**US Army Corps
of Engineers**
**Construction Engineering
Research Laboratories**

**USACERL Technical Report 98/04
December 1997**

CONSTRUCTION PRODUCTIVITY ADVANCEMENT RESEARCH (CPAR) PROGRAM

Design and Performance Testing of Prestressed Precast Reinforced Concrete Hybrid Joists

by

Mohsen A. Saleh, Pamalee A. Brady,
Amin Einea, Maher K. Tadros, and Curtis L. Decker

Approved for public release; distribution is unlimited.

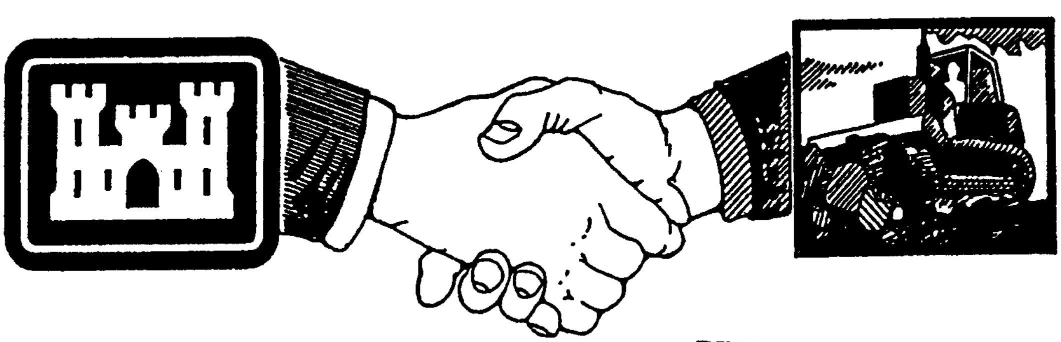

**A Corps/Industry Partnership To Advance
Construction Productivity and Reduce Costs**

USER EVALUATION OF REPORT

REFERENCE: USACERL Technical Report 98/04, *Design and Performance Testing of Prestressed Precast Reinforced Concrete Hybrid Joists*

Please take a few minutes to answer the questions below, tear out this sheet, and return it to USACERL. As user of this report, your customer comments will provide USACERL with information essential for improving future reports.

1. Does this report satisfy a need? (Comment on purpose, related project, or other area of interest for which report will be used.)

____

____

____

2. How, specifically, is the report being used? (Information source, design data or procedure, management procedure, source of ideas, etc.)

____

____

3. Has the information in this report led to any quantitative savings as far as manhours/contract dollars saved, operating costs avoided, efficiencies achieved, etc.? If so, please elaborate.

____

____

4. What is your evaluation of this report in the following areas?

a. Presentation: ______________________________

b. Completeness: ______________________________

c. Easy to Understand: ______________________________

d. Easy to Implement: ______________________________

e. Adequate Reference Material: ______________________________

f. Relates to Area of Interest: ______________________________

g. Did the report meet your expectations? ______________________________

h. Does the report raise unanswered questions? ______________________________

i. General Comments. (Indicate what you think should be changed to make this report and future reports of this type more responsive to your needs, more usable, improve readability, etc.)

____

____

____

____

____

____

5. If you would like to be contacted by the personnel who prepared this report to raise specific questions or discuss the topic, please fill in the following information.

Name: ______________________________

Telephone Number: ______________________________

Organization Address: ______________________________

____

____

6. Please mail the completed form to:

Department of the Army
CONSTRUCTION ENGINEERING RESEARCH LABORATORIES
ATTN: CECER-TR-I
P.O. Box 9005
Champaign, IL 61826-9005

REPORT DOCUMENTATION PAGE

Form Approved
OMB No. 0704-0188

1. AGENCY USE ONLY *(Leave Blank)*	2. REPORT DATE	3. REPORT TYPE AND DATES COVERED
	December 1997	Final

4. TITLE AND SUBTITLE
Design and Performance Testing of Prestressed Precast Reinforced Concrete Hybrid Joists

5. FUNDING NUMBERS
CPAR
LT3

6. AUTHOR(S)
Moshen A. Saleh, Pamalee A. Brady, Amin Einea,Maher K. Tadros, and Curtis L. Decker

7. PERFORMING ORGANIZATION NAME(S) AND ADDRESS(ES)
U.S. Army Construction Engineering Research Laboratories (USACERL)
P.O. Box 9005
Champaign, IL 61826-9005

8. PERFORMING ORGANIZATION REPORT NUMBER
TR 98/04

9. SPONSORING / MONITORING AGENCY NAME(S) AND ADDRESS(ES)
Headquarters, U.S. Army Corps of Engineers
ATTN: CERD-C
20 Massachusetts Ave. NW
Washington, DC 20314-1000

10. SPONSORING / MONITORING AGENCY REPORT NUMBER

11. SUPPLEMENTARY NOTES
Copies are available from the National Technical Information Service, 5285 Port Royal Road, Springfield, VA 22161.

12a. DISTRIBUTION / AVAILABILITY STATEMENT
Approved for public release; distribution is unlimited.

12b. DISTRIBUTION CODE

13. ABSTRACT (Maximum 200 words)
This report describes an innovative design for prestressed precast reinforced concrete joists. The joist is a hybrid design that uses large web openings for passage of environmental pipes and ducts, replicating an advantage of steel truss construction. The design also exploits the stiffness and strength of precast concrete double-tee beams.

Alternative designs were investigated by varying parameters such as concrete strength, prestressing strand layout, and reinforcement. Test results from eight hybrid joists are presented to substantiate finite element analysis results, and a simple method for designing the beams is presented.

It is concluded that hybrid joist demonstrates remarkable performance and the capability to behave like a conventional double-tee beam. The behavior of the hybrid joist meets the requirements of ACI 318-95. Experimental failure loads were very high compared with design service and ultimate loads. The analytical and experimental results indicate that the hybrid joist has a predictable ductile response, and the experimental results verify that the analytical model provides a reliable and simple method for determining the load-deflection response. Vibration analysis showed that the hybrid joist has acceptable response to established criteria and compares well with the response of both concrete and steel bar joists.

14. SUBJECT TERMS
Construction Productivity Advancement Research (CPAR)
concrete testing
precast concrete
prestressed concrete
hybrid joists

15. NUMBER OF PAGES
120

16. PRICE CODE

17. SECURITY CLASSIFICATION OF REPORT	18. SECURITY CLASSIFICATION OF THIS PAGE	19. SECURITY CLASSIFICATION OF ABSTRACT	20. LIMITATION OF ABSTRACT
Unclassified	Unclassified	Unclassified	SAR

NSN 7540-01-280-5500

Standard Form 298 (Rev. 2-89)
Prescribed by ANSI Std 239-18
298-102

Foreword

This research was performed for Headquarters, U.S. Army Corps of Engineers, under Construction Productivity Advancement Research (CPAR) Work Unit LT3, "Optimization of Prefabricated Joists." The technical monitors were Daniel Chen, CEMP-ET, and Stanley Green, CEMP-CE.

The work was performed by the Engineering Division (FL-E) of the Facilities Technology Laboratory (FL), U.S. Army Construction Engineering Research Laboratories (USACERL). The USACERL Principal Investigator was Pamalee Brady, CECER-FL-E. The CPAR research and development partner was the Center for Infrastructure Research at the University of Nebraska, Omaha. The University of Nebraska Principal Investigator was Dr. Maher K. Tadros. Larry M. Windingland is Acting Chief, CECER-FLE, and Donald F. Fournier is Acting Chief, CECER-FL. The USACERL technical editor was Gordon L. Cohen, Technical Information Team.

The contributions of the following individuals to this research are gratefully acknowledged:

- Mr. Larry Fischer of Concrete Industries, Inc., a CPAR industry participant
- Mr. Ervell Staab of Missouri River Division, a Corps of Engineers participant in the work.

COL James A. Walter is the Commander of USACERL and Dr. Michael J. O'Connor is the Director.

Contents

List of Figures and Tables

Figures

Tables

1 Introduction

Background

Precast concrete double-tee beams, which are widely used as floor and roof members, may be made structurally and economically more efficient by taking advantage of concepts used for steel truss joist systems. One means of increasing the economy of precast concrete joists is to add large web openings in the joist to permit the passage of mechanical ducts through the webs instead of under them. This approach reduces the floor-to-floor height in a building, and reduces wind and earthquake forces on the building through weight optimization. Cost savings may therefore be achieved in structural and foundation systems, and mechanical and electrical systems.

There are other potential advantages to such a configuration. Increasing the flange width of the double tee from a maximum of 8 ft (2.44 m) to 10 ft (3.05 m) or 12 ft (3.66 m) may provide greater efficiencies. Making the double tee wider would reduce the weight of the double tee per square foot (square meter) by using only two webs for a width of 12 ft (versus two webs for a width of 8 ft). Furthermore, the erection time of a structure may be reduced because fewer double tees would be needed to support a given area. Also, fewer trips would be needed to haul double tees to the job site, fewer crane picks would be required to place the double tees, and fewer double tees would need to be leveled and connected in the field.

Another approach to optimization is the development of a new *hybrid joist* that benefits from the design strengths of both the steel bar joist and the concrete double tee. Such a hybrid joist could be used for either floor or roof framing, and the concept could be extended for application in bridge decks.

The U.S. Army Construction Engineering Research Laboratories (USACERL) investigated designs for a new hybrid joist using a truss configuration of precast concrete with steel tendons in the top and bottom chords of the member. The research was conducted under the U.S. Army Corps of Engineers Construction

Productivity Advancement Research (CPAR) program. The CPAR Partner in this study was the University of Nebraska, Omaha.

Objective

The first objective of this CPAR work unit was to modify the existing precast concrete double-tee shape, which is widely used as floor and roof members, to make it more structurally and economically efficient. The project was to focus on adding the largest web openings possible, which will allow passage of mechanical ducts through the webs instead of under them. The addition of web openings in double tees will reduce the floor-to-floor height in a building and reduce wind and earthquake forces on the building through weight optimization. Cost savings may therefore be achieved in structural and foundation systems, and mechanical and electrical systems.

Increasing the width of the double tee from a maximum of 8 ft (2.44 m) to 10 ft (3.05 m) or 12 ft (3.66 m) was another modification to be investigated. This change in width may be possible in part through the use of high-strength concrete. Making the double tee wider will reduce the weight of the double tee per square foot (or square meter) by using only two webs for a width of 12 ft versus two webs for a width of 8 ft. Also, the increased width will reduce the erection time of a structure because there will be fewer double tees to erect. This approach would require fewer trips to bring double tees to the job site, fewer crane picks to place the double tees, and fewer double tees to be leveled and connected in the field.

The second objective of the program involved the relatively "high-risk, high-reward" development of a new hybrid joist that combines benefits of both the steel bar joist and the concrete double tee. This hybrid joist could be used for either floor or roof framing. The working ideas for the new joist involve using a truss configuration of precast concrete, with steel tendons in the top and bottom chords of the member.

This report encompasses the second objective of the CPAR project only. Documentation of the first objective is available in USACERL Technical Report 98/03, *Design and Performance Testing of Prestressed Precast Reinforced Concrete Double-Tee Beams With Web Openings* (Saleh et al., December 1997).

Approach

The program approach stated in the CPAR Cooperative Research and Development Agreement (CPAR-CRDA) encompasses the following steps:

1. Information on the state-of-the-art technology in the areas of steel joists, precast concrete framing systems, prestressed beams with web openings, and emerging structural materials such as high-strength concrete, lightweight concrete, high-strength steel, and fiber-reinforced plastics for possible use in the hybrid joist will be compiled for documentation. The performance of existing systems will be evaluated, standard designs will be assessed, and methods of testing both the modified tees and the hybrid joist will be reviewed.
2. Material strengths, opening size and placement, and reinforcement details will be refined for double-tee joist designs. Effects of span length and widening the double tees will be evaluated. Analysis of the modified double tees will be conducted, and design guidelines will be developed.
3. Two different systems of the hybrid joist will be developed. Prototype materials and joist configurations will be selected for the new joist designs. Analysis of prototype designs will be conducted for a number of spans and loading conditions. The designs will be optimized and final designs will be prepared for testing.
4. Double-tee specimens with web openings and hybrid joist specimens will be manufactured. These specimens may be full scale or small scale. For the hybrid joist, the components of the joist and the full joist itself will be tested. A test program will be defined, and the equipment and instrumentation requirements will be assessed.
5. Experimental tests to evaluate the performance of the hybrid joist components will be conducted. Double tees with web openings and complete hybrid joists will also be tested to determine their structural performance. Test data will be collected. The specimens will be produced by industry with input from both NTDC and USACERL. Testing of the double tees will be conducted by NTDC; testing of the hybrid joists will be conduced by USACERL.
6. Detailed analysis will be conducted on the experimental test results to evaluate the performance of the modified double tee and the hybrid joist. Further analysis, design and testing of the final joist designs will be demonstrated in a field project. USACE-MRD will assist in identification of an appropriate filed demonstration project.
7. The industry design method for elements of each type of joist will be established. Design aids in the form of tables or charts will be developed. The design philosophy will be articulated for structural engineering designers.
8. A final report will be prepared that documents the joist development, test verification, final prototype design, design procedure, plans for commercialization

and technology transfer and conclusions as to the extent of the products' application and benefits to the U.S. construction industry.

This approach was followed in the conduct of this CPAR project. The current report documents work related to hybrid joist designs. Documentation of the work with double-tee designs is available in (USACERL TR 98/03).

Units of Weight and Measure

U.S. standard units of measure are used throughout this report. A table of conversion factors for Standard International (SI) units is provided below.

SI conversion factors

1 in.	=	25.4 cm
1 ft	=	0.305 m
1 sq in.	=	6.452 cm^2
1 sq ft	=	0.093 m^2
1 lb	=	0.453 kg
1 kip	=	453 kg
1 psi	=	6.89 kPa
1 psf	=	4.88 kg/m^2

2 Existing Joist Systems

Open Web Steel Joist Systems

The open web steel joist (OWSJ) system, or *bar joist* system, consists of top and bottom chords constructed of steel double-angles with diagonal steel bars welded to the angles. This joist system is used to support cold-formed corrugated steel sheets with a cast-in-place slab. Different series of OWSJs are available on the North American market, such as K-Series, CS-Series, LH-Series, DLH-Series, and SLH-Series (Vulcraft 1995), for example.

The *K-Series* is designed to support uniformly distributed loads. The design of this series is based on a yield strength of 50,000 pounds per square inch (psi). The depth of K-Series joists ranges from 8 to 30 in. covering spans from 8 to 60 ft. *The CS-Series* was introduced to address concentrated or nonuniform loading. For the chords, uniform design moment and shear diagrams are used. That is, the moment and shear capacity are constant throughout the span. Also, all webs are designed for 100 percent stress reversal.

The *LH-* and *DLH-Series* were developed to address longer spans. The LH-Series is suitable for the direct support of floors and roof decks in buildings, and the DLH-Series is suitable for the direct support of roof decks in buildings. In the design of LH- and DLH-Series, the chord or web sections are based on a yield strength of at least 36,000 psi. The depth of LH-Series ranges from 18 to 48 in., which can cover spans from 21 to 96 ft. The DLH-Series has a range of depth from 52 to 72 in., covering spans from 61 to 144 ft. The SLH-Series are "Super Longspan Steel Joists." This term refers to open web, load-carrying members utilizing hot-rolled steel shapes. The SLH-Series is suitable for the direct support of roof decks in buildings. The joists have a range of depth from 80 to 120 in., which can cover spans from 80 to 240 ft.

Steel joist systems have some disadvantages, however. First, they have low overall stiffness, which may result in excessive vibrations and deflections. Also, the low stiffness and light weight of this structural system requires that effects

of uplift loads be examined in design. Furthermore, steel joist systems have very low resistance to fire and corrosion, and they require intensive labor to construct.

Precast Prestressed Joist Systems

Precast prestressed joist systems are used as either floor or roof members. The most popular sections in these systems are solid flat plates, hollow core sections, and double-tee sections. *Solid flat plates* have a depth range of 4 to 8 in. and the span range is from 10 to 35 ft. The depth of *hollow core sections* ranges from 6 to 15 in. and spans range from 12 to 50 ft. *Double-tee sections* are between 12 to 36 in. in depth and span between 40 and 90 ft. The main advantages of these systems are:

1. They are made under controlled conditions, so their quality is high.
2. Steel reinforcement is protected against corrosive and fire environments.
3. The sections have high stiffness, which reduces vibrations and deflections.
4. Using these systems reduces the amount of field labor required for erection.

However, these systems have some disadvantages. They, like CIP systems, are relatively heavy compared to the steel joist systems, so they require stronger structures and foundations for their support. This will lead to higher seismic loads. They also do not allow passage of service ducts through their webs.

Web Openings in Concrete Joists

To address a major disadvantage in precast concrete double tees several studies have been undertaken since 1967 to develop precast prestressed concrete beams with web openings. The research has focused on designing for flexural failure, preventing shear failure, limiting deflections, and optimizing shape, size, and location of web openings. The following paragraphs provide a summary of these research studies.

Experimental Research

Ragan and Warwaruk (1967) conducted the first experimental study on prestressed concrete T-beams with large web openings. Four model beams and two full-size T-beams were tested in the program. All model beams were subjected to two-point loads while the loading of full-size beams was approximately uniform. The results showed that the failure moment was two to three times that at

which cracking was first observed. The researchers concluded that sizable web openings could be accommodated without sacrificing strength and that deflections of beams with openings were not significantly greater than for beams without openings.

Suave (1970) conducted experimental work on prestressed concrete T-beams with large web openings. He investigated varying two-point load positions, shear reinforcement, and additional longitudinal reinforcement in the shear spans. He tested nine beams, one of which was solid and the rest with eight openings, 8 in. tall by 16 in. wide, separated by 8 in. wide posts. Suave drew the following conclusions:

1. Additional shear reinforcement served to increase the load-carrying capacity of a beam with large web openings.
2. Increasing the supplementary longitudinal reinforcement did not significantly increase the shear capacity of the beams.
3. Additional vertical reinforcement placed in the posts gave these posts the capacity required to localize the failure in the lower chord if this chord had no vertical reinforcement.
4. The reinforcing of both the posts and the lower chord resulted in a redistribution of stresses in the shear span such that all sections were more equally stressed in diagonal tension.

LeBlanc (1971) conducted tests on prestressed T-beams. He investigated the behavior of beams with different opening shapes, number of prestressing strands, and amount of shear reinforcement. Ten beams were tested. Six contained 8 in. tall x 16 in. wide parallelogram-shaped openings, three contained rectangular openings of the same overall dimensions, and one beam had no openings. He concluded that beams with parallelogram-shaped openings performed better than the beams with rectangular shaped openings. Increasing the number of prestressing strands required an increase in shear reinforcement to ensure that the beam failed in flexure.

Barney, Corley, Hansan, and Parmelee (1977) expanded on the work done by Ragan and Warwaruk (1967). They tested 5 short span and 13 long span full-size precast prestressed concrete T-beams. Figure 2.1* shows the details of the long-span beam sections; Figure 2.2 shows the loading location for the tested beams. The variables investigated were size and location of opening along the span, type and amount of shear reinforcement, and amount of primary flexural reinforcement. The capacity of specimens with openings in high shear regions

* Figures and tables are presented at the end of the chapter in which they are first discussed.

was limited by an unrestrained shear crack extending from the lower side of the opening toward the support. These cracks normally propagated along the prestressing strands. In some beams, the cracks extended into the region required for strand embedment causing the strand to slip. The variables having greatest effect on beam strength and behavior were the location of web openings along the span and the amount of web shear reinforcement. The behavior of these beams was similar to a Vierendeel* truss. Barney et al. recommended that adjacent web openings be separated by web elements (posts) having overall width-to-depth ratios of at least 2.0, where the width of the post is the distance between adjacent stirrups. The authors concluded that large web openings can be placed in prestressed concrete beams without sacrificing strength or serviceability. However, openings must be located outside the required strand embedment length and adequate shear reinforcement must be provided adjacent to openings. They developed a design procedure for prestressed double-tee beams with multiple web openings.

Salam and Harrop (1979) studied the effects of circular web openings on the performance of prestressed concrete beams. The parameters studied were opening size, location, and reinforcement. Consideration was given to the prediction of beam strength and to different methods of reinforcement around the openings. It was concluded that beams with multiple circular openings had peak stresses below those for beams with a single hole. Also, compensation for the presence of the holes is best provided by vertical stirrups at the sides of the holes. This reinforcement resists the horizontal splitting due to prestress and diagonal tensile stress at working load. The researchers concluded that a perforated beam can be as strong as a similar solid beam provided the holes do not protrude into the ultimate rectangular stress block required to produce flexure failure.

Kennedy and El-Laithy (1982) investigated both theoretically and experimentally the behavior of prestressed concrete beams with rectangular openings. They were particularly interested in behavior at the prestressing force transfer stage. Eighteen post-tensioned concrete beams were used for the experimental program. The main parameters studied were the depth of the opening and its horizontal and vertical location. The results indicated that the depth and the vertical location of the opening were the two parameters that significantly affected the stresses around the opening. The horizontal location of the openings did not have an appreciable influence on the stresses at the transfer stage. The analyses also revealed that the maximum vertical tensile stress occurs at or near the mid-depth of the opening, and this stress increases linearly with the increase

* Vierendeel truss: a Pratt truss without diagonal members having rigid joints between the chords and verticals.

in the prestressing force until a horizontal crack is formed. The presence of the opening also gives rise to significant shear stresses near the four corners of the opening. The influence of transverse reinforcement on the cracking load was also studied. It was found that reinforcing against the vertical tension force was effective in increasing the cracking load by approximately 30 percent for both rectangular and T-beams. It was concluded that:

1. The presence of an opening gives rise to a potential splitting-tension field, followed by a compression field, whose distances are functions of the depth and vertical location of the opening.
2. The assumption of plane sections remaining planar does not apply in the vicinity of the opening.
3. The presence of an opening increases the deflection only slightly at the transfer stage.

Dinakaran and Sastry (1984) conducted tests on T-beams with openings. The variables considered were the size of opening, location of openings, and type of reinforcement around openings. The openings were positioned both in the shear span as well as in the interior of the span. The results showed that the first crack appeared from the side of the opening closest to the support for beams having openings in the shear span due to the shear concentration at the opening corners. This crack propagated toward the support. Beams having openings in the constant moment zone did not exhibit crack propagation from the corner of the opening. The test results also revealed that the location of the opening has the greatest effect on the strength and the behavior of the beams. It was concluded that post-tensioned prestressed concrete T-beams with large openings behave similarly to a Vierendeel truss. Also, beams with openings in the high-moment region behave better than those having openings in the shear span, and their ultimate moment capacity is also greater. It was found that vertical stirrups and hooks provided adjacent to openings control cracking. Compressive struts and tensile struts carry external shear in proportion to their cross-sectional areas. The influence of openings on deflection is minor in properly reinforced beams.

Kennedy and Abdalla (1992) investigated the response of prestressed beams with openings for the purpose of developing a design procedure to overcome cracking at openings. This study focused on the potential splitting forces that may develop at the edges of the openings at prestressing force transfer stage and at the corners of the openings at service load stage. A parameter study of specific variables was also conducted analytically. These variables were horizontal and vertical locations of the openings, opening width and depth, and type of cross

section. An experimental study of post-tensioned beams with web openings was also conducted to justify the proposed design process. Tests were carried out on 13 post-tensioned beams. Six of the beams were rectangular in section, five were T-section, and the remaining two were I-section. The layout of the specimens is shown in Figure 2.3. As shown in Figure 2.4, the experimental results revealed five critical locations for potential cracking of prestressed beams with openings:

1. the edges of the opening due to prestressing force
2. at the corners of the opening due to the framing action at the opening
3. in the opening chords due to the flexural stresses resulting from the secondary moments in these chords
4. in the tension chord due to the normal tensile stresses in that chord
5. in the opening chords due to shear.

The first of the above five types of potential cracking was assumed to occur at the transfer stage due to the prestressing force only. The rest of the cracking would occur at the service load stage due to applied vertical loads. The last two types of cracking may cause the complete collapse of the beam. Kennedy and Abdalla's design method was developed for beams with a single web opening.

Savage (1993) at University of Nebraska investigated variables including the effect of two prestressing strand depression points, opening size and location, and use of high-strength concrete on double-tee beams with openings. Figure 2.5 shows the typical dimensions of the test specimens. The design of the specimen, was based on finite element analysis and the design procedure by Barney et al. (1977). Four full-sized specimens were tested to failure. Figure 2.6 shows the reinforcement details of these specimens. They concluded that:

1. The ultimate strength of the beams was not affected by the presence of web openings.
2. The double tees with web openings behaved like Vierendeel trusses.
3. None of the compression chords above the openings exhibited buckling behavior.
4. The beams should be designed not to crack under service loads.
5. The addition of prestressing strands above the openings was effective in counteracting the tensile stress concentrations caused by end moments acting on the compression chord.

Analytical Methods

Several researchers have developed procedures for the analysis and design of prestressed concrete beams with web openings.

Barney et al. (1977) developed both a simplified and an iterative analysis procedure. Barney explains that primary stress results from the two chords resisting moment in unison; secondary flexural stresses in the chords are also created due to a statically indeterminate portion of the total shear force acting at the section. In the design method, hinges are assumed at the mid-length of each chord (Figure 2.7). Resulting equations for top and bottom chord compression and tension are derived as a function of moment, prestress force, distance of prestress force from the neutral axis, and distance between centroidal axes of the chords. These equations assume no cracking has taken place and apply to load stages at transfer of prestress service.

With cracking, a redistribution of forces takes place and Barney presents a conservative iterative technique to find values for chord shear forces at ultimate load that are based upon a cracked section moment of inertia. This technique is valid for all loads up to those causing full-depth cracks in the bottom chord member of the beam. Barney's test results indicated that after full-depth cracking of the bottom chord, additional shear is carried entirely by the compressive (top) chord.

This analytical procedure is also applicable to beams with concrete toppings. It is necessary to distinguish between the loads that are applied to the beam itself and the loads applied to the composite system. In an uncracked state, the beam is assumed to carry all the dead load and prestress force. Once cracking ensues, some of the dead load and prestress force, along with all of the load applied after the concrete topping is cast is assume to be carried by the composite system. The models by Barney et al. are valid when the chords behave primarily as flexural members and for beams having straight prestressing strands.

Kennedy and Abdalla (1992) performed a theoretical study using a nonlinear finite element program. Based on the results from the finite element solution, which were substantiated by experimental tests, a simple method was developed to estimate the vertical tensile force around web openings due to the prestressing force. The model permitted placement of reinforcement at different locations (running in horizontal, vertical, and inclined directions) around the opening with various cross-sectional areas and arrangements. The concrete under compression was modeled by an elastic-plastic theory and isotropic hardening was accounted for. The model was a "smeared crack" model in that it did not track individual macro cracks. However, at each integration point of the finite element model, the presence of cracks was entered in the calculations by the way in which the cracks affected the stresses and the material stiffness associated with the

integration point. The finite element model was an idealization and used to get an overall idea of beam behavior and stresses.

The most relevant analysis process for this particular study is that developed by Savage (1993). The objective of the model was to get an idea of the deflection characteristics of beams with web openings and the location and magnitude of stress concentrations. The method began with a working stress analysis for critical sections at the beam end and at midspan through an opening. Variables included concrete strength, number of prestressing strands, and opening depth. This analysis was an approximation as secondary moments caused by shear in the chords, above and below the openings, were neglected. The working stress model was used as a basis to begin finite element analysis.

The finite element analysis produced estimations of axial stresses at transfer as well as service, and shear and principal tensile stresses at ultimate load. The longitudinal stresses were checked against American Concrete Institute (ACI) working stress limits (ACI 318, 1995). Shear and principal tensile stresses at ultimate load were used to aid in the design of shear stirrups. The finite element analysis showed areas of high stress concentration. The model is an elastic one and does not take cracking into account. Thus loads at ultimate load—and to a lesser degree, service load—are not exact.

Discussion of Previous Research Findings

The previous research indicates that the prestressed concrete beam with web openings behaves similarly to a Vierendeel truss. The deflection of these beams is similar to that of beams without web openings. The most common failure mode observed in the experimental tests of beams with web openings is the formation of a hinging mechanism in the posts. Web openings should be placed outside of the strand development length and the high shear zone. Vertical stirrups should be placed on each side of an opening to control cracking. The chord below an opening may crack at loads less than the service load.

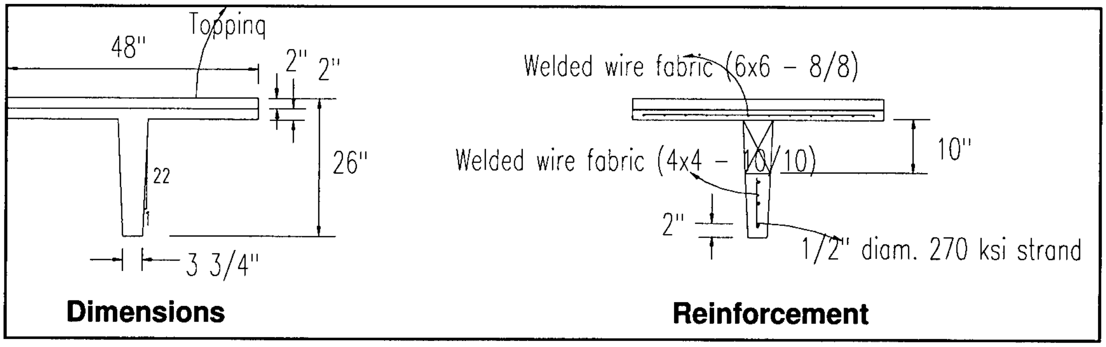

Figure 2.1. Long-span test beam sections from Barney et al. 1977).

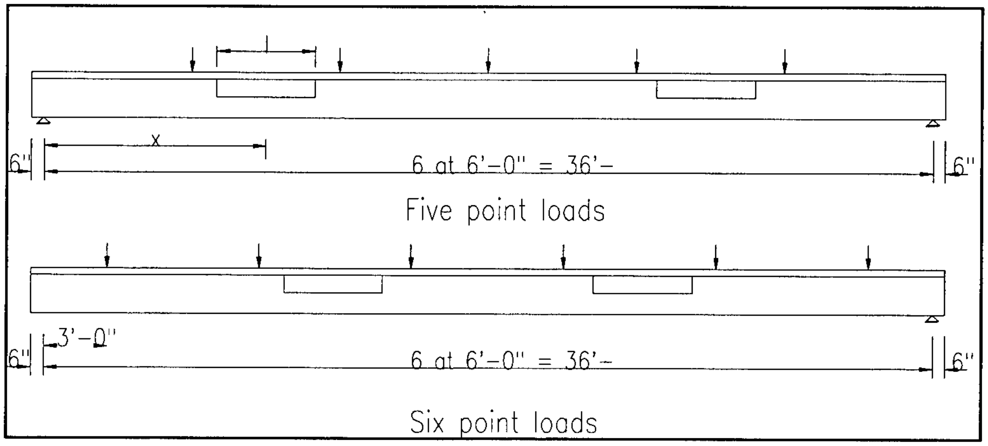

Figure 2.2. Loading location for test beams from Barney et al. (1977).

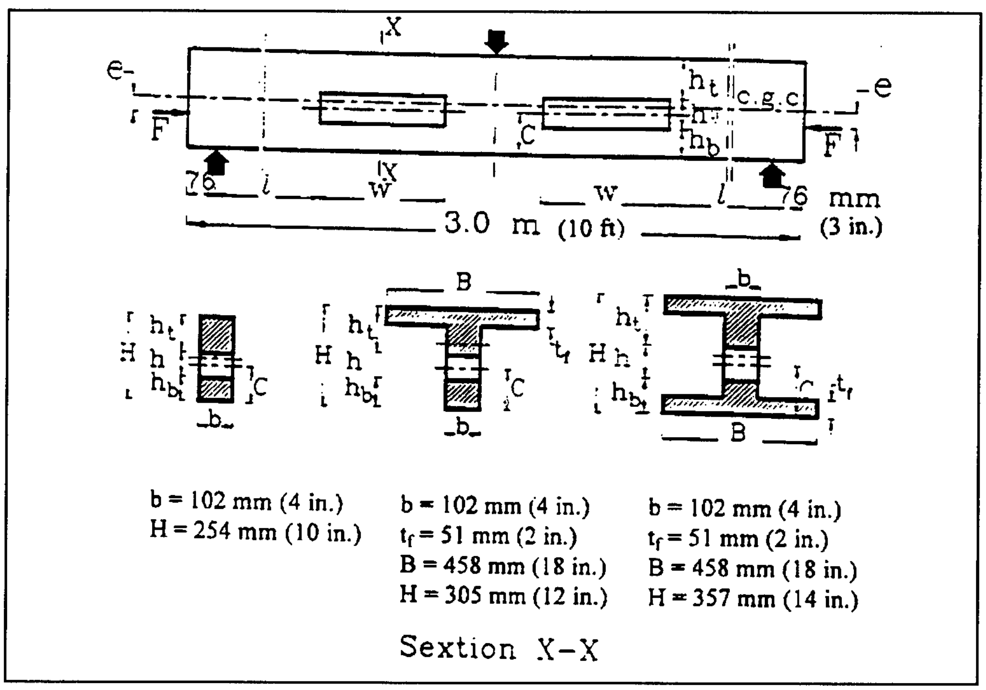

Figure 2.3. Layout of test beams as adapted from Abdella (1993).

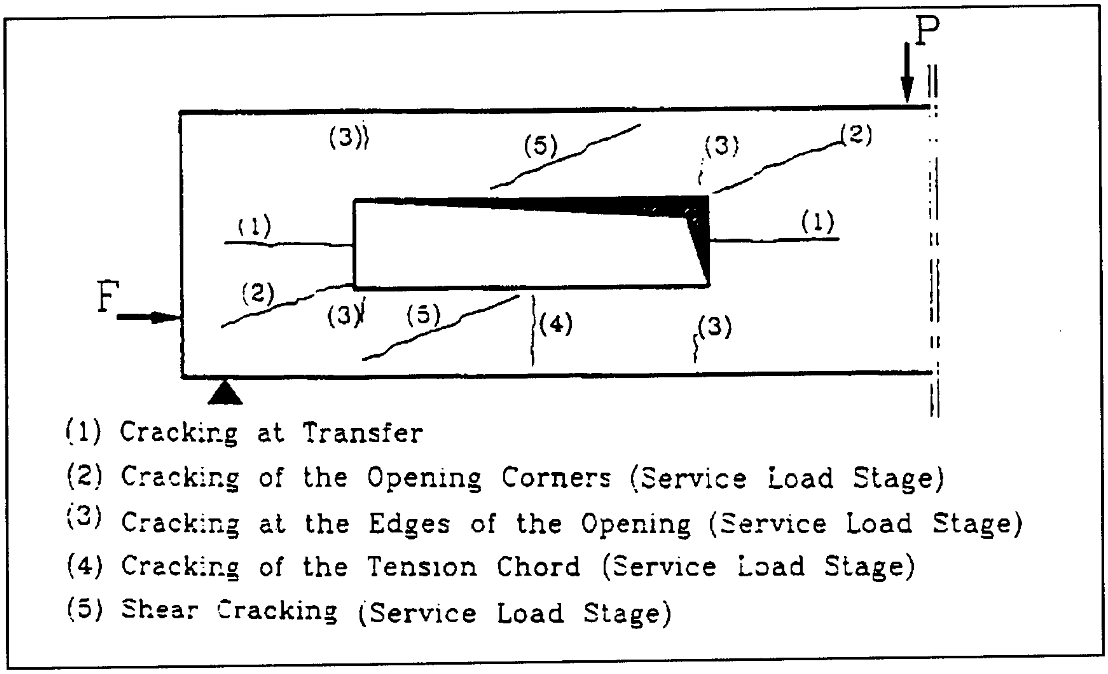

Figure 2.4. Different types of cracking around beam opening, adapted from Abdella (1993).

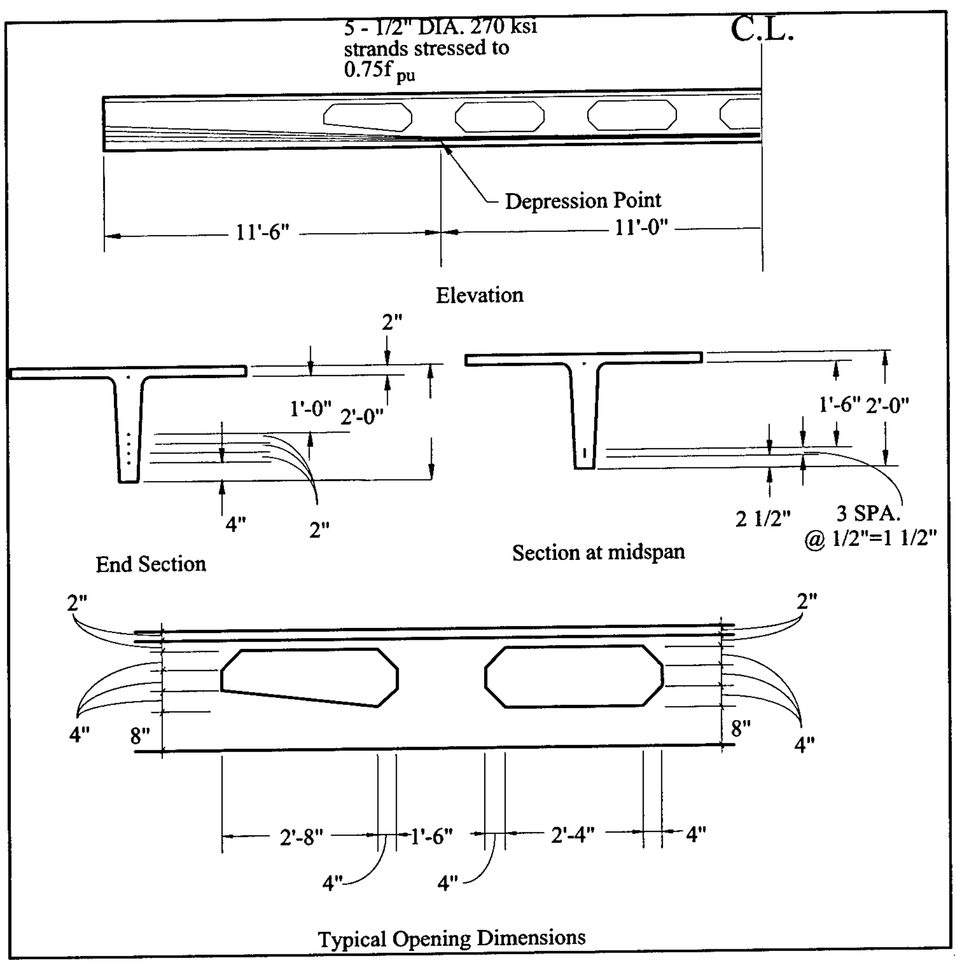

Figure 2.5. Concrete dimensions and strand profile from Savage 1993.

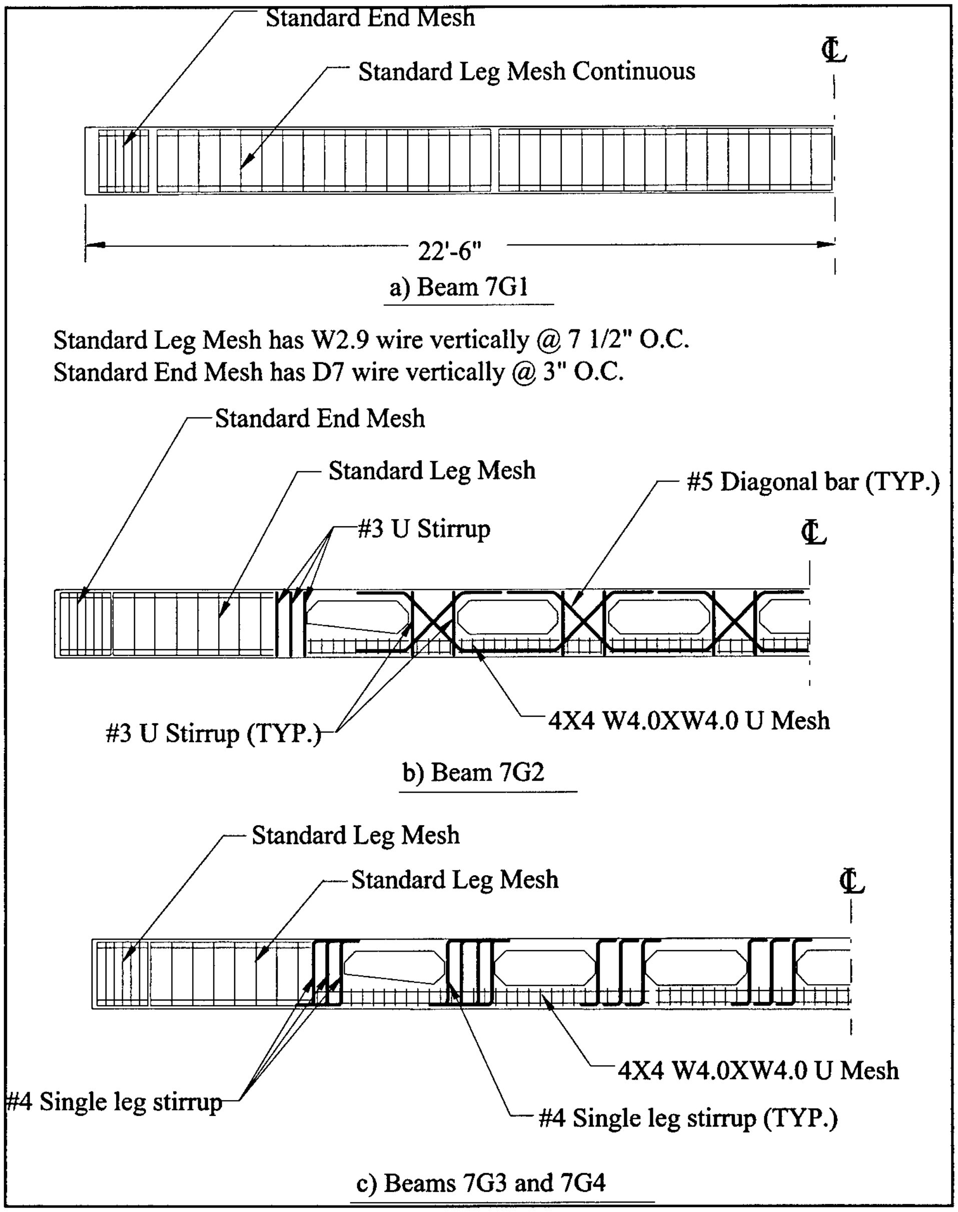

Figure 2.6. Reinforcement details from Savage (1993).

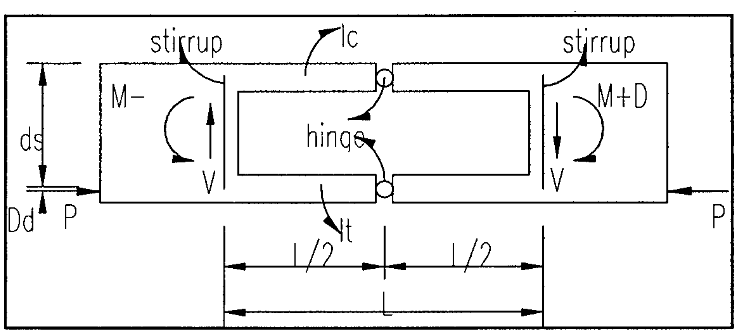

Figure 2.7. Idealized model of beam with web openings, as adapted from Barney et al. (1977).

3 Joist Design

Introduction

This chapter describes the development of a prototype design for a prestressed precast concrete joist with integral web openings. The joist was designed to be easy to fabricate and erect and capable of covering a wide variety of building applications. Another important design consideration was to provide a joist that avoids certain problems with open-web steel joist applications, including floor vibrations, corrosion, fireproofing, and ponding due to excessive deflections. Thus, the joist design is intended to combine the benefits of prestressed concrete double tees and open-web steel joists but overcome their shortcomings.

Description of Proposed System

The design concept for the hybrid joist was a prestressed precast concrete joist with integral web openings and a precast or cast-in-place slab. The web had top and bottom chords connected with vertical and inclined members, as shown in Figure 3.1. Figure 3.2 shows the overall dimensions for a joist having a depth of 24 in. The joists may have different depths to cover a variety of spans. The main variables in the design were the depth of the openings, depth of top and bottom chords, the length of exterior prismatic segment (L_1), and the length of interior opening (L_2). Changes in depth are obtained by varying the thickness of the top and bottom chords, and the height of the opening. Large increments of span lengths may be made by changing dimension L_2 in increments of 5 ft, and small increments may be made by changing dimension L_1 in fractions of 5 ft. The inclined part of the joist used the same angle for all joists. The variation in dimensions of the inclined portion of the joist depends on the depth of the joist; for any specific joist depth this inclined portion has fixed dimensions.

The hybrid joist was envisioned for use in office construction (floors and roofs) and similar applications characterized by uniform loading. A span of 32 ft and a tributary spacing s of 4 ft between the web were chosen for the initial design. Loads of 50 psf office live load and 20 psf superimposed (SI) dead load were

assumed. A 50 psf dead load also represented 4-in. thick precast or cast-in-place slab. The total uniform superimposed service load was therefore 120 psf. Self-weight of the joist, 18 psf, was considered uniformly distributed along the span. This resulted in a total uniform service load of 138 psf and an ultimate load of 201 psf. The specimens were designed according to specifications from American Concrete Institute (ACI) 318-95, *Building Code Requirements for Structural Concrete and Commentary*. (This publication is cited hereinafter for brevity as "ACI 318-95.")

The joist had a constant thickness of 6 in. For a 24-in. deep joist, the top, bottom, and inclined chord members had a depth of 6 in. while the end members had a depth of 10 in. There were two vertical members, 6 in. wide, which act as compression members. Figure 3.3 shows the strand profile and distribution. The prestressed reinforcement consisted of 6 strands; two strands were located in the top chord and four strands were located in the bottom chord. Strands were separated by 2 in. along the length of the joist.

Construction of the web is best done in the horizontal position with two joists cast simultaneously to balance the anchorage forces of prestressing. Figure 3.4 shows a schematic of the forming with the strands. Figure 3.5 shows the three-dimensional shape of the web. Figure 3.6 shows the final appearance of the hybrid joist system with the web and cast-in-place slab on top.

Design Analysis

The shape of the joist was finalized based on several trial and error analyses. When this preliminary selection was made, analysis in two stages was performed. First, working stress analysis was conducted to ensure the satisfaction of the stresses at different construction and loading stages. Second, finite element modeling was carried out to predict the behavior of the joist and identify stress concentration regions.

In all analyses prestressing strands were assumed to be 1/2 in. diameter with 270 ksi and low relaxation properties. Mild reinforcing was assumed in the form of Grade 60 deformed bars. Concrete strength was chosen to benefit from state-of-the-art of materials technology. High-performance concrete with a compressive strength of 7000 psi at prestressing transfer and 12,000 psi at 28 days was assumed.

A working stress analysis was undertaken to check the stresses at different stages during construction and application; the stages were as shown in Table 3.1. Some of loads acted on a non-composite section (web only), and some on a composite section (web plus slab). Critical sections were determined to be at the joist end, at the top chord midspan, at the bottom chord midspan, and at the start of the inclined part of the strand. The RISA2D (Rapid Interactive Structural Analysis – 2 Dimensional) structural software program* was used to calculate the internal forces at these sections. For service loads, the stresses at critical sections were lower than allowable ACI Code requirements.

To assess the overall behavior of the joist using finite elements, it was modeled as a linear, elastic two-dimensional structure. Several element types from the element library in ANSYS50A† were tested to choose the appropriate element for each material, concrete and prestressing strand. A three-dimensional (3-D) shell element with a specified thickness, SHELL63, was used to model the concrete. SHELL63 has both bending and membrane capabilities, both in-plane and out-of-plane. This element was used with a 6 in. thickness to simulate the web and a 48 in. thickness to simulate the slab. Because the created model was two-dimensional (2-D), the out-of-plan degrees of freedom were constrained. A 2-D spar element from ANSYS50A — LINK1 — was used to model the prestressing strand. The two-node element is a uniaxial tension-compression element with two degrees of freedom at each node. Initial strain in this element was used to introduce the prestressing forces into the model. This element was used to simulate four strands in the bottom chord and two strands in the top chord.

The finite element model represented a 32 ft span joist consisting of web and cast-in-place slab. The targeted results from the finite element analyses were axial stresses, principal tensile stresses, and shear stresses at transfer of prestressing force all at service loads and ultimate loads. The results from the finite element analyses showed several stress concentration areas. There was tension stress concentration at the points of inclination of the draped strands because of the vertical component of the prestressing force at this point. There was also tension stress concentration at the edge of the triangular openings. The finite element analyses also showed that the camber and deflection of the joist at different loading stages were acceptable under ACI 318-95 requirements. The model was used only to check the behavior of the hybrid joist and to predict the magnitude of stress and deflection values. This information was beneficial in calculating and placing appropriate reinforcement in the test specimens.

---

* RISA Technologies, 26212 Dimension Drive, Suite 200, Lake Forest, CA 92630.

† ANSYS, a finite element analysis software package, version 5.0A, ANSYS, Inc., Canonsburg, PA 15357.

Selection of Test Designs

Based on the working stress and finite element analysis results final joists designs were selected for experimental testing. The analyses showed stress concentrations around the web openings, particularly at the corners of the triangular openings and in the web piers. The final joist thickness was 6 in.; all members had a 6 in. depth except for the end members, which were 10 in. in depth to provide adequate shear capacity. The prestressing strand profile was chosen to coincide with the center of gravity (c.g.) of the members. A total of six strands were to be used; two straight strands were aligned with the c.g. of the top web chord. The remaining four strands were designed to run along the inclined members and were located in the c.g. of the web bottom chord. Minimal vertical shear reinforcement was provided to connect the cast-in-place slab with the web.

Table 3.1. Load stages.

Stage	Type of section
release of the strands	non-composite section
self weight of the web	non-composite section
self weight of the slab	non-composite section
superimposed dead load	composite section
superimposed live load	composite section

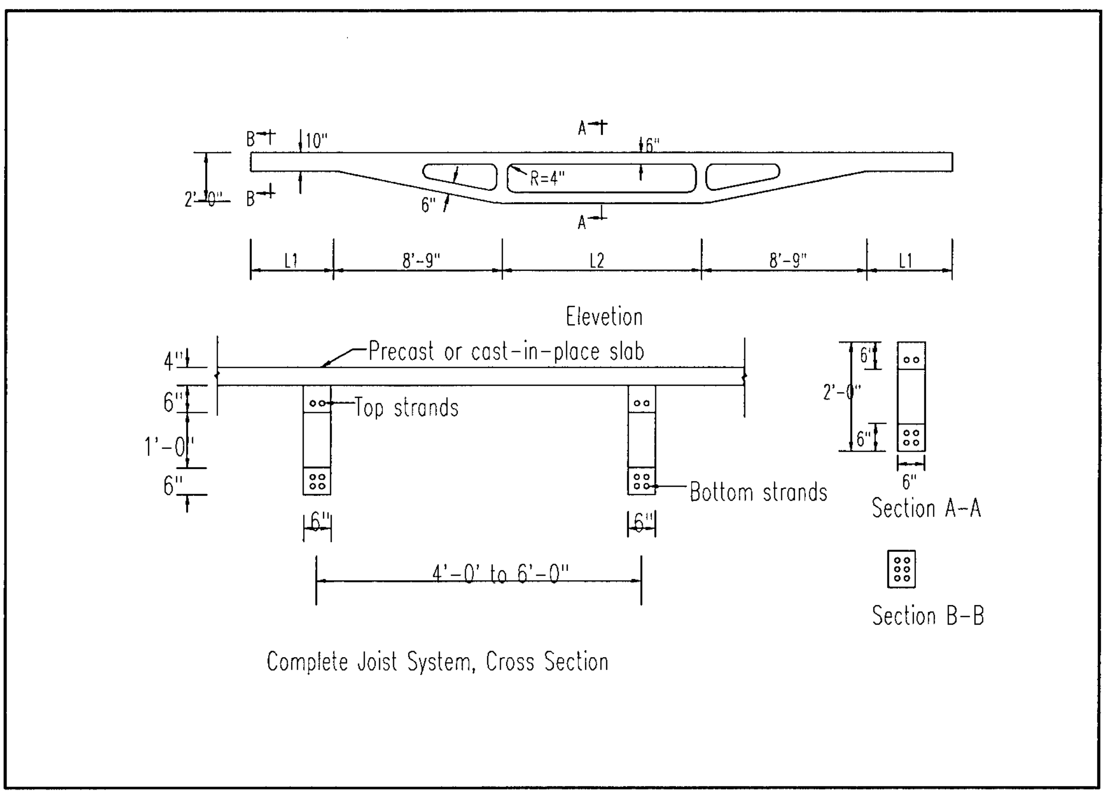

Figure 3.1. Hybrid joist concept.

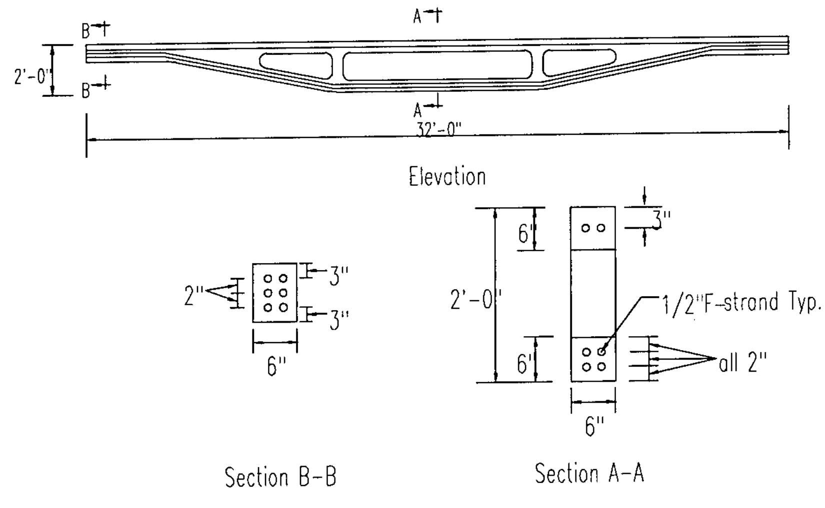

Figure 3.2. Dimensions for proposed hybrid joist design.

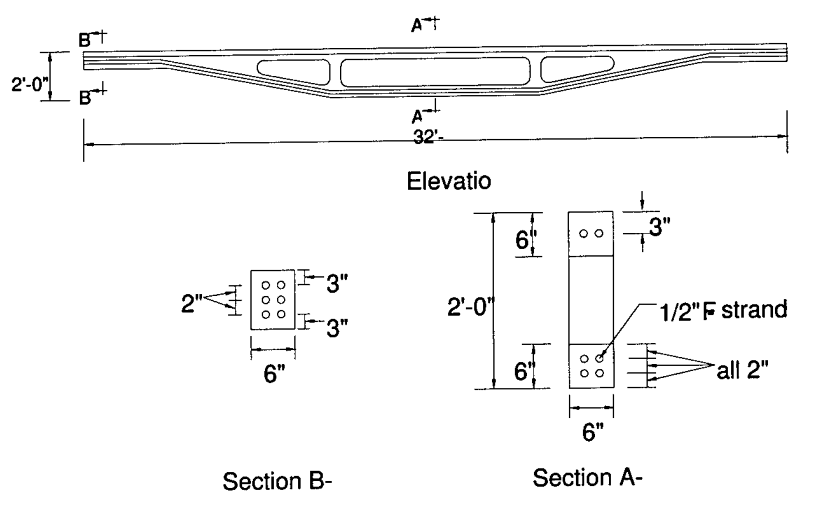

Figure 3.3. Hybrid joist prestressing strand configuration.

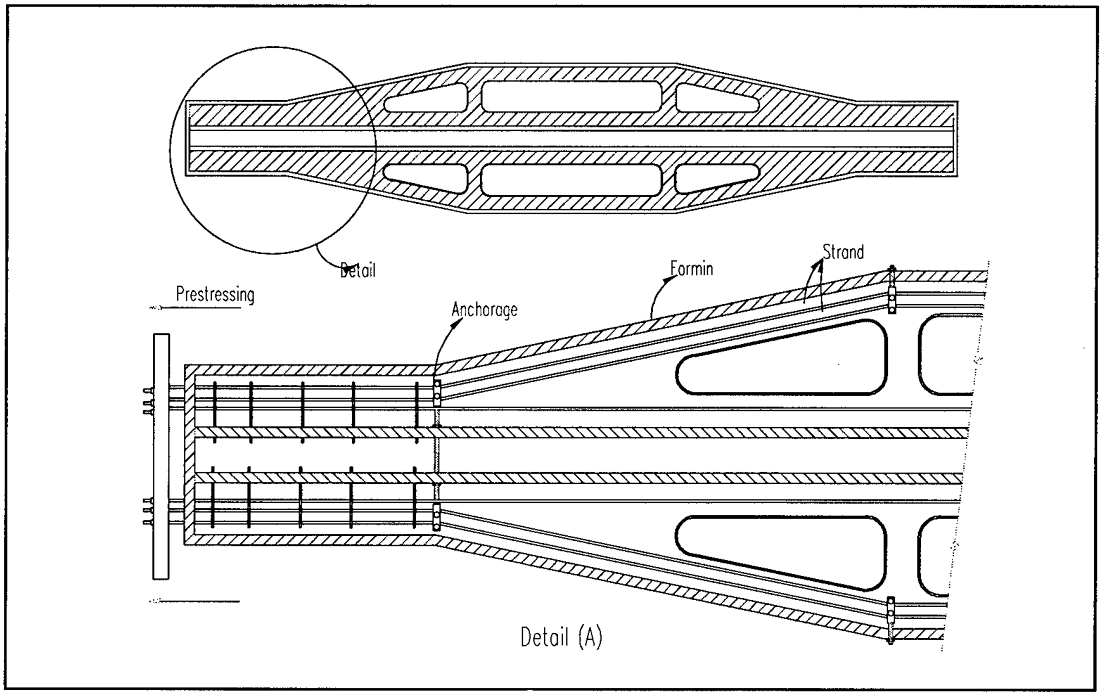

Figure 3.4. Schematic of strand formation.

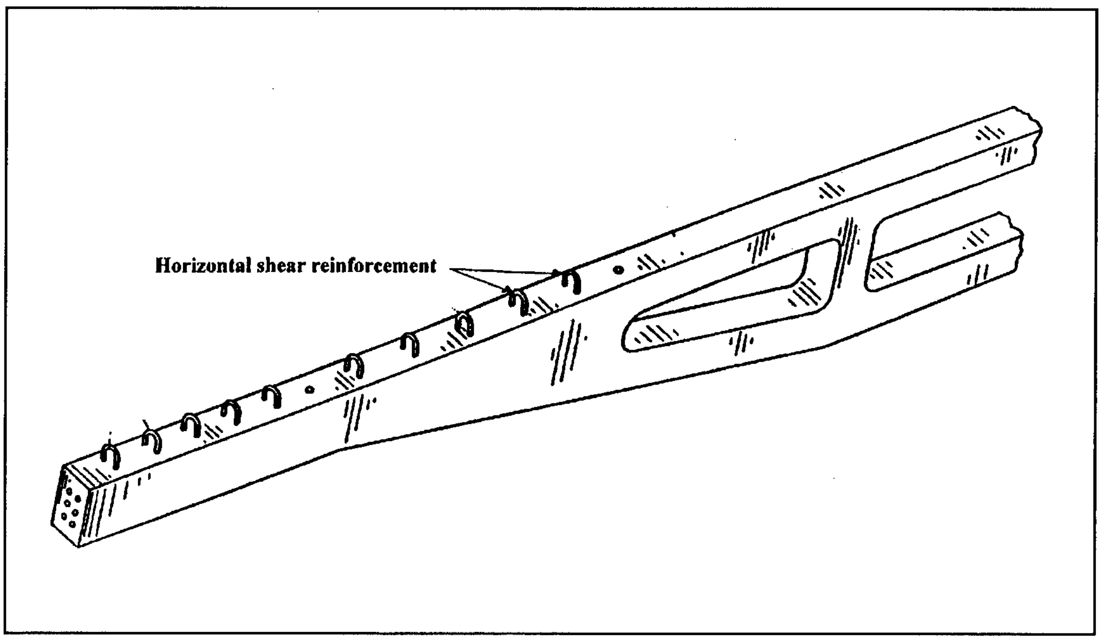

Figure 3.5. Three-dimensional form of hybrid joist web.

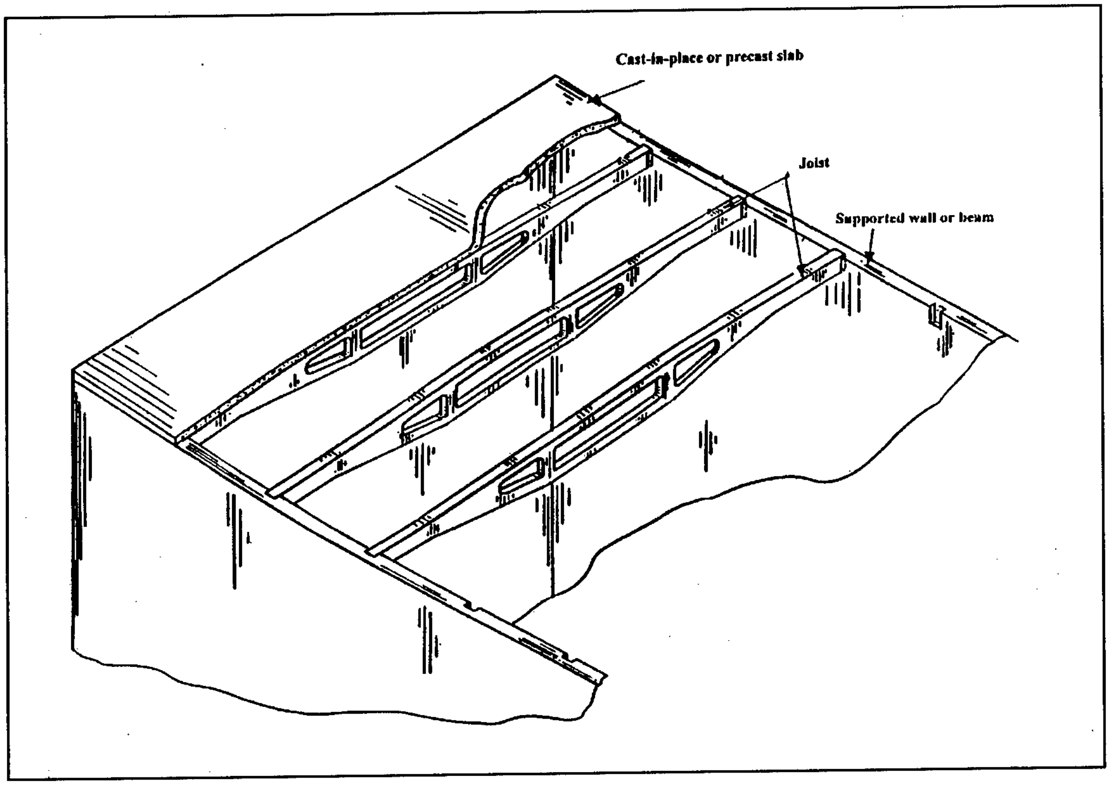

Figure 3.6. Cutaway view of hybrid joist system supporting a concrete slab.

4 Experimental Test Specimens

Introduction

This chapter describes the eight full-scale prestressed reinforced concrete hybrid joists fabricated in the structures lab at the University of Nebraska, Omaha (UNO) and the structures lab at USACERL. The webs of all joists were constructed at UNO. The slabs of two joists were placed at UNO. The balance of the joist webs were shipped to USACERL and the slabs cast at that location.

Description

The design of the joists was based on the preliminary analysis described in Chapter 3. As in the design analysis, test structures utilized cross-sectional symmetry in that half of a double hybrid joist was constructed. One web supported one half of the normal slab width. The first series of joists was designated HJ-1 and HJ-2. Shape and dimensions of these joists are shown in Figure 4.1. The joists had a constant thickness of 6 in. Joist ends were 10 in. deep; the depth of all other joist elements was 6 in. To reduce stress concentrations at the openings, the corners were curved with a radius of 4 in. The tendon profile is shown in Figure 4.2. Six tendons were used, two straight and four draped. In the prismatic portion of the joist end the six tendons dispersed at a spacing of 2 in. each way. The center of gravity of these six tendons coincided with the center of gravity of the section end. The top two tendons were located in the middle of the top chord. The four bottom tendons had a draped profile, with draping points at the start of the inclined member. The center of gravity of these tendons coincided with the center of gravity of the inclined members and bottom chords.

Shear reinforcement consisted of #4 vertical stirrups as shown in Figure 4.3, extending above the top chord to ensure anchorage to the cast-in-place slab. These stirrups were placed in each end of the joist over a distance of 9.0 ft. Figure 4.3 shows the details of the shear reinforcement. Additional closed stirrups were placed at the draping points and at the edge of the triangular web

openings. These closed stirrups were #4 C-shaped for easy placement. The vertical struts between openings were longitudinally reinforced with three #3 bars 20 in. long, and #2 spirals with a 3 in. diameter, 1 in. pitch, and 15 in. length.

The cast-in-place concrete slab had a thickness of 4 in. and was reinforced with #4 bars running longitudinally at approximately 2 in. height through the stirrups protruding from the joist web. Welded wire fabric (WWF), 4 X 4-W4.0 X W4.0, was placed using rebar chairs throughout the slab at a height of 2 in. Figure 4.4 shows a plan view of joist slab reinforcement.

The shape and dimensions of the second series of joists, designated HJ-3, HJ-4, HJ-5, and HJ-6, were the same as for the first series. Prestressing tendons in all joists were placed as they were for HJ-1 and HJ-2. Shear reinforcement and the width of the cast-in-place concrete slab, however, were varied. Figure 4.5 shows the web reinforcement of HJ-3 and HJ-4 Along the top of the beam web #4 U-shaped stirrups were placed to extend into the cast-in-place slab. Additional #4 C-shaped stirrups were located at the tendon hold-down point and at the edge of the triangular web opening. In HJ-5 and HJ-6, web shear reinforcement was reduced to two #4 U-shaped stirrups (Figure 4.6). C-shaped stirrups were as for HJ-3and HJ-4 Slabs cast for HJ-5 and HJ-6 were 4 in. thick and 4 ft wide. The width of the cast-in-place slab for HJ-3 and HJ-4 was 6 ft. Slab reinforcement for all joists consisted of 4 X 4-W4.0 X W4.0 WWF and two #4 longitudinal bars, similar to that for the first joist series.

A third series of joists, designated HJ-7 and HJ-8, were constructed. Shear reinforcement for these joists was the same as that for the first series, but the shape of the stirrups was changed as shown in Figure 4.7. Additional C-shaped stirrups were placed around the prestressing tendons at the same spacing as the U-shaped stirrups; this reinforcement size was #3. C-shaped stirrups were also located at the tendon hold-down location in the prismatic beam section and at the edge of the triangular web opening. These joists were each cast with a 4 in., 4 ft wide slab. Slab reinforcement was as for all other joists.

Construction

The webs of the joists were prestressed and cast horizontally, i.e., on their sides as shown in Figure 4.8. Hold-down devices were used at the draping points to position the prestressing tendons and resist the forces shown as F_1 and F_2.

Figure 4.9 shows the forces that resulted from applying the pre-tension on the tendons. The fabrication steps for each joist are summarized below.

A 3/4 in. plywood bed was placed inside a prestressing bed. Steel draping frames were placed in position on the top of the plywood. The hold-down devices were attached to the draping steel frames using high-strength 1-in. diameter threaded rods. The tendons were inserted through the hold-down devices and the prestressing bed. The tendons were anchored from one end and fully prestressed, as shown in Figure 4.10.

The sides and the openings of the joist web forms were then constructed of 2 x 6 (nominal) lumber. These forms were nailed to the plywood bed. Holes were drilled in the top of the upper chord form to permit the U-shaped stirrups to extend above the web. These stirrups were placed along the web according to each joist design. The C-shaped stirrups were placed along the tendons, at the draping points, and at the edge of the triangular openings per each joist design. Blockouts were placed along the top chord to create shear keys. Electrical strain gages were placed along the tendon length. The locations are identified in the instrumentation plan for each joist and are illustrated in Figure 4.11. Additional strain gages were mounted on the closed stirrups at the draping points.

The forms were oiled. The concrete mix was placed in the forms and vibrated to ensure consolidation of the specimens. The specimens were covered with wet burlap that was kept moist for the first 3 days. The specimens cured at room temperature for 7 days. Cylinders measuring 4 in. diameter by 8 in. tall were cast and cured with the joists under the same conditions. The concrete strength was monitored by compression testing of cylinders to assess when the required release strength was achieved. When concrete strength reached 7000 psi the tendons were released by alternately torch-cutting tendons on each face at the joist ends. Casting and release dates for each specimen are shown in Table 4.1. The webs were then turned vertically and stored in the lab, as shown in Figure 4.12.

For HJ-1 and HJ-2, forms for casting the top slab of the joist were located on the laboratory floor at UNO (Figure 4.13). Slabs for each joist web were separated by spacers. Slab reinforcement was placed and located in position by rebar chairs. The webs were turned upside down and positioned in place on the forms. The slabs were cast, covered with wet burlap and left at room temperature to cure. After curing for 7 days, the joists were flipped over and stored in the lab until the testing day. The webs of HJ-5 through HJ-8 were shipped to USACERL after completion. Here the webs were positioned vertically and upright, and

leveled. The slab forms were then constructed around them. Forms were oiled and reinforcement was positioned with rebar chairs. Concrete was placed with an overhead bucket and shoveled into place. Test cylinders measuring 4 in. in diameter and 8 in. tall were cast at the same time. After concrete placement the forms and test cylinders were covered with wet burlap followed by plastic sheets. The burlap was maintained moist for 4 days following casting. After 7 days the forms were stripped. Figure 4.14 shows the final shape of the joists.

Material Properties

Concrete

The concrete mix used in the hybrid joist specimen webs was a high-performance concrete (HPC) that meets special performance and uniformity requirements. These requirements are ease of placement and consolidation without compromising strength, superior long-term mechanical properties, early high strength, volume stability, and long life in severe environments. Table 4.2 shows the components of this mix. The HPC used in this study was designed to achieve a strength of 12,000 psi at 28 days, but it must be noted that no test specimens actually reached the intended strength or stiffness at 28 days.

The main concern with HPC is the hydration temperature. The temperature of the mix was monitored in two locations, one in a test cylinder and the other in the joist web. Figure 4.15 shows the time versus temperature for both locations of a representative concrete placement. The highest temperature reached was 90 °F, which is below the maximum recommended temperature of 180 °F. Table 4.3 shows the average compressive strength for each concrete placement of each joist web. Figure 4.16 shows the time versus strength curves for the concrete used in the webs.

The concrete mix used in the slab of HJ-1 and HJ-2 was designed to have a 28-day strength of 7000 psi. Concrete used in the slabs of specimens HJ-3 through HJ-8 was obtained from a local ready-mix plant and delivered to the site. The mix was specified to be 5000 psi and consisted of Type I cement with a maximum aggregate size of 1.0 in. limestone. The mix corresponded to dry weight proportions of 1.0 : 3.0 : 2.6 (cement : fine aggregate : course aggregate). On the day of testing all cylinders were also tested. Compression tests were conducted in accordance with ANSI/ASTM C39-86.

Reinforcement

The tendons used were manufactured by the American Spring Wire Corporation (26300 Miles Rd., Cleveland, OH 44146). These tendons were 1/2 in. diameter, 270 ksi, low relaxation. The stress-strain curve for these tendons is shown in Figure 4.17. The shear reinforcement in the webs consisted of bar reinforcement, Grade 60. A welded wire fabric mesh, Grade 75, was used as reinforcement for the cast-in-place slab.

Table 4.1. Casting and release dates for each hybrid joist web.

Specimen	Casting Date	Release Date
HJ-1	5/2/95	5/6/95
HJ-2	5/2/95	5/6/95
HJ-3	1/29/96	2/5/96
HJ-4	1/29/96	2/5/96
HJ-5	2/12/96	2/16/96
HJ-6	2/12/96	2/16/96
HJ-7	6/20/96	6/24/96
HJ-8	6/20/96	6/24/96

Table 4.2. Mix components for 12,000 psi HPC concrete.

Item	Quantity
Cement (Type I)	750 lb
Fly Ash (Class C)	200 lb
Silica Fume (Master Builders)	50 lb
Water	240 lb
Sand (ASTM C-33)	990 lb
1/2" Limestone	1860 lb
Air Content (Entrapped)	2.0 %
Water reducer (WRDA-82)	4 oz./100 lb
High range water reducer (WRDA-19)	30 oz./100 lb

Table 4.3. Average compressive concrete strength.

Concrete Placement Designation	Average Compressive Concrete Strength, f'_c (ksi)
HJ-1 & HJ-2 web	11.0
HJ-1 & HJ-2 top flange	6.8
HJ-5 & HJ-6 web	9.3
HJ-5 & HJ-6 top flange	6.9
HJ-7 & HJ-8 web	11.5
HJ-7 & HJ-8 top flange	6.4

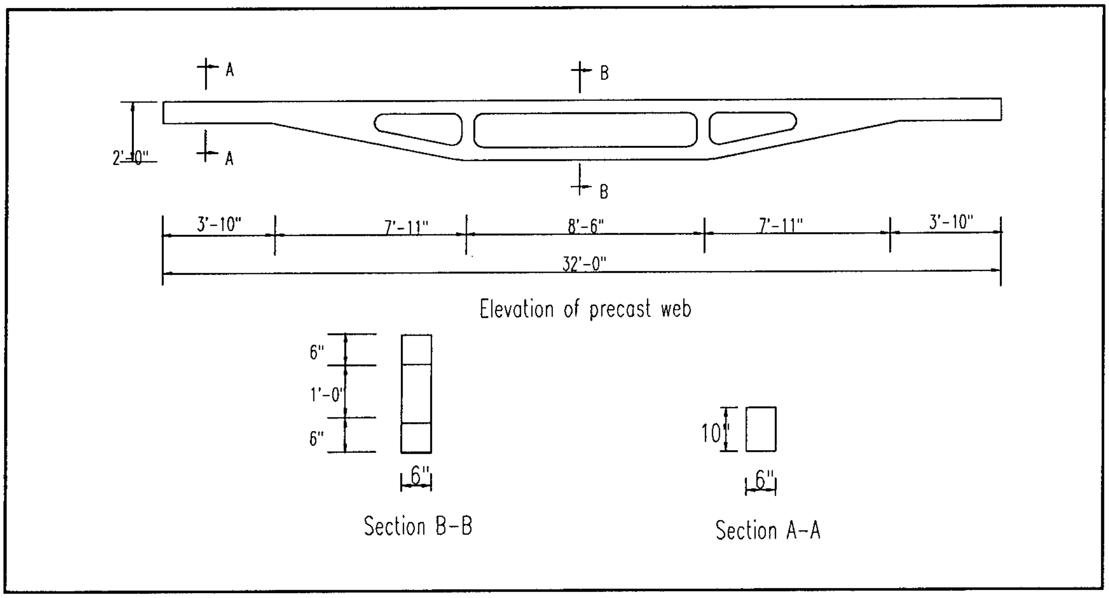

Figure 4.1. Dimensions of HJ-1 and HJ-2.

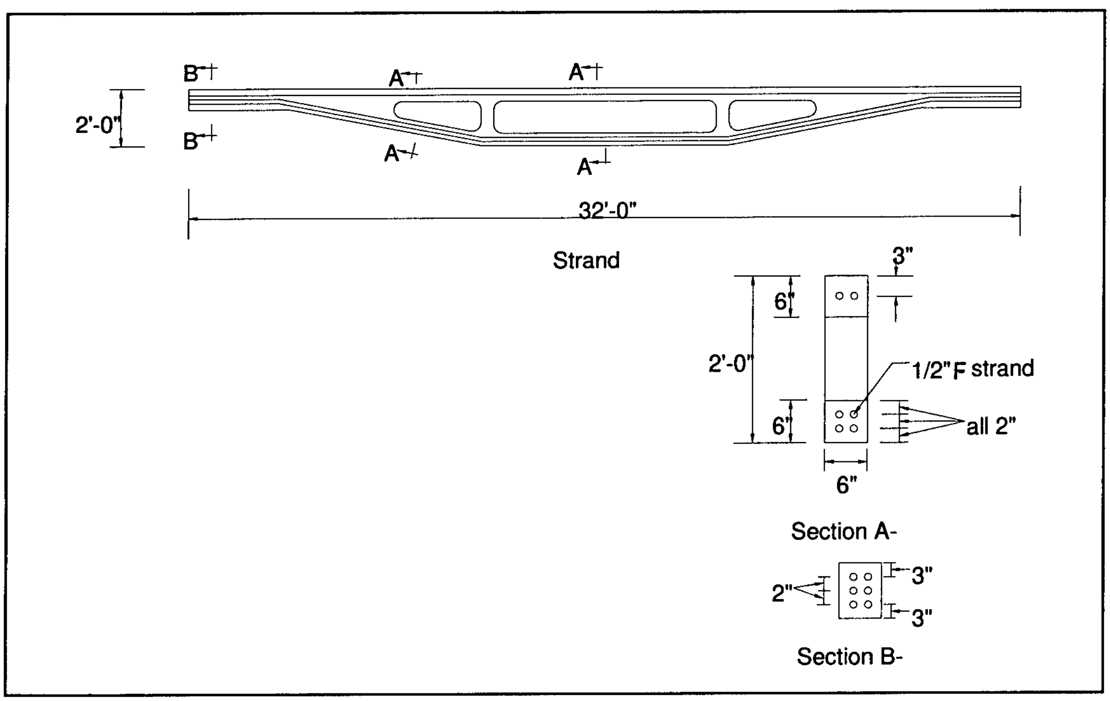

Figure 4.2. Hybrid joist strand profile.

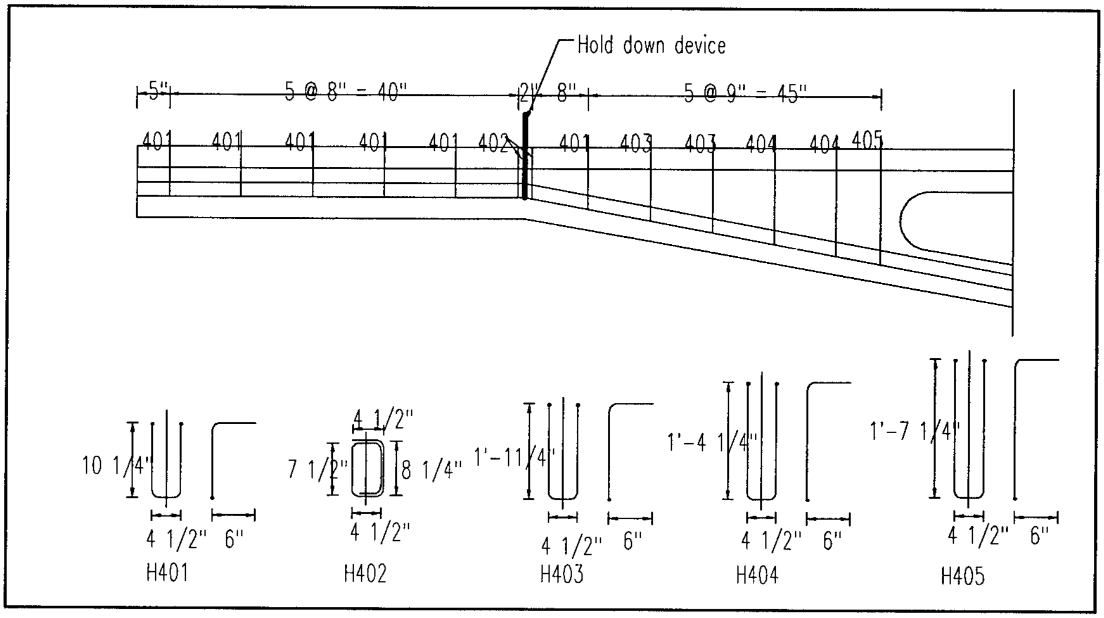

Figure 4.3. HJ-1 and HJ-2 web reinforcement details.

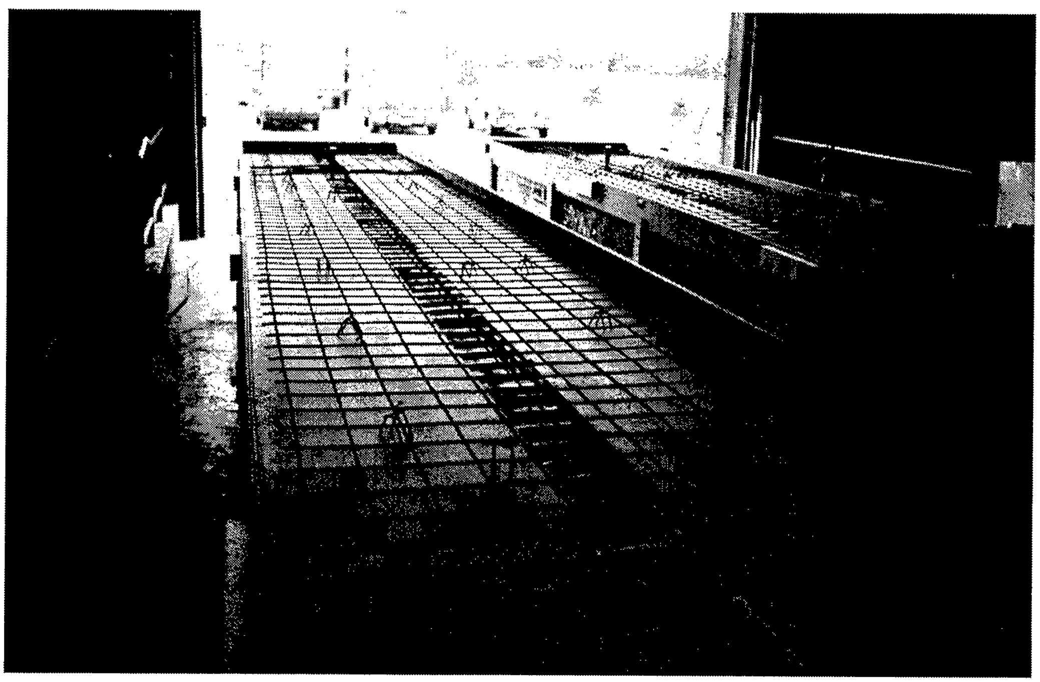

Figure 4.4. Plan view of slab reinforcement.

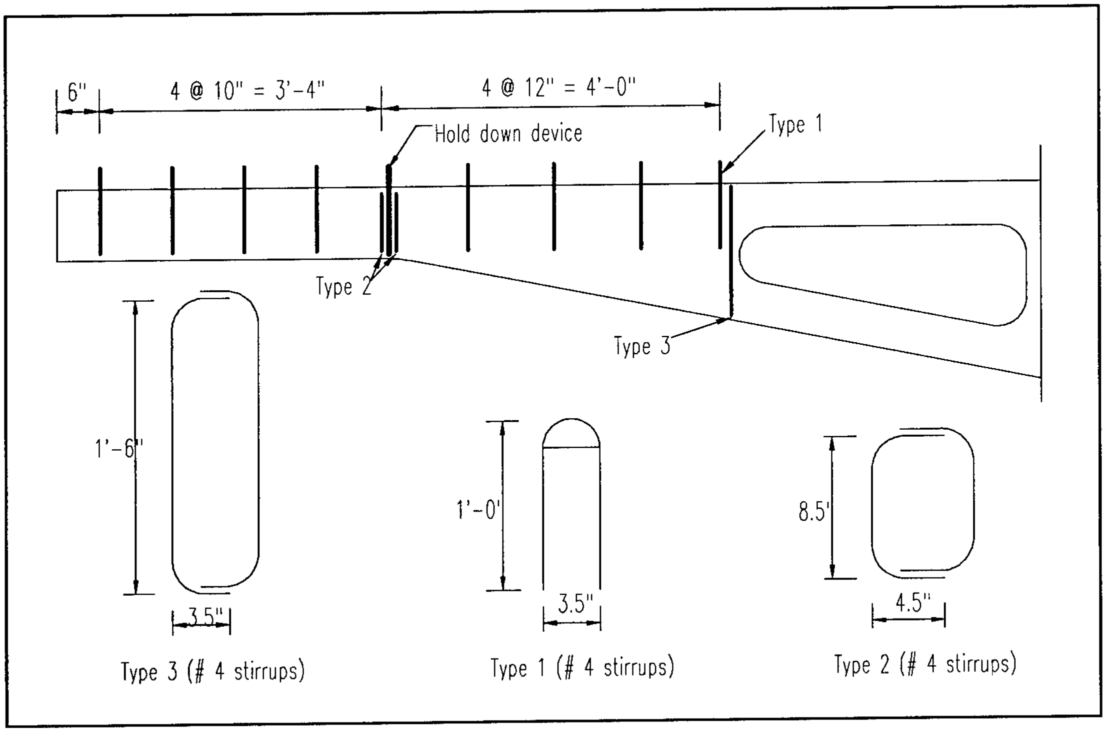

Figure 4.5. HJ-3 and HJ-4 web reinforcement.

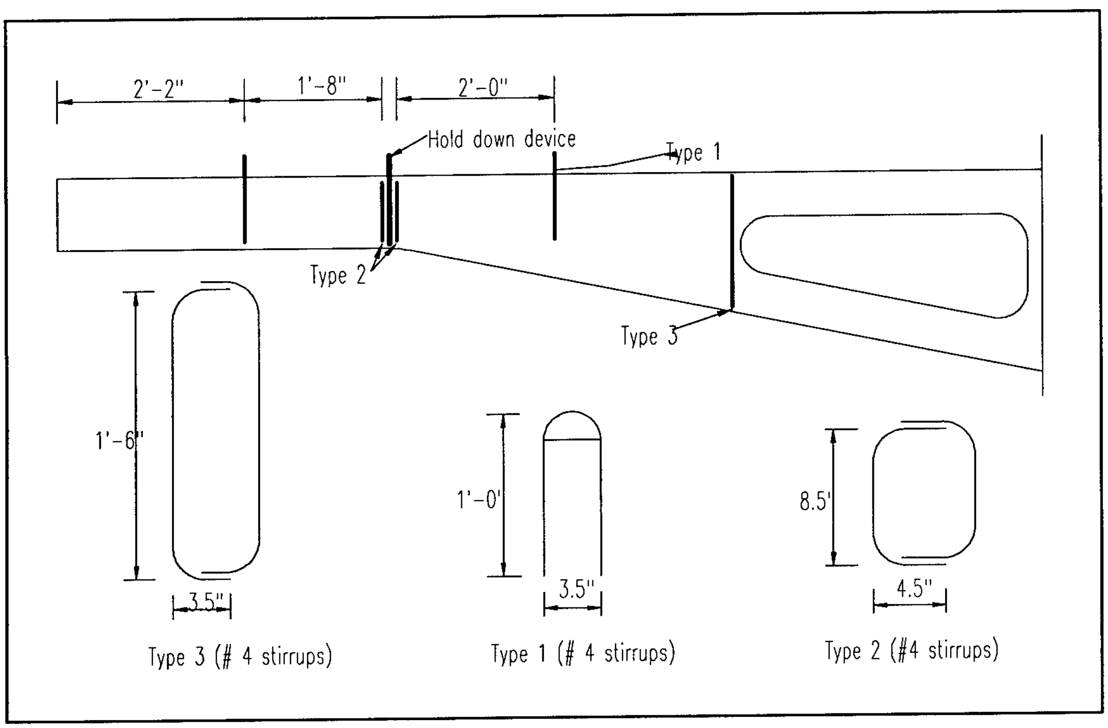

Figure 4.6. HJ-5 and HJ-6 web reinforcement.

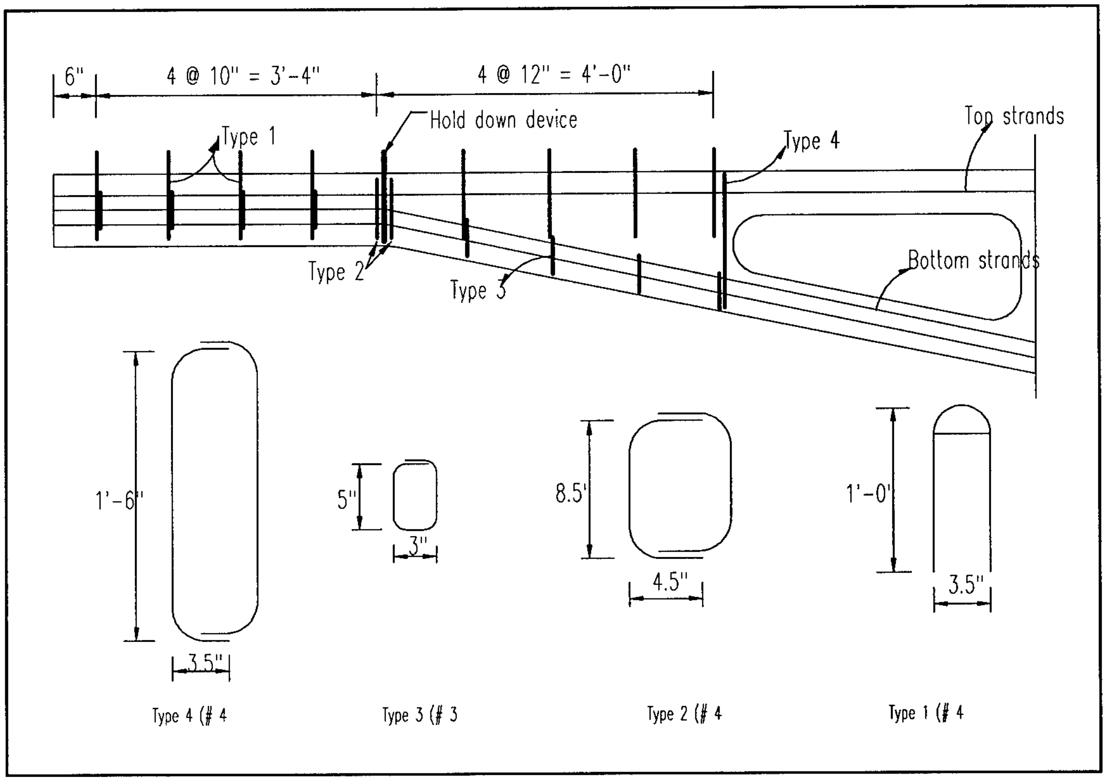

Figure 4.7. HJ-7 and HJ-8 web reinforcement.

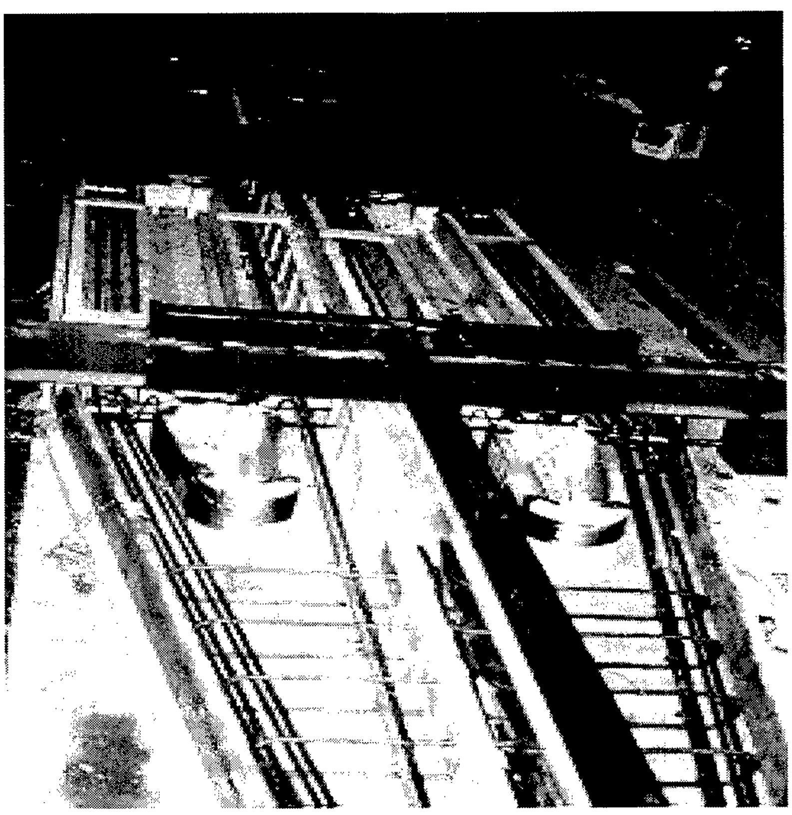

Figure 4.8. Formwork and prestressing tendons for hybrid joist web.

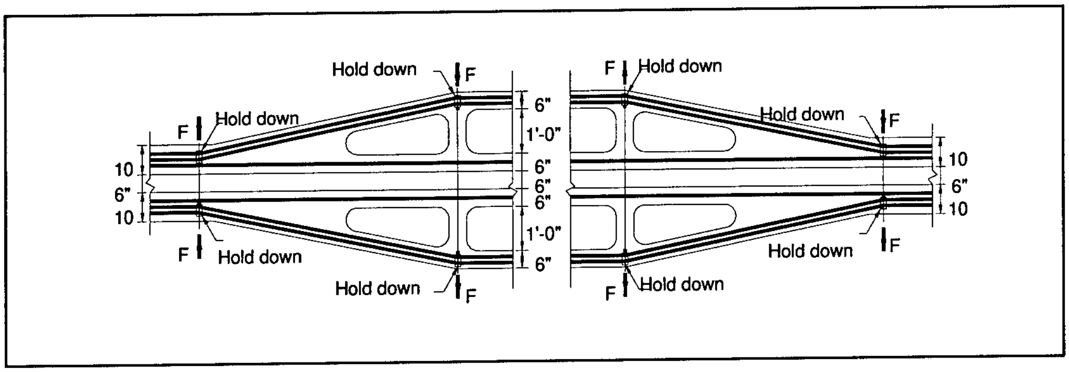

Figure 4.9. Plan view of pre-tensioning forces.

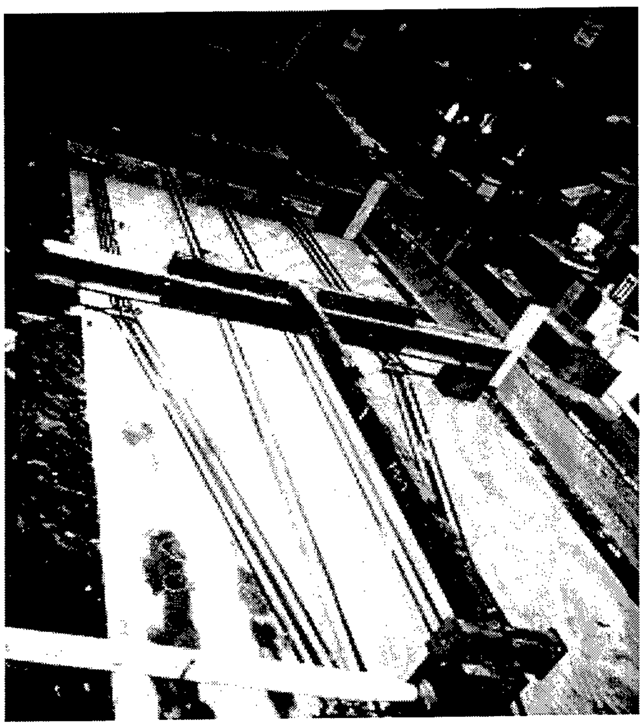

Figure 4.10. Application of pre-tensioning forces.

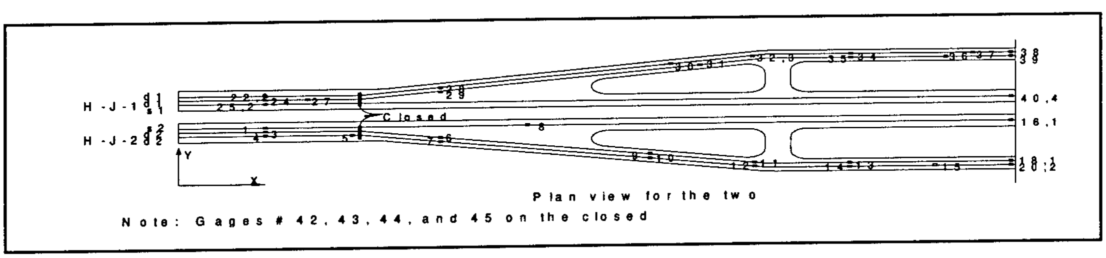

Figure 4.11. Internal strain gage layout on reinforcement.

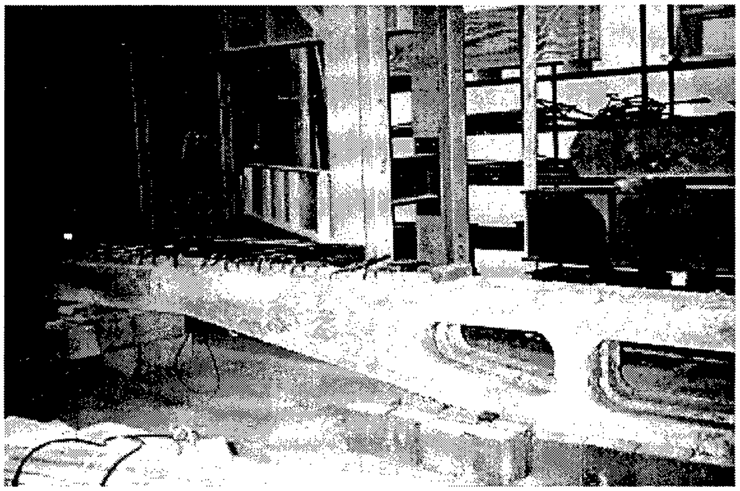

Figure 4.12. Vertical storage of hybrid joist webs.

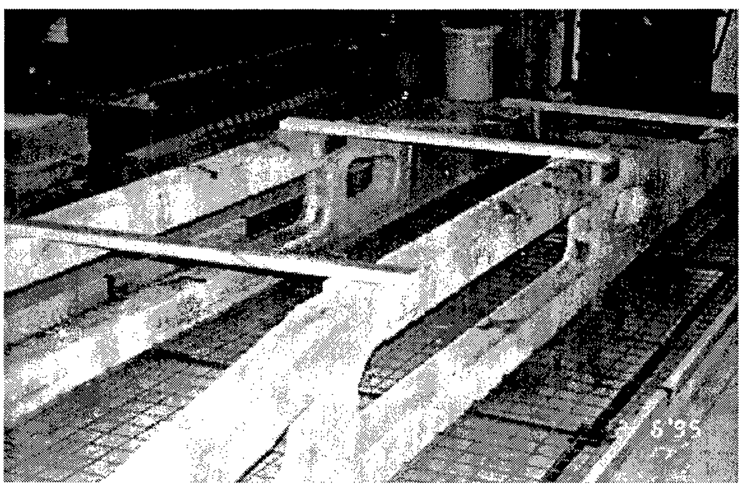

Figure 4.13. HJ-1 and HJ-2 forming and casting of top slab.

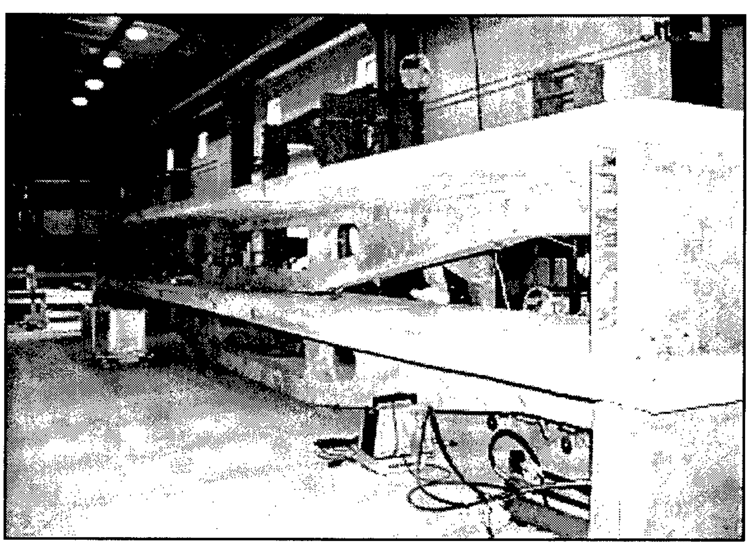

Figure 4.14. Completed hybrid joist construction.

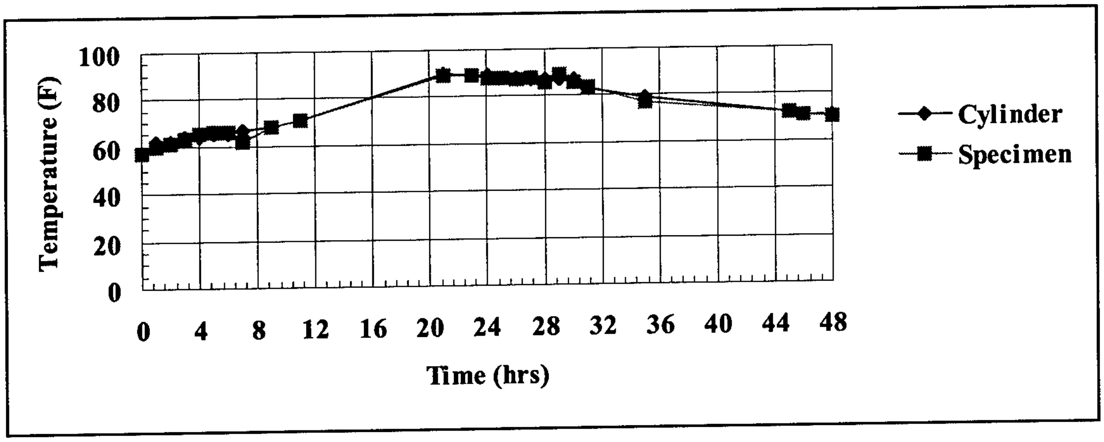

Figure 4.15. High-performance concrete hydration temperature versus time.

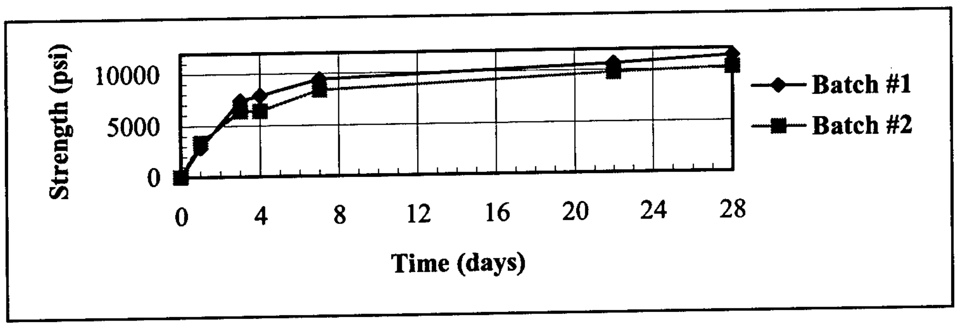

Figure 4.16. High-performance concrete strength versus time.

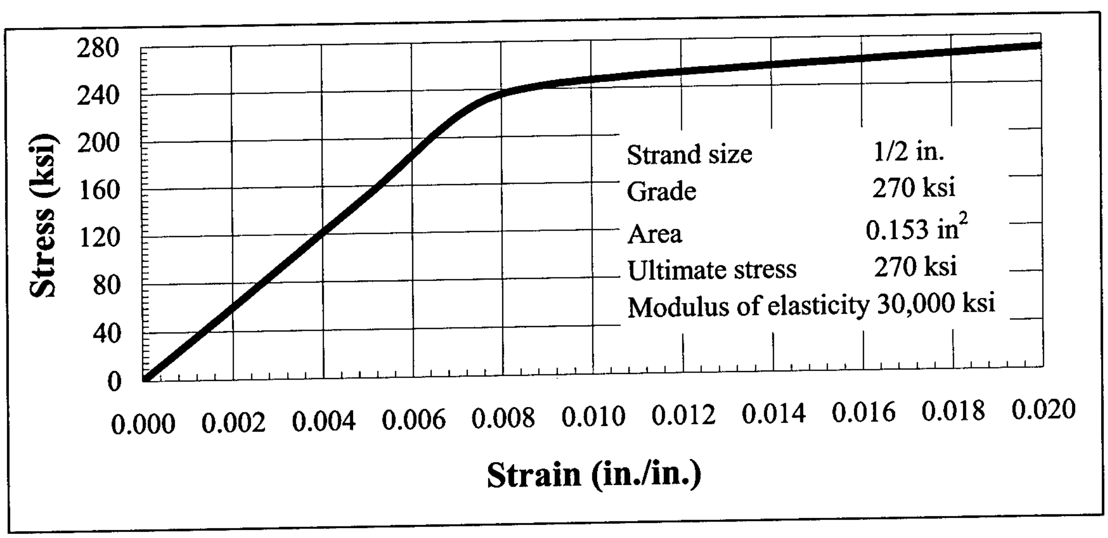

Figure 4.17. Prestressing tendon stress versus strain.

5 Experimental Program

Introduction

The primary objective of this experimental investigation was to evaluate the new hybrid joist system under service and ultimate loads. HJ-1 and HJ-2 were tested at the Structures Laboratory of the University of Nebraska at Omaha. HJ-5 through HJ-8 were tested on the Structural Load Floor at USACERL. Details of the test setup and instrumentation, test program, and data acquisition are discussed.

Test Setup

To the extent feasible within laboratory constraints, the test configuration was designed to simulate loading and support conditions of a typical hybrid joist application in a floor or roof structure. The test setup at the Structures Laboratory at the University of Nebraska is shown in Figure 5.1. Two specimens, HJ-1 and HJ-2, were tested in this configuration. Each specimen had a clear span of 31 ft and was supported at each end by a concrete saddle. Hydraulic actuators were suspended from an overhead steel reaction beam supported by DYWIDAG bars braced and connected to the structural load floor. A total of two 100-kip capacity actuators were used. These actuators loaded a distribution beam located along the center of the joist and supported above the joist web posts. The load was thus applied at a distance of 10 ft, 8 in. from the centerline of the support at each end. Figure 5.2 shows the photo of the test setup.

A similar configuration was used for testing joists HJ-5, HJ-6, HJ-7, and HJ-8 on the USACERL Structural Load Floor.* Specimens were simply supported by a concrete saddle at each end. These saddles provided lateral stability during testing but offered no resistance to rotation. Specimens HJ-6, HJ-7, and HJ-8

* Specimens HJ-3 and HJ-4, which were similar in configuration to HJ-5 and HJ-6, were not tested in this experimental program. When the latter two specimens performed poorly in testing, it was determined that there was nothing further to be learned by testing HJ-3 and HJ-4.

were tested in a configuration with a clear span of 31 ft (Figure 5.3). HJ-5 was tested in a configuration with a clear span of 23 ft, 4 in. (Figure 5.4). Vertical loads were applied by 50-kip hydraulic actuators suspended from a load frame. The actuators were centered directly over the web posts of the specimens; steel beams and plates were used as needed to eliminate the gap between the actuator and the joist and maximize actuator stroke capacity.

Test Programs

The objective of the incremental load testing was to determine corresponding strain and deflection readings at critical locations on the joist. Additionally, visual identification of crack development and determination of failure mode were of interest. Table 5.1 shows the dates and locations of testing.

In the test program at UNO, actuators were load-controlled. Load was applied in average increments of 2 kips. Two 10,000 psi load-pressure cells were used to measure the hydraulic pressure and monitor applied loads. After each load step, the hydraulic pump was stopped until the cracks were marked.

In testing at USACERL the stroke of each actuator was calibrated to zero after making contact with the specimen; a small pre-load was associated with this positioning. Specimens were loaded at a constant rate to a specified stroke limit. The actuators were maintained at this stroke while the joist was inspected for cracks; these were marked. Measured readings of deflections were taken at selected locations and the deflection data were checked. Stroke was then further applied to the specimen until the stroke limit of the actuators was reached. Beams were used to maintain the deflected specimen. The full stroke (i.e., the full load) was then removed. Steel plates were added between the actuator and the beam. The actuators were then moved into contact with the specimen again; this was associated with a small pre-load. The test was continued in the same manner until the specimen failed. A representative test program is shown in Table 5.2. Data were recorded during loading and unloading cycles.

Instrumentation and Data Recording

Test specimens HJ-1 and HJ-2 were instrumented with displacement potentiometers and strain gages. Tables 5.3 and 5.4 summarize the instrumentation plans for HJ-1 and HJ-2. Figure 5.5 shows the layout of internal strain gages for specimens HJ-1 and HJ-2. Internal and external strain gages were

located so as to measure strains in both prestressing tendons and reinforcement, and on concrete surfaces. Electrical resistance strain gages were installed on several locations on the steel reinforcing bars embedded in the concrete. The steel reinforcing bars were instrumented with Measurements Group* Model EA-06-125BT-120 electrical resistance strain gages with constant grids and complete polyamide encapsulation. The sensing grid is 0.125 in. long by 0.062 in. wide. Each gage was connected to data acquisition system to measure the strain. Also, electrical resistance strain gages were installed on several locations on the surface of the concrete. The strain gages used were Texas Measurements† Model PL-60-11 with nominal resistance 120 ± 0.3 ohms. The gage length is 2.362 in. (60 mm) long by 0.039 in. (1 mm) wide. Each gage was connected to the data acquisition system to measure the strain.

Position Transducer Model P-10A‡ variable resistance displacement transducers were used to measure the absolute displacement at various locations on the test beam. These units employ a spring-loaded precision rotary potentiometer with a flexible steel cable wrapped around the potentiometer shaft. The other end of the cable is attached to the point where the displacement is to be measured. When displacement occurs, the cable motion rotates the shaft of the potentiometer, which causes a change in resistance. These transducers were mounted on the floor but independent of the test beam. All recorded potentiometer displacements were absolute, measured with respect to the laboratory floor.

In the Structures Laboratory of UNO the loading system consisted of two Enerpac§ Model RRH-6010 double-acting, hollow-plunger hydraulic cylinders. The cylinders include transducers that measure the applied pressure (Omega Model PX-602). The load was applied using an Enerpac 30,000 Series Dump Pump (1.5 horsepower, 10,000 psi).

All transducers and strain gauges were connected to a desktop computer for continuous data acquisition during specimen loading and unloading. The data acquisition system was Megadac** Series 3000. Figure 5.6 is a functional block diagram of the instrumentation, data acquisition, and test control systems. The system was controlled by computer through an instrument controller interface bus. The recording channels were scanned at a predetermined sampling rate,

* Measurements Group, Inc., P.O. Box 27777, Dept. TR, Raleigh, NC 27611-7777.
† Texas Measurements, Inc., College Station, TX 77841.
‡ MagneTek, Simi Valley, CA 93065.
§ Applied Power, Inc., Butler, WI 53007.
** Data Acquisition and Control Systems, Germantown, MD 20874.

and the data were recorded and then transformed to ASCII* text files on the computer.

Specimens HJ-5, HJ-6, HJ-7, and HJ-8 were instrumented with displacement potentiometers, linear variable displacement transducers (LVDTs), and strain gages. No external strain gages were used in these specimens. Instrumentation tables for these four specimens are shown in Tables 5.5 through 5.8.

For specimens HJ-5 through HJ-8, absolute displacements were measured by potentiometers at three locations along the joist length: at the center of the joist, beneath one web post, and at a distance 25 percent of the span length from a support along the inclined portion of the joist. Celesco† Model PT101-10 and PT101-60A variable resistance displacement transducers were used to measure the absolute displacements. These units are of similar design to the ones described above. They rested on the laboratory floor and were attached to the joist bottom using stranded steel extension wires. These transducers were connected to Endevco‡ Model 4471.3 signal conditioners, which provide direct current (dc) power and electrical balancing, but no amplification. Displacement measurements were also taken manually at the front and back face of the slab at each joist end, and along the front slab face at the center and beneath each actuator. Potentiometer locations were the same for joists HJ-5 through HJ-8 (Figure 5.7).

LVDTs were designed to monitor displacement across a specific gage length regardless of crack development. Schaevitz§ Model 200HR LVDTs were used to measure the relative displacements at various locations on the joists' concrete surface. The 200HR LVDTs have a range of ±0.2 in. These transducers are powered by alternating current (ac) and contain a set of transformer windings and a moveable metal core. The core is attached to the measurement point, and when displacement occurs, the movement of the core changes the electrical coupling between the windings, which in turn changes the output signal. The LVDTs were connected to Endevco Model 4478.1A signal conditioners that provide ac power, signal amplification, ac to dc conversion, and electrical balancing. LVDT locations were the same for joists HJ-5 through HJ-8 (Figure 5.8).

* ASCII: American Standard Code for Information interchange.

† Celesco Transducer Products, Inc., 7800 Deering Ave., Canoga Park, CA 91304.

‡ Endevco Corp., 30700 Viejo Rd., San Juan Capistrano, CA 92675.

§ Schaevitz 1000 Lucas Way, Hampton, VA 23666.

The locations of internal strain gages were the same for specimens HJ-5 and HJ-7. HJ-6 and HJ-8 had internal strain gages located in the same locations. Only selected strain gage measurements were monitored from the numerous gages placed in the specimens by UNO. Strains measured are shown in Figure 5.9. Electrical resistance strain gages as were used in specimens HJ-1 and HJ-2 were also used in these latter four joists. The steel reinforcing bars were instrumented with Measurements Group Model EA-06-125BT-120 electrical resistance strain gages with constant grids and complete polyamide encapsulation. The sensing grid is 0.125 in. long by 0.062 in. wide.

Figure 5.10 is a functional block diagram of the instrumentation, data acquisition and test control systems used at USACERL. All of the transducer output signals were connected to a Hewlett Packard* Model 3052A data logging system. The system was controlled by computer through an instrument controller interface bus. The record channels were scanned at a predetermined sampling rate, and the data were recorded in ASCII text files on the computer.

The loading system consisted of two CGS/Lawerence Model 307-50 electro-hydraulic actuators (controlled by closed-loop servo controllers) and a function generator. The actuators were operated in a displacement-control mode. In this mode, the function generator supplies a slowly changing command signal to the controllers. The controllers send a drive signal to each of the actuators, which causes the actuators to move until the displacement measured by LVDTs located inside each actuator is equal to the command signal. The actuators also include load transducers that measure the applied load.

Table 5.1. Test program.

Specimen	Date of Testing	Location of Testing
HJ-1	1 Aug 1995	UNO
HJ-2	2 Aug 1995	UNO
HJ-6	9 May 1996	USACERL
HJ-5	14 May 1996	USACERL
HJ-8	10 Oct 1996	USACERL
HJ-7	24 Oct 1996	USACERL

* Hewlett Packard Co., 5301 Stevens Creek Blvd., Santa Clara, CA 95052-8059.

Table 5.2. Representative loading program for HJ-5 through HJ-8.

Displacement	Loading Rate	Steps	Time/Step
0-1.0 in.	10 min/1 in.	Increments of .10 in	1 min
1.0 - 14.0 in. or failure	10 min/1 in.	Increments of .50 in.	5 min

Table 5.3. Instrumentation plan for HJ-1.

Instrument	CIR Name	Location (X - Dir.) (in.)	Location (Y - Dir.) (in.)
POT_W	N / A	46.000	N / A
POT_Mid	N / A	192.000	N / A
POT_E	N / A	243.000	N / A
Int_22	s22	23.000	3.000
Int_23	s23	23.000	3.000
Int_24	s24	23.000	5.000
Int_25	s25	23.000	7.000
Int_26	s26	23.000	7.000
Int_27	s27	36.000	3.000
Int_28	s28	58.000	-0.232
Int_29	s29	58.000	1.768
Int_30	s30	78.000	-8.495
Int_31	s31	78.000	-6.495
Int_32	s32	135.000	-12.000
Int_33	s33	135.000	-12.000
Int_34	s34	147.000	-12.000
Int_35	s35	147.000	-10.000
Int_36	s36	167.000	-12.000
Int_37	s37	170.000	-10.000
Int_38	s38	192.000	-12.000
Int_39	s39	192.000	-10.000
Int_40	s40	192.000	7.000
Int_41	s41	192.000	7.000

Table 5.4. Instrumentation plan for HJ-2.

Instrument	CIR Name	Location (X - Dir.) (in.)	Location (Y - Dir.) (in.)
POT_W	N / A	46.000	N / A
POT_Mid	N / A	192.000	N / A
POT_E	N / A	243.000	N / A
Int_1	s1	23.000	7.000
Int_2	s2	23.000	7.000
Int_3	s3	23.000	5.000
Int_4	s4	23.000	3.000
Int_5	s5	43.000	3.000
Int_6	s6	58.000	3.232
Int_7	s7	58.000	1.232
Int_8	s8	64.000	7.000
Int_9	s9	78.000	-6.495
Int_10	s10	78.000	-8.495
Int_11	s11	135.000	-10.000
Int_12	s12	135.000	-12.000
Int_13	s13	147.000	-10.000
Int_14	s14	147.000	-12.000
Int_15	s15	167.000	-12.000
Int_16	s16	192.000	7.000
Int_17	s17	192.000	7.000
Int_18	s18	192.000	-10.000
Int_19	s19	192.000	-10.000
Int_20	s20	192.000	-12.000
Int_21	s21	192.000	-12.000

Table 5.5. Instrumentation plan for HJ-5.

Instrument	CERL Name / Cable #	CIR Name	Conversion Factor (per volt)	Location (X - Dir.) (in.)	Location (Y - Dir.) (in.)	Gage Length (in.)	Comments
Cell_N		N / A	5.000 kips	141.000	N / A	N / A	Concentrated Load - 50 Kip Actuator
Stroke_N		N / A	0.300 inches	141.000	N / A	N / A	
Cell_S		N / A	5.000 kips	250.000	N / A	N / A	Concentrated Load - 50 Kip Actuator
Stroke_S		N / A	0.300 inches	250.000	N / A	N / A	
POT_N	P1	N / A	1.994 inches	141.000	N / A	N / A	Third span Deflection - Potentiometer
POT_Mid	P2	N / A	1.996 inches	192.000	N / A	N / A	Midspan Deflection - Potentiometer
POT_S	P3	N / A	2.000 inches	278.000	N / A	N / A	Quarter span Deflection - Potentiometer
Int_1	IS1 / 3	s3	0.00150 in/in	23.000	7.000	N / A	Placed by the CIR-Measured from slab top
Int_2	IS2 / 2	s2	0.00150 in/in	23.000	9.000	N / A	Placed by the CIR-Measured from slab top
Int_3	IS3 / 1	s1	0.00150 in/in	23.000	11.000	N / A	Placed by the CIR-Measured from slab top
Int_4	IS4 / 12	s12	0.00150 in/in	135.000	26.000	N / A	Placed by the CIR-Measured from slab top
Int_5	IS5 / 11	s11	0.00150 in/in	135.000	24.000	N / A	Placed by the CIR-Measured from slab top
Int_6	IS6 / 10	s10	0.00150 in/in	135.000	26.000	N / A	Placed by the CIR-Measured from slab top
Int_7	IS7 / 15	s15	0.00150 in/in	147.000	7.000	N / A	Placed by the CIR-Measured from slab top
Int_8	IS8 / 14	s14	0.00150 in/in	147.000	24.000	N / A	Placed by the CIR-Measured from slab top
Int_9	IS9 / 13	s13	0.00150 in/in	147.000	26.000	N / A	Placed by the CIR-Measured from slab top
Int_10	IS10 / 18	s18	0.00150 in/in	192.000	7.000	N / A	Placed by the CIR-Measured from slab top
Int_11	IS11 / 17	s17	0.00150 in/in	192.000	24.000	N / A	Placed by the CIR-Measured from slab top
Int_12	IS12 / 16	s16	0.00150 in/in	192.000	26.000	N / A	Placed by the CIR-Measured from slab top
LVDT_1	D1	N / A	0.00494 inches	70.000	1.000	3.976	Measured from the Top of the Slab
LVDT_2	D2	N / A	0.00497 inches	70.000	3.000	7.441	Measured from the Bottom Face of the Slab
LVDT_3	D3	N / A	0.00495 inches	70.000	12.500	2.756	Measured from the Bottom Face of the Slab
LVDT_4	D4	N / A	0.00497 inches	143.500	1.000	6.299	Measured from the Top of the Slab
LVDT_5	D5	N / A	0.00496 inches	143.000	2.500	6.260	Measured from the Bottom Face of the Slab
LVDT_6	D6	N / A	0.00496 inches	142.000	10.500	2.559	Measured from the Bottom Face of the Slab
LVDT_7	D7	N / A	0.00496 inches	142.000	23.250	2.638	Measured from the Bottom Face of the Slab
LVDT_8	D8	N / A	0.00495 inches	167.500	1.000	5.827	Measured from the Top of the Slab
LVDT_9	D9	N / A	0.00496 inches	167.500	2.250	5.433	Measured from the Bottom Face of the Slab
LVDT_10	D10	N / A	0.00499 inches	168.000	23.250	7.165	Measured from the Bottom Face of the Slab
LVDT_11	D11	N / A	0.00489 inches	195.500	1.000	6.417	Measured from the Top of the Slab
LVDT_12	D12	N / A	0.00496 inches	193.500	2.250	2.874	Measured from the Bottom Face of the Slab
LVDT_13	D13	N / A	0.00496 inches	194.500	23.500	5.236	Measured from the Bottom Face of the Slab
LVDT_14	D14	N / A	0.00491 inches	194.500	N / A	7.677	Placed on top of Slab
LVDT_15	D15	N / A	0.00496 inches	220.000	1.000	4.882	Measured from the Top of the Slab
LVDT_16	D16	N / A	0.00500 inches	194.500	N / A	5.709	Placed on bottom side of Web
LVDT_17	D17	N / A	**-0.00503 in.**	220.000	3.500	6.378	Measured from the Bottom Face of the Slab
LVDT_18	D18	N / A	0.00487 inches	220.500	23.500	5.157	Measured from the Bottom Face of the Slab
LVDT_19	D19	N / A	**-0.00501 in.**	244.000	11.000	1.811	Measured from the Bottom Face of the Slab
LVDT_20	D20	N / A	0.00500 inches	245.000	23.000	2.677	Measured from the Bottom Face of the Slab

*** +X direction is defined as running north to south with north being 0. Measurements taken to the north face of the LVDT blocks.
*** +Y direction is defined as running up to down with 0 being the bottom face of the slab, except where noted that measurement was taken from the top of the slab. Measurement was taken to the middle of the circular opening in the block.

Table 5.6. Instrumentation plan for HJ-6.

Instrument	CERL Name / Cable #	CIR Name	Conversion Factor (per volt)	Location (X - Dir.) (in.)	Location (Y - Dir.) (in.)	Gage Length (in.)	Comments
Cell_N		N / A	5.000 kips	141.000	N / A	N / A	Concentrated Load - 50 Kip Actuator
Stroke_N		N / A	0.300 inches	141.000	N / A	N / A	
Cell_S		N / A	5.000 kips	250.000	N / A	N / A	Concentrated Load - 50 Kip Actuator
Stroke_S		N / A	0.300 inches	250.000	N / A	N / A	
POT_N	P1	N / A	1.994 inches	141.000	N / A	N / A	Strut Deflection - Potentiometer
POT_Mid	P2	N / A	1.996 inches	192.000	N / A	N / A	Midspan Deflection - Potentiometer
POT_S	P3	N / A	2.000 inches	278.000	N / A	N / A	Quarter span Deflection - Potentiometer
Int_1	IS1 / 19	s19	0.00150 in/in	23.000	7.000	N / A	Placed by the CIR-Measured from slab top
Int_2	IS2 / 20	s20	0.00150 in/in	23.000	9.000	N / A	Placed by the CIR-Measured from slab top
Int_3	IS3 / 21	s21	0.00150 in/in	23.000	11.000	N / A	Placed by the CIR-Measured from slab top
Int_4	IS4 / 28	s28	0.00150 in/in	135.000	7.000	N / A	Placed by the CIR-Measured from slab top
Int_5	IS5 / 26	s26	0.00150 in/in	102.000	20.495	N / A	Placed by the CIR-Measured from slab top
Int_6	IS6 / 30	s30	0.00150 in/in	135.000	26.000	N / A	Placed by the CIR-Measured from slab top
Int_7	IS7 / 31	s31	0.00150 in/in	147.000	7.000	N / A	Placed by the CIR-Measured from slab top
Int_8	IS8 / 27	s27	0.00150 in/in	102.000	22.495	N / A	Placed by the CIR-Measured from slab top
Int_9	IS9 / 33	s33	0.00150 in/in	147.000	26.000	N / A	Placed by the CIR-Measured from slab top
Int_10	IS10 / 34	s34	0.00150 in/in	192.000	7.000	N / A	Placed by the CIR-Measured from slab top
Int_11	IS11 / 35	s35	0.00150 in/in	192.000	24.000	N / A	Placed by the CIR-Measured from slab top
Int_12	IS12 / 36	s36	0.00150 in/in	192.000	26.000	N / A	Placed by the CIR-Measured from slab top
LVDT_1	D1	N / A	0.00494 inches	69.375	1.000	4.843	Measured from the Top of the Slab
LVDT_2	D2	N / A	0.00497 inches	69.750	3.375	2.913	Measured from the Bottom Face of the Slab
LVDT_3	D3	N / A	0.00495 inches	69.375	12.250	2.559	Measured from the Bottom Face of the Slab
LVDT_4	D4	N / A	0.00497 inches	142.500	1.250	6.772	Measured from the Top of the Slab
LVDT_5	D5	N / A	0.00496 inches	142.750	3.000	6.260	Measured from the Bottom Face of the Slab
LVDT_6	D6	N / A	0.00496 inches	142.750	11.750	2.402	Measured from the Bottom Face of the Slab
LVDT_7	D7	N / A	0.00496 inches	142.750	23.500	7.756	Measured from the Bottom Face of the Slab
LVDT_8	D8	N / A	0.00495 inches	167.000	1.000	2.638	Measured from the Top of the Slab
LVDT_9	D9	N / A	0.00496 inches	167.250	2.500	7.362	Measured from the Bottom Face of the Slab
LVDT_10	D10	N / A	0.00499 inches	167.250	24.000	6.142	Measured from the Bottom Face of the Slab
LVDT_11	D11	N / A	0.00489 inches	193.750	1.000	6.496	Measured from the Top of the Slab
LVDT_12	D12	N / A	0.00496 inches	192.000	3.250	3.780	Measured from the Bottom Face of the Slab
LVDT_13	D13	N / A	0.00496 inches	192.000	24.000	5.669	Measured from the Bottom Face of the Slab
LVDT_14	D14	N / A	0.00491 inches	193.750	N / A	5.433	Placed on top of Slab
LVDT_15	D15	N / A	0.00496 inches	219.000	1.250	5.512	Measured from the Top of the Slab
LVDT_16	D16	N / A	0.00500 inches	193.750	N / A	5.866	Placed on bottom side of Web
LVDT_17	D17	N / A	**-0.00503 in.**	219.000	3.500	2.638	Measured from the Bottom Face of the Slab
LVDT_18	D18	N / A	0.00487 inches	219.000	24.000	5.551	Measured from the Bottom Face of the Slab
LVDT_19	D19	N / A	**-0.00501 in.**	245.000	11.500	2.559	Measured from the Bottom Face of the Slab
LVDT_20	D20	N / A	0.00500 inches	244.000	24.000	5.669	Measured from the Bottom Face of the Slab

*** +X direction is defined as running north to south with north being 0. Measurements taken to the north face of the LVDT blocks.
*** +Y direction is defined as running up to down with 0 being the bottom face of the slab, except where noted that measurement was taken from the top of the slab. Measurement was taken to the middle of the circular opening in the block.

Table 5.7. Instrumentation plan for HJ-7.

Instrument	CERL Name / Cable #	CIR Name	Conversion Factor (per volt)	Location (X - Dir.) (in.)	Location (Y - Dir.) (in.)	Gage Length (in.)	Comments
Cell_N		N / A	5.000 kips	141.000	N / A	N / A	Concentrated Load - 50 Kip Actuator
Stroke_N		N / A	0.300 inches	141.000	N / A	N / A	
Cell_S		N / A	5.000 kips	250.000	N / A	N / A	Concentrated Load - 50 Kip Actuator
Stroke_S		N / A	0.300 inches	250.000	N / A	N / A	
POT_N	P1	N / A	2.000 inches	96.000	N / A	N / A	Strut Deflection - Potentiometer
POT_Mid	P2	N / A	2.000 inches	192.000	N / A	N / A	Midspan Deflection - Potentiometer
POT_S	P3	N / A	2.000 inches	243.000	N / A	N / A	Quarter span Deflection - Potentiometer
Int_1	IS1	s3	0.00150 in/in	23.000	7.000	N / A	Placed by the CIR-Measurement from slab top
Int_2	IS2 / 2	s2	0.00150 in/in	23.000	9.000	N / A	Placed by the CIR-Measurement from slab top
Int_3	IS3 / 1	s1	0.00150 in/in	23.000	11.000	N / A	Placed by the CIR-Measurement from slab top
Int_4	IS4	s12	0.00150 in/in	135.000	7.000	N / A	Placed by the CIR-Measurement from slab top
Int_5	IS5	s11	0.00150 in/in	135.000	24.000	N / A	Placed by the CIR-Measurement from slab top
Int_6	IS6 / 10	s10	0.00150 in/in	135.000	26.000	N / A	Placed by the CIR-Measurement from slab top
Int_7	IS7 / 15	s15	0.00150 in/in	147.000	7.000	N / A	Placed by the CIR-Measurement from slab top
Int_8	IS8 / 14	s14	0.00150 in/in	147.000	24.000	N / A	Placed by the CIR-Measurement from slab top
Int_9	IS9 / 13	s13	0.00150 in/in	147.000	26.000	N / A	Placed by the CIR-Measurement from slab top
Int_10	IS10 / 18	s18	0.00150 in/in	192.000	7.000	N / A	Placed by the CIR-Measurement from slab top
Int_11	IS11 / 17	s17	0.00150 in/in	192.000	24.000	N / A	Placed by the CIR-Measurement from slab top
Int_12	IS12 / 16	s16	0.00150 in/in	192.000	26.000	N / A	Placed by the CIR-Measurement from slab top
LVDT_1	D1	N / A	0.00500 inches	69.875	1.000	7.559	Measured from the Top of the Slab
LVDT_2	D2	N / A	0.00500 inches	70.500	4.000	5.591	Measured from the Bottom Face of the Slab
LVDT_3	D3	N / A	0.00500 inches	70.500	13.000	5.315	Measured from the Bottom Face of the Slab
LVDT_4	D4	N / A	0.00500 inches	143.000	1.000	7.953	Measured from the Top of the Slab
LVDT_5	D5	N / A	0.00500 inches	142.000	5.500	5.709	Measured from the Bottom Face of the Slab
LVDT_6	D6	N / A	0.00500 inches	144.000	13.750	2.717	Measured from the Bottom Face of the Slab
LVDT_7	D7	N / A	0.00500 inches	143.500	23.750	5.748	Measured from the Bottom Face of the Slab
LVDT_8	D8	N / A	0.00500 inches	168.000	1.000	5.984	Measured from the Top of the Slab
LVDT_9	D9	N / A	0.00500 inches	168.250	3.500	8.071	Measured from the Bottom Face of the Slab
LVDT_10	D10	N / A	0.00500 inches	168.500	24.000	6.535	Measured from the Bottom Face of the Slab
LVDT_11	D11	N / A	0.00500 inches	194.750	1.000	6.339	Measured from the Top of the Slab
LVDT_12	D12	N / A	0.00500 inches	194.000	3.250	2.756	Measured from the Bottom Face of the Slab
LVDT_13	D13	N / A	0.00500 inches	194.000	24.500	3.150	Measured from the Bottom Face of the Slab
LVDT_14	D14	N / A	0.00500 inches	194.750	N / A	6.732	Placed on top of Slab
LVDT_15	D15	N / A	0.00500 inches	220.625	1.000	N / A	Measured from the Top of the Slab
LVDT_16	D16	N / A	0.00500 inches	194.000	N / A	3.189	Placed on bottom side of Web
LVDT_17	D17	N / A	-0.00500 in.	218.500	3.500	5.709	Measured from the Bottom Face of the Slab
LVDT_18	D18	N / A	0.00500 inches	219.500	24.500	6.772	Measured from the Bottom Face of the Slab
LVDT_19	D19	N / A	-0.00500 in.	244.000	12.500	3.150	Measured from the Bottom Face of the Slab
LVDT_20	D20	N / A	0.00500 inches	243.000	22.000	4.528	Measured from the Bottom Face of the Slab

*** +X direction is defined as running north to south with north being 0. Measurements taken to the north face of the LVDT blocks.
*** +Y direction is defined as running up to down with 0 being the bottom face of the slab, except where noted that measurement was taken from the top of the slab. Measurement was taken to the middle of the circular opening in the block.

Table 5.8. Instrumentation plan for HJ-8.

Instrument	CERL Name / Cable #	CIR Name	Conversion Factor (per volt)	Location (X - Dir.) (in.)	Location (Y - Dir.) (in.)	Gage Length (in.)	Comments
Cell_N		N / A	5.000 kips	141.000	N / A	N / A	Concentrated Load - 50 Kip Actuator
Stroke_N		N / A	0.300 inches	141.000	N / A	N / A	
Cell_S		N / A	5.000 kips	250.000	N / A	N / A	Concentrated Load - 50 Kip Actuator
Stroke_S		N / A	0.300 inches	250.000	N / A	N / A	
POT_N	P1	N / A	2.000 inches	95.000	N / A	N / A	Third span Deflection - Potentiometer
POT_Mid	P2	N / A	2.000 inches	193.313	N / A	N / A	Midspan Deflection - Potentiometer
POT_S	P3	N / A	2.000 inches	241.500	N / A	N / A	Quarter span Deflection - Potentiometer
Int_1	IS1 / 22	s22	0.00150 in/in	56.000	7.000	N / A	Placed by the CIR-Measurement from slab top
Int_2	IS2 / 20	s20	0.00150 in/in	23.000	9.000	N / A	Placed by the CIR-Measurement from slab top
Int_3	IS3 / 21	s21	0.00150 in/in	23.000	11.000	N / A	Placed by the CIR-Measurement from slab top
Int_4	IS4 / 25	s25	0.00150 in/in	102.000	7.000	N / A	Placed by the CIR-Measurement from slab top
Int_5	IS5 / 26	s26	0.00150 in/in	102.000	20.495	N / A	Placed by the CIR-Measurement from slab top
Int_6	IS6 / 30	s30	0.00150 in/in	135.000	26.000	N / A	Placed by the CIR-Measurement from slab top
Int_7	IS7 / 31	s31	0.00150 in/in	147.000	7.000	N / A	Placed by the CIR-Measurement from slab top
Int_8	IS8 / 27	s27	0.00150 in/in	102.000	22.495	N / A	Placed by the CIR-Measurement from slab top
Int_9	IS9 / 33	s33	0.00150 in/in	147.000	26.000	N / A	Placed by the CIR-Measurement from slab top
Int_10	IS10 / 34	s34	0.00150 in/in	192.000	7.000	N / A	Placed by the CIR-Measurement from slab top
Int_11	IS11 / 35	s35	0.00150 in/in	192.000	24.000	N / A	Placed by the CIR-Measurement from slab top
Int_12	IS12 / 36	s36	0.00150 in/in	192.000	26.000	N / A	Placed by the CIR-Measurement from slab top
LVDT_1	D1	N / A	0.00500 inches	70.625	1.000	7.283	Measured from the Top of the Slab
LVDT_2	D2	N / A	0.00500 inches	69.500	3.375	5.197	Measured from the Bottom Face of the Slab
LVDT_3	D3	N / A	0.00500 inches	69.250	11.250	4.803	Measured from the Bottom Face of the Slab
LVDT_4	D4	N / A	0.00500 inches	145.625	1.000	7.677	Measured from the Top of the Slab
LVDT_5	D5	N / A	0.00500 inches	144.750	3.250	5.748	Measured from the Bottom Face of the Slab
LVDT_6	D6	N / A	0.00500 inches	144.750	12.500	2.835	Measured from the Bottom Face of the Slab
LVDT_7	D7	N / A	0.00500 inches	144.750	23.500	5.079	Measured from the Bottom Face of the Slab
LVDT_8	D8	N / A	0.00500 inches	168.625	1.000	6.024	Measured from the Top of the Slab
LVDT_9	D9	N / A	0.00500 inches	168.250	2.750	7.480	Measured from the Bottom Face of the Slab
LVDT_10	D10	N / A	0.00500 inches	169.500	23.750	6.378	Measured from the Bottom Face of the Slab
LVDT_11	D11	N / A	0.00500 inches	196.750	1.000	6.496	Measured from the Top of the Slab
LVDT_12	D12	N / A	0.00500 inches	195.000	3.250	2.756	Measured from the Bottom Face of the Slab
LVDT_13	D13	N / A	0.00500 inches	195.625	24.250	3.150	Measured from the Bottom Face of the Slab
LVDT_14	D14	N / A	0.00500 inches	196.688	N / A	6.299	Placed on top of Slab
LVDT_15	D15	N / A	0.00500 inches	221.125	1.000	2.795	Measured from the Top of the Slab
LVDT_16	D16	N / A	0.00500 inches	196.000	N / A	3.110	Placed on bottom side of Web
LVDT_17	D17	N / A	-0.00500 in.	220.000	3.250	5.630	Measured from the Bottom Face of the Slab
LVDT_18	D18	N / A	0.00500 inches	221.500	24.000	6.220	Measured from the Bottom Face of the Slab
LVDT_19	D19	N / A	-0.00500 in.	245.875	12.625	2.913	Measured from the Bottom Face of the Slab
LVDT_20	D20	N / A	0.00500 inches	247.750	23.250	4.291	Measured from the Bottom Face of the Slab

*** +X direction is defined as running north to south with north being 0. Measurements taken to the north face of the LVDT blocks.
*** +Y direction is defined as running up to down with 0 being the bottom face of the slab, except where noted that measurement was taken from the top of the slab. Measurement was taken to the middle of the circular opening in the block.

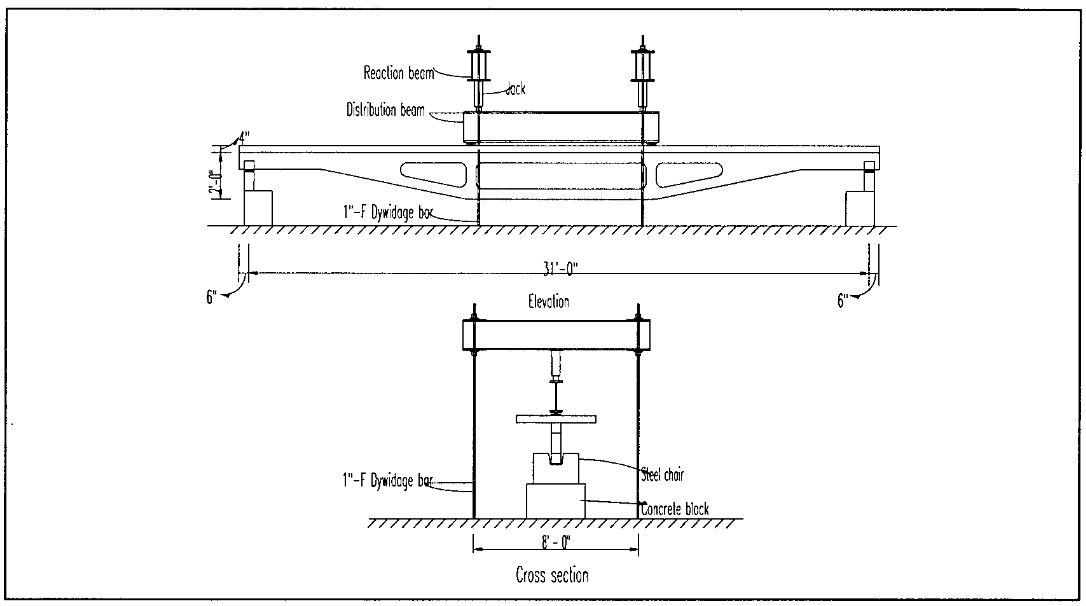

Figure 5.1. Schematic of test setup at UNO for HJ-1 and HJ-2.

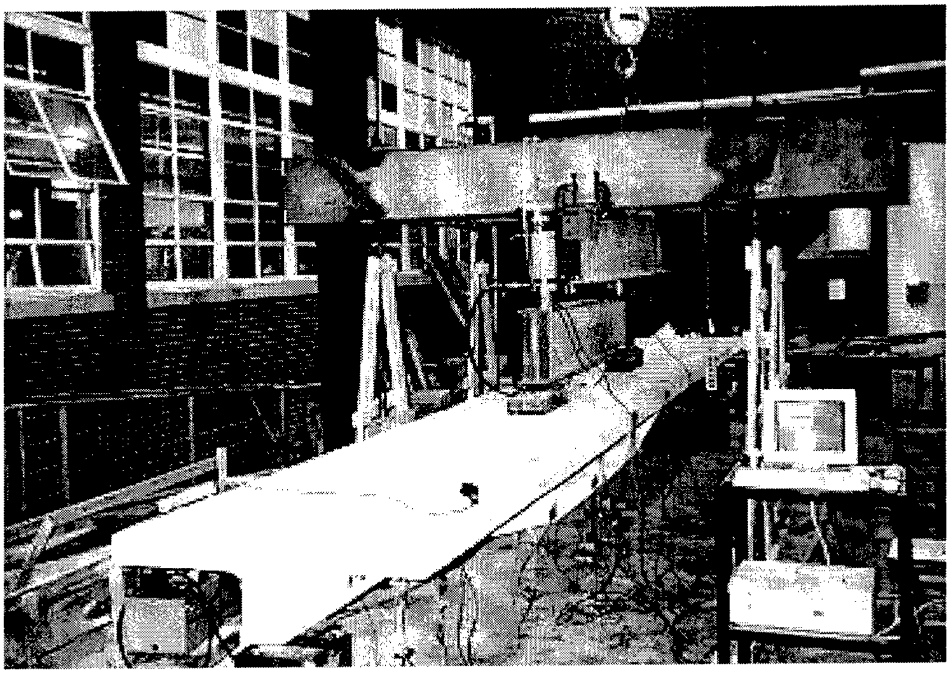

Figure 5.2. Photograph of test setup at UNO for HJ-1 and HJ-2.

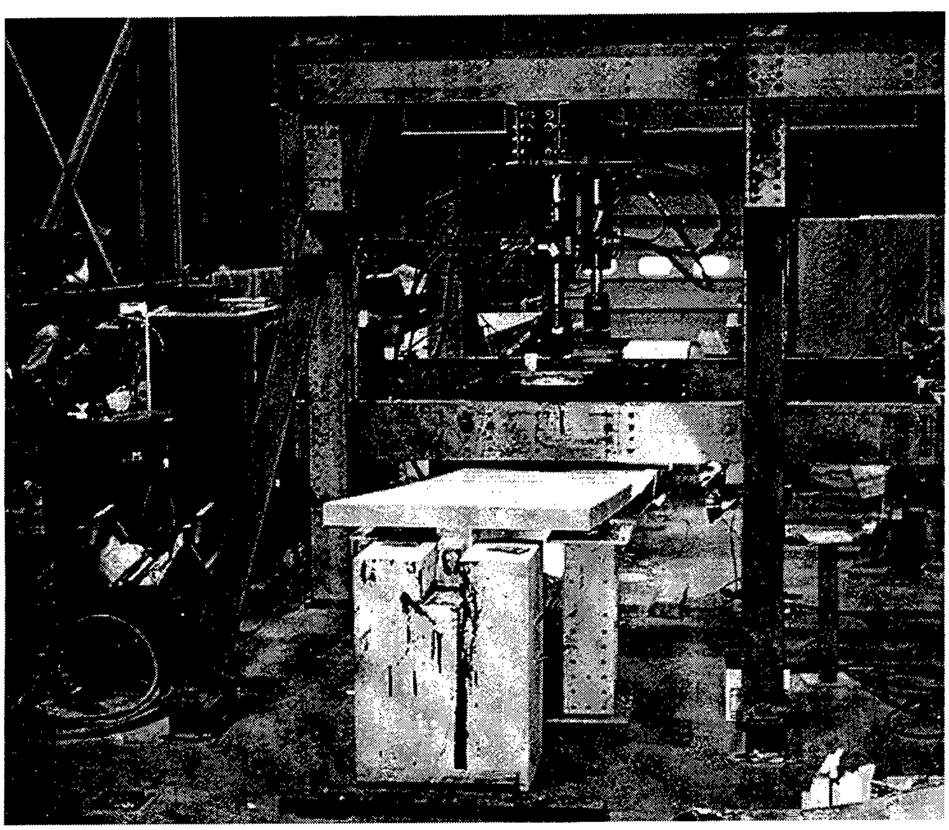

Figure 5.3. USACERL test setup – 31 ft clear span.

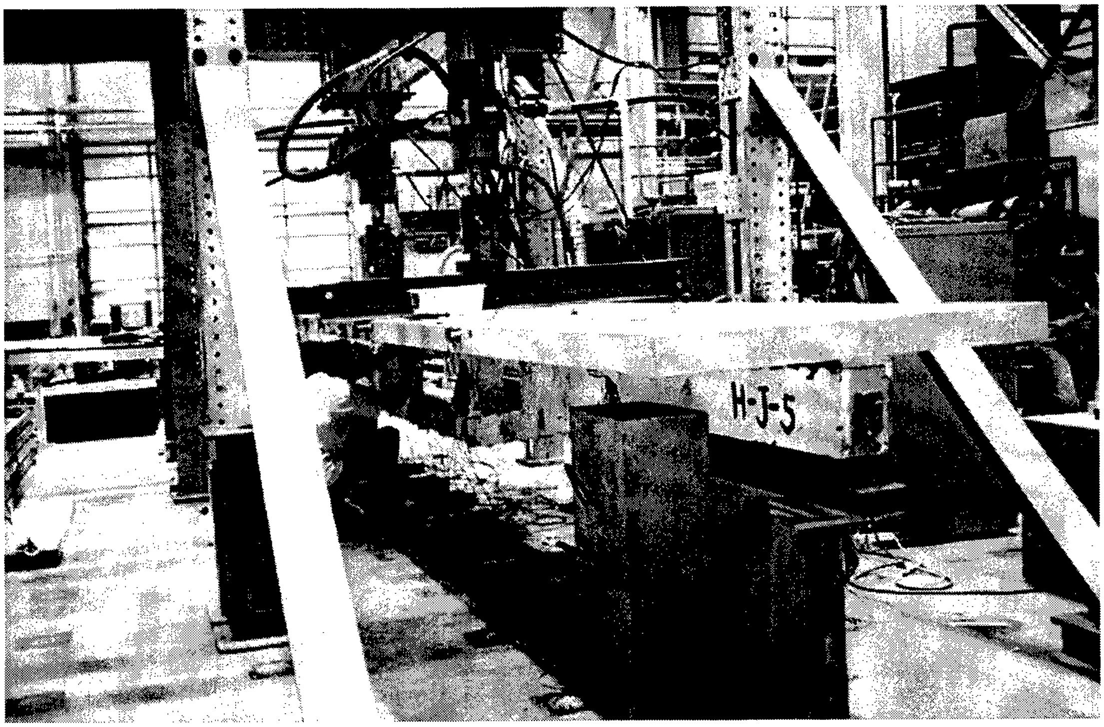

Figure 5.4. USACERL test setup – 23 ft clear span.

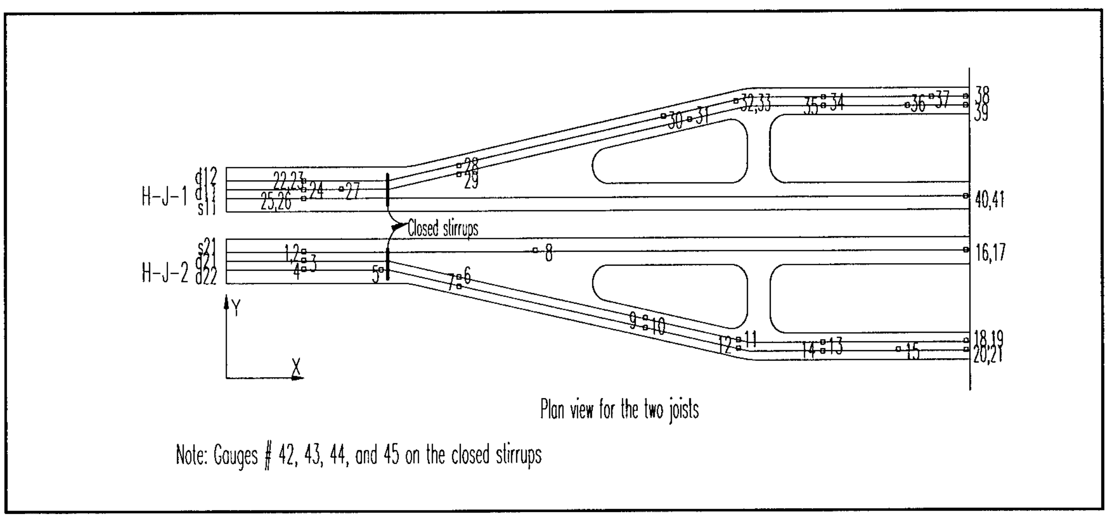

Figure 5.5. Internal strain gage layout for HJ-1 and HJ-2.

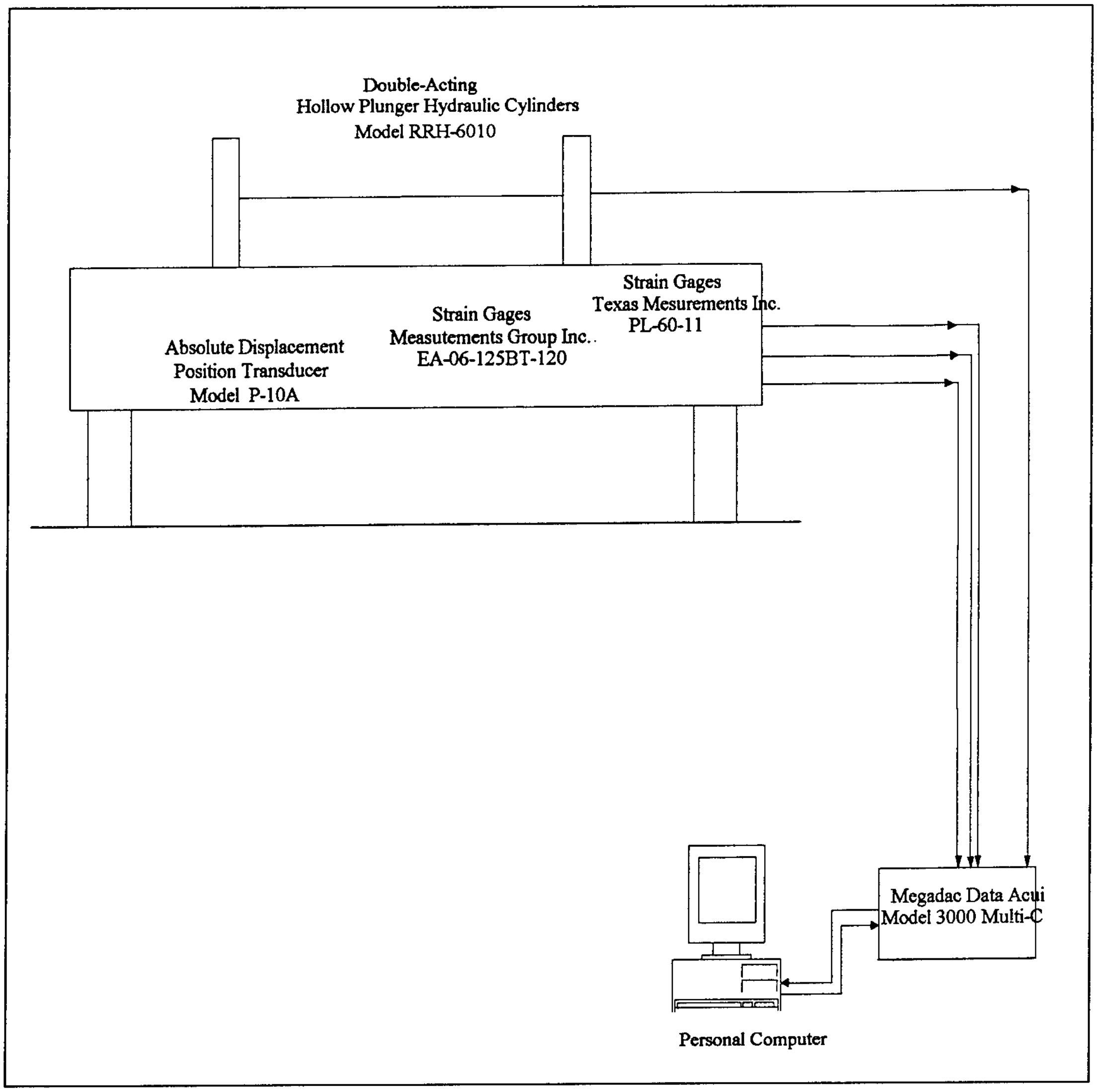

Figure 5.6. Functional block diagram of UNO data acquisition system.

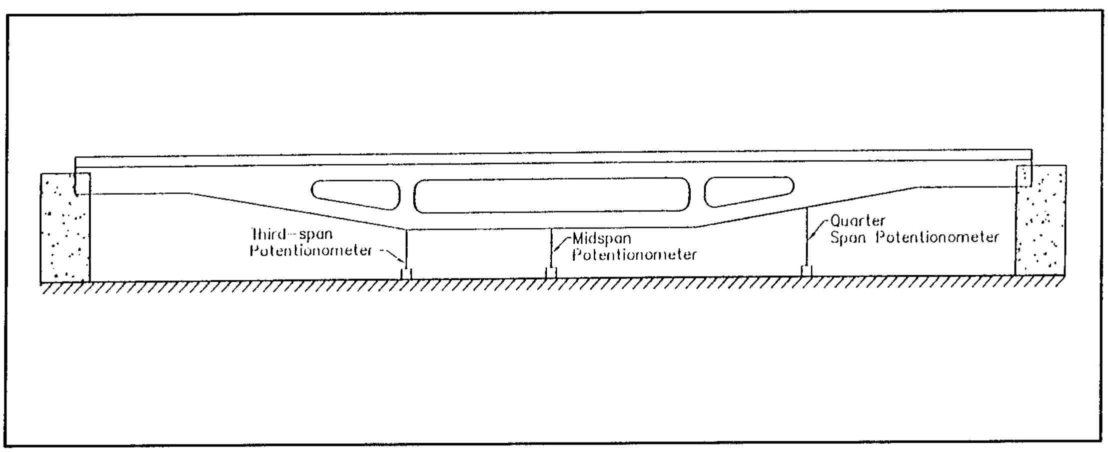

Figure 5.7. Potentiometer locations on test specimens HJ-5, HJ-6, HJ-7, and HJ-8.

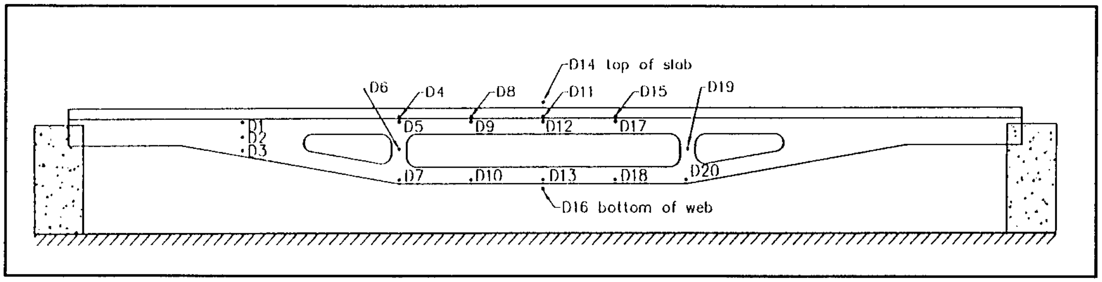

Figure 5.8. LVDT locations on test specimens HJ-5, HJ-6, HJ-7, and HJ-8.

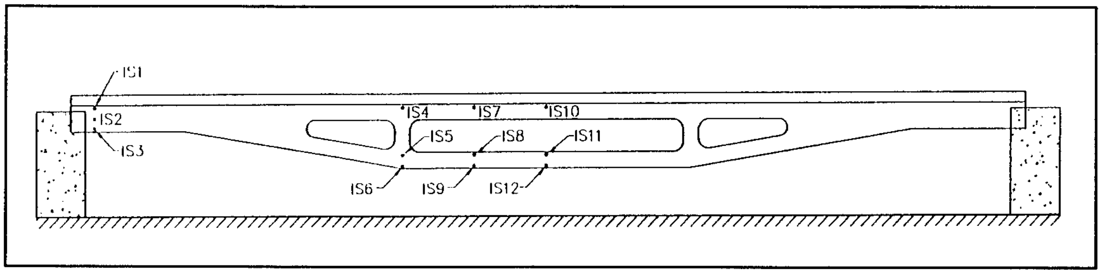

Figure 5.9. Internal strain gage locations on test specimens HJ-5, HJ-6, HJ-7, and HJ-8.

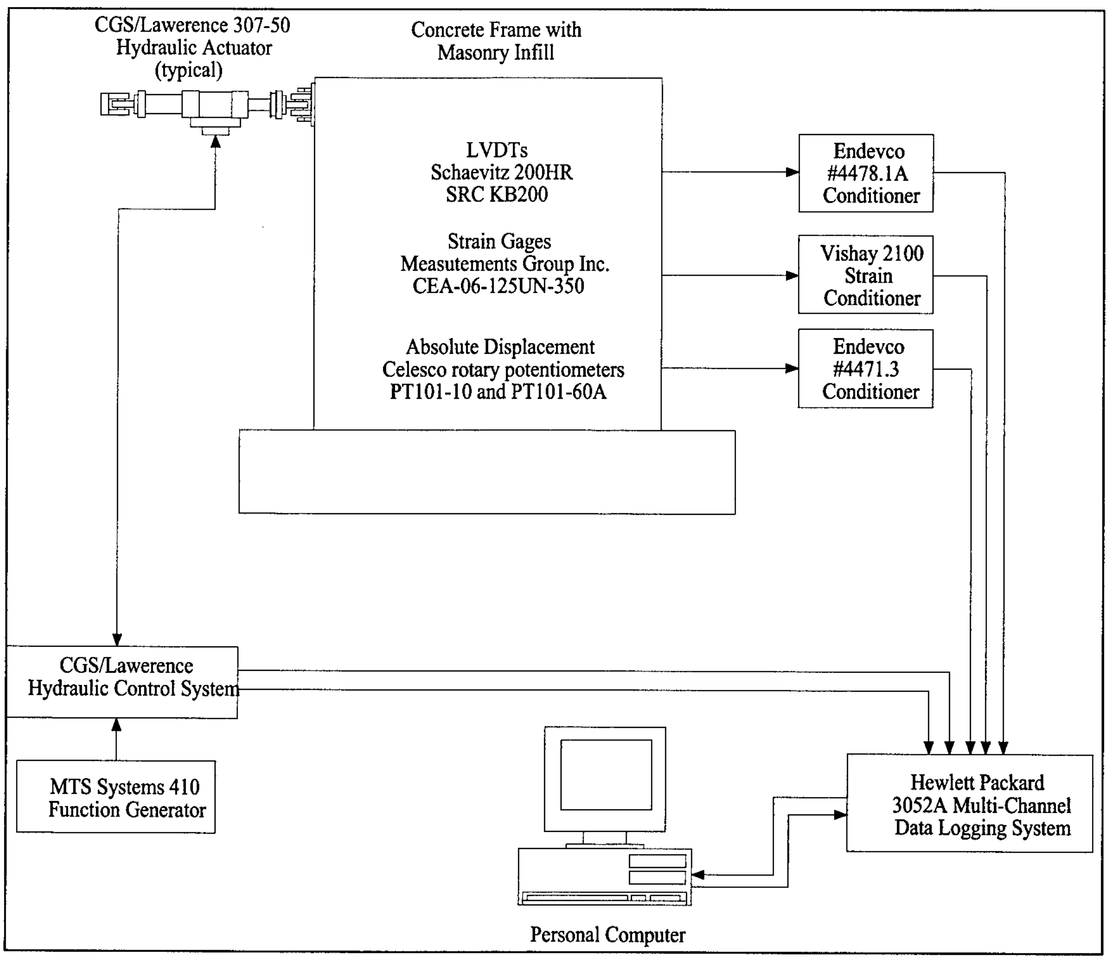

Figure 5.10. Functional block diagram of USACERL data acquisition system.

6 Experimental Results

Introduction

This chapter presents the experimental results from the tests of specimens HJ-1 and HJ-2, performed at the UNO Structures Laboratory, and the tests of HJ-5, HJ-6, HJ-7, and HJ-8, performed at the USACERL Structures Laboratory. Load and displacement, concrete and prestressing steel strains, and specimen failure modes are discussed in detail.

Load and Deflection

Table 6.1 summarizes principal test results, including cracking load, location of first crack, failure load, equivalent uniform load at failure for the test configuration, and type of failure. All load values in the table represent the sum of the two actuator loads. The experimental cracking load was determined at the time the first crack was observed. Total failure loads represent the sum of all beams and plates used in loading in addition to the actuator loads. Joist HJ-1 failed at a load of 60.0 kips, approximately 660 percent of the superimposed service load or 317 percent of the superimposed ultimate load. Joist HJ-2 failed at a load of 62.0 kips, approximately 689 percent of the superimposed service load or 328 percent of the superimposed ultimate load. Joist HJ-6 was then tested, and failed at a load of 48.7 kips, well below the anticipated capacity but still 504 percent of the ultimate superimposed (SI) design load. The premature failure was attributed to insufficient shear reinforcement (but it may also have been negatively affected by the concrete's failure to reach a strength of 12,000 psi.at 28 days, as specified in the design). HJ-5 was reinforced similarly, so it was decided to test that specimen in a smaller clear span of 23.33 ft; consequently, its failure load was significantly greater — 83.7 kips. The effects of this joist's lower concrete strength cannot directly be determined from the experimental results. HJ-7 and HJ-8 failed at loads of 65.0 and 63.0 kips, respectively. These represented 675 percent and 653 percent of the ultimate SI design load.

Deflection parameters, including camber at tendon release and experimental deflections due to the applied loads are summarized in Table 6.2. For the 31 ft clear span, the experimental deflections at the load equivalent to live load (LL), 0.85 kips, and the load equivalent to SI dead load (DL) + LL, 3.0 kips, are much lower than the ACI 318-95 limitations of L/360 (1.0 in.), and L/240 (1.55 in.), respectively, for specimens HJ-6, HJ-7, and HJ-8. Equivalent point loads for the same conditions for the 23.33 ft clear span are 0.71 kips (LL) and 2.5 kips (SIDL). Deflection limits for the 23.33 ft span are 0.78 in. (LL) and 1.17 in. (SIDL). Measured deflections for HJ-5 are also below these limits. The experimental load versus midspan deflection curves for joists HJ-1 and HJ-2 are shown in Figure 6.1. Similar curves for HJ-5 through HJ-8 are shown in Figure 6.2. The greater stiffness of HJ-5 is a function of the different clear span used in testing. Initial stiffnesses of HJ-6 through HJ-8 were very similar. HJ-6 began to degrade at a much lower load level than HJ-7 and HJ-8. HJ-7 and HJ-8 had very similar force-versus-displacement performance.

Deflection profiles along the length of joist were approximated based on the measured deflections. They are shown for HJ-1 and HJ-2 with respect to load increments of a single actuator in Figures 6.3 and 6.4. Similar plots for the other tested joists are shown in Figure 6.5. The data used for approximating these latter curves were measured at potentiometers P1 – P3 and manually at points T1 – T5 as specified in the instrumentation plans. These shapes reflect the constant moment between load points and the marked stiffness variation along the specimen length. The increased curvature with increasing load also reflects progressively greater cracking in the center section of the joists.

Strains

Three types of strain readings were used in testing the family of hybrid joists: internal strain of reinforcement and external strain on concrete surfaces — both measured by strain gages — and displacement measured over a specified gage length on concrete surfaces by LVDTs. For the latter measurements cracks may have developed within the gage length, and the strain (displacement/displacement) may be greater than the maximum concrete strain range of 0.003 – 0.004 for compression or 0.0001 – 0.0002 for tension.

Strain distribution over section depth is shown in Figures 6.6 and 6.7 for three critical sections of HJ-1 and HJ-2. The distribution was approximated from concrete strain measurements near the top of the section and prestressing strand strains at the bottom of the section. Similar plots are shown in Figures

6.8 through 6.11 for HJ-5 through HJ-8, respectively. Strains at the end of HJ-5 were so small that they did not show up on a plot. Specimens HJ-1, HJ-2, HJ-7, and HJ-8 show similar strain maxima for comparable load levels. The neutral axis is located within or at the slab depth of 4 in. in all four joists. HJ-5 and HJ-6 were unable to develop significant strain in the prestressing strands due to their early shear failures. The neutral axis in these two specimens is also lower, at approximately 6 in. below the top of the slab. The midspan strains were used to calculate the experimental moment versus curvature (M-Φ) plots for HJ-1 and HJ-2. These are shown with the theoretical curve in Figure 6.12. The experimental curves were calculated by taking the difference in the strain values between the top and bottom gages and dividing by the vertical distance between them. Experimental and theoretical M-Φ are comparable in the elastic range and the analytical model bounds the experimental values beyond this range.

Figures 6.13 and 6.14 show the results of internal strain measurements along the strands for both top and bottom strands of HJ-1 and HJ-2. Top strand strains were not available. Figures 6.15 through 6.18 show strand strain measurements for HJ-5 through HJ-8. To assess the stress in the strands, the strains shown must be added to the strain due to prestressing and related to the elastic modulus of the material. The strand was fully tensioned, so the effective strain due to the prestress is approximately 6705 micro strain [(f_{se}/E_s) = 0.75 (270) / (30,000) (10^6) = 6750 micro strain]. All strains were below the ultimate strand strain of 35,000 microstrain. Again, the lack of strain developed in the strand indicates the poor performance of HJ-5 and HJ-6. During testing it was observed that the bottom chord of joists HJ-7 and HJ-8 appeared to arch upward between the struts; this may be related to the larger strains shown at the struts than the midspan for some load levels.

Cracking and Failure Mechanism

None of the joists experienced any cracking when the prestressing tendons were released. Before testing it was observed that HJ-1 had a hairline horizontal crack at the outside corner of the triangular opening near the support. This crack probably occurred due to the mislocation of the closed stirrups at this area. During handling, specimen HJ-7 developed a crack across the slab through its depth near the south strut.

Cracks were marked on each of the joists throughout testing. Specimens HJ-1, HJ-2, HJ-7, and HJ-8 each had similar crack patterns over the test series. The crack patterns of HJ-1 and HJ-2 are shown in Figures 6.19 and 6.20 respectively.

Figures 6.21 and 6.22 show crack development for HJ-7 and HJ-8. In all cases initial flexural cracks formed along the bottom chord at midspan. Cracks were regularly spaced, and they became more numerous and closely spaced as the displacement was increased. Near the end of testing, when the load was not increasing but the specimen was able to deflect significantly more, inclined cracks developed in the shear spans of the members.

In HJ-1 there was no significant breakage except for chipping of concrete from the right corner of the top chord, as shown in Figure 6.23. In HJ-2 a wide crack started to appear at the left corner of the bottom chord, as shown in Figure 6.24. Eventually, one of the tendons broke at this location, as shown in Figure 6.25. No actual failure was observed in specimens HJ-7 or HJ-8. Both joist continued to deflect after reaching an ultimate load capacity.

Early in the test series, limited cracking occurred in the bottom chords of HJ-6 and HJ-5. As actuator stroke was increased, cracking in the shear spans became evident but the cracks in the bottom chord did not develop further. In HJ-6 an inclined crack developed near the support and progressed upward along the web/slab interface (Figure 6.26). This crack progressed into the slab and failure ultimately occurred in this north end of the joist (Figure 6.27). Inclined shear cracks were also very evident in HJ-5, and the test was stopped when a large crack developed over the full end of the joist (Figure 6.28).

Discussion of Experimental Results

The results of the testing show the importance of adequate shear reinforcement in prestressed concrete joists. The performance of specimens HJ-5 and HJ-6 was severely degraded by insufficient shear reinforcement. Connectivity between the joist web and slab were also shown to be very important as all test joists tended to separate along this interface after testing was completed. HJ-6 failed along this interface. Based on the experimental results, the shear reinforcement details used in HJ-7 and HJ-8 are determined to be the most effective configuration. The shear reinforcement in these specimens is designed in this manner to anchor the tendons, confine the concrete, and provide sufficient anchorage to the cast-in-place slab.

When designed with adequate shear reinforcement, the behavior of the test joists was exceptional. Failure loads for specimens HJ-1, HJ-2, HJ-7, and HJ-8 were very high compared with design service and ultimate loads. Failure was also very ductile for these members, with deflection capacity extending well beyond

the point at which the ultimate load was reached. The hybrid joist behaved very much like a traditional prestressed precast concrete beam except that the hybrid system had the capability to carry 30 percent more load than the conventional prestressed double tee before first cracks appeared.

Based on the test results, it was decided that the triangular openings near the joist ends could be eliminated without hurting joist performance. These openings had been intended to minimize weight, but the hybrid joist performed so effectively in the tests that this weight reduction provided no significant benefit. Elimination of the triangular openings will simplify the joist production process and avoid any potential for cracks in the shear span facilitated by the openings.

Table 6.1. Principal experimental test results for hybrid joists.

Joist designation	Experimental cracking load* (kips)	First Crack Location	Applied Failure load* (kips)	Total Failure Load (kips)	Equivalent Uniform Load (ksf)	Type of failure
HJ-1	24.0	midspan, bottom chord	60.0	61.0	0.71	flexure
HJ-2	30.0	midspan, bottom chord	62.0	63.0	0.74	flexure
HJ-5	20.0	midspan, bottom chord	83.0	84.0	1.14	shear
HJ-6	11.7	midspan, bottom chord	48.0	49.0	0.57	shear
HJ-7	31.5	midspan bottom chord	64.0	65.0	0.76	flexure
HJ-8	30.0	midspan bottom chord	62.0	63.0	0.74	flexure

* Sum of two actuators.

Table 6.2. Camber and deflection for hybrid joists (in.).

Joist designation	Camber at release	LL Deflection	SIDL + LL Deflection	Deflection at failure load
HJ-1	0.38	0.10	0.14	7.5
HJ-2	0.50	0.15	0.20	9.5
HJ-5	0.35	0.01	0.05	2.37
HJ-6	0.45	0.03	0.16	3.52
HJ-7	0.38	0.02	0.14	16.6
HJ-8	0.50	0.01	0.14	18.4

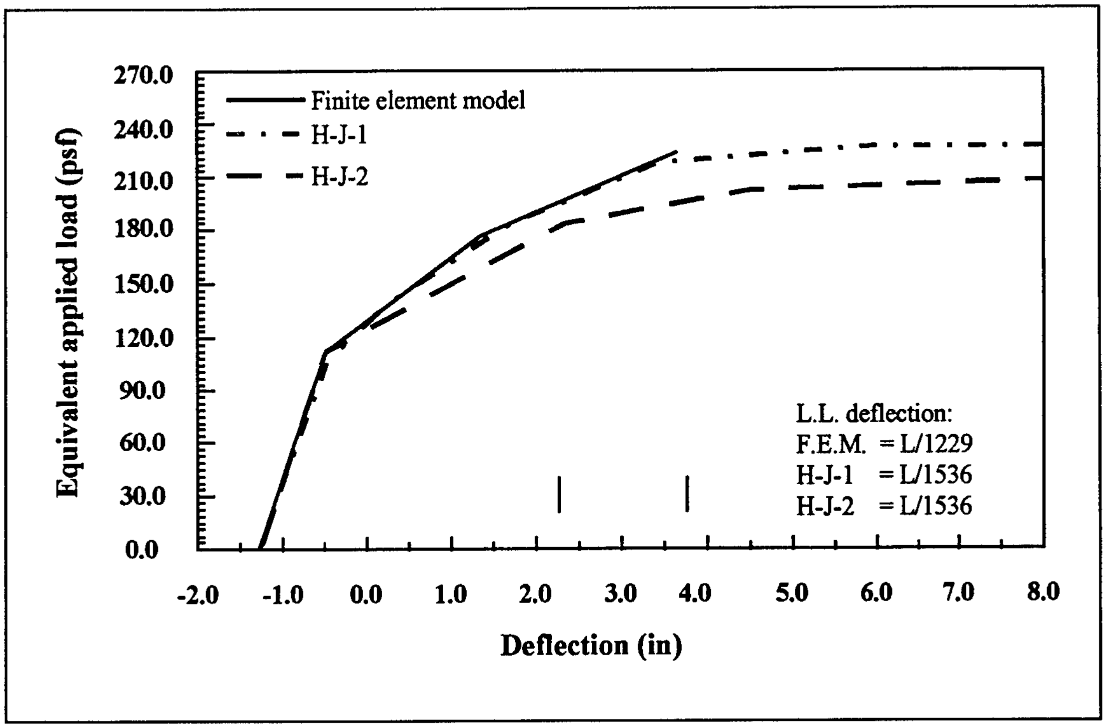

Figure 6.1. Load vs deflection for HJ-1 and HJ-2.

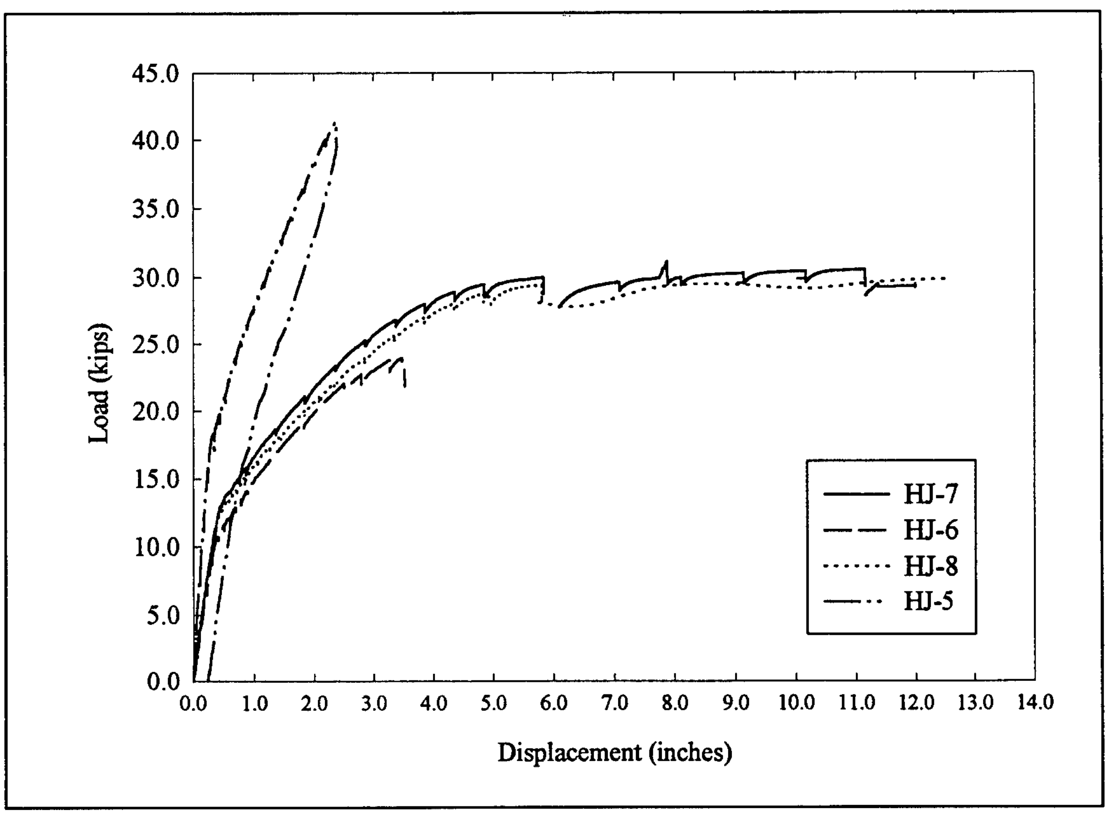

Figure 6.2. Load vs deflection for HJ-5 – HJ-8.

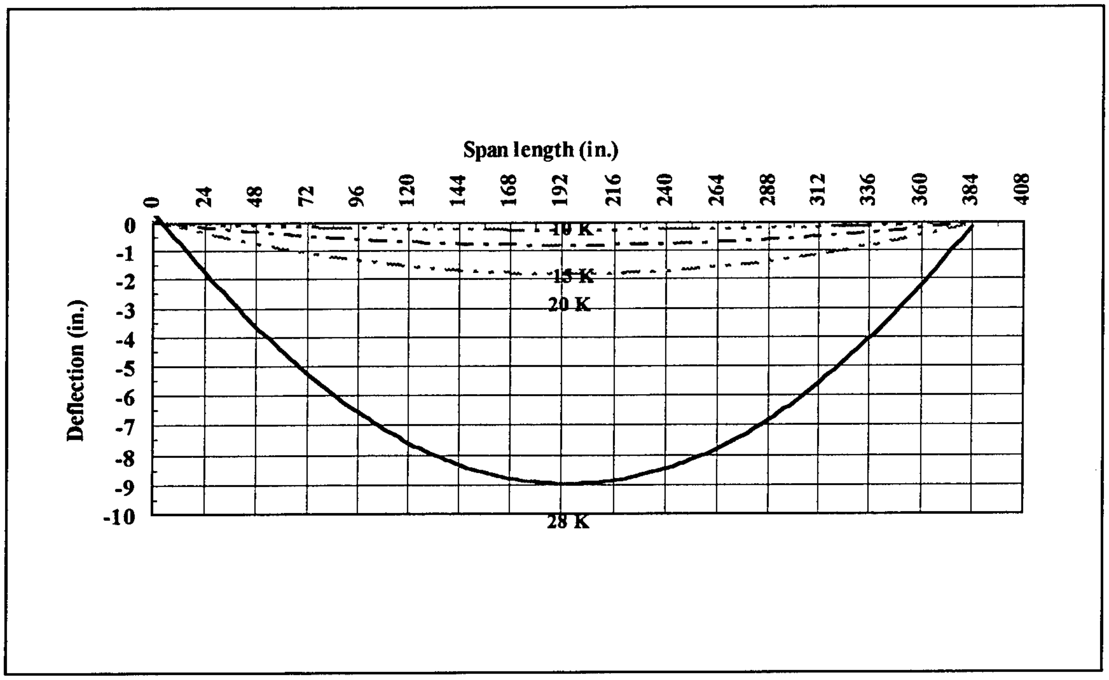

Figure 6.3. Deflected shape for HJ-1.

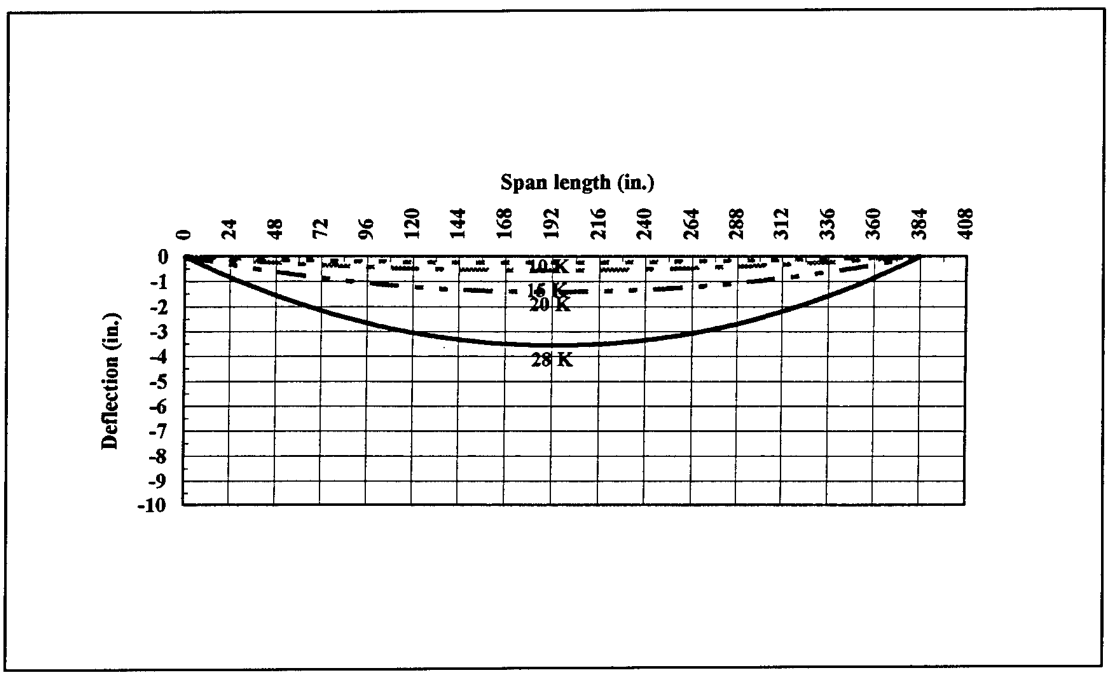

Figure 6.4. Deflected shape for HJ-2.

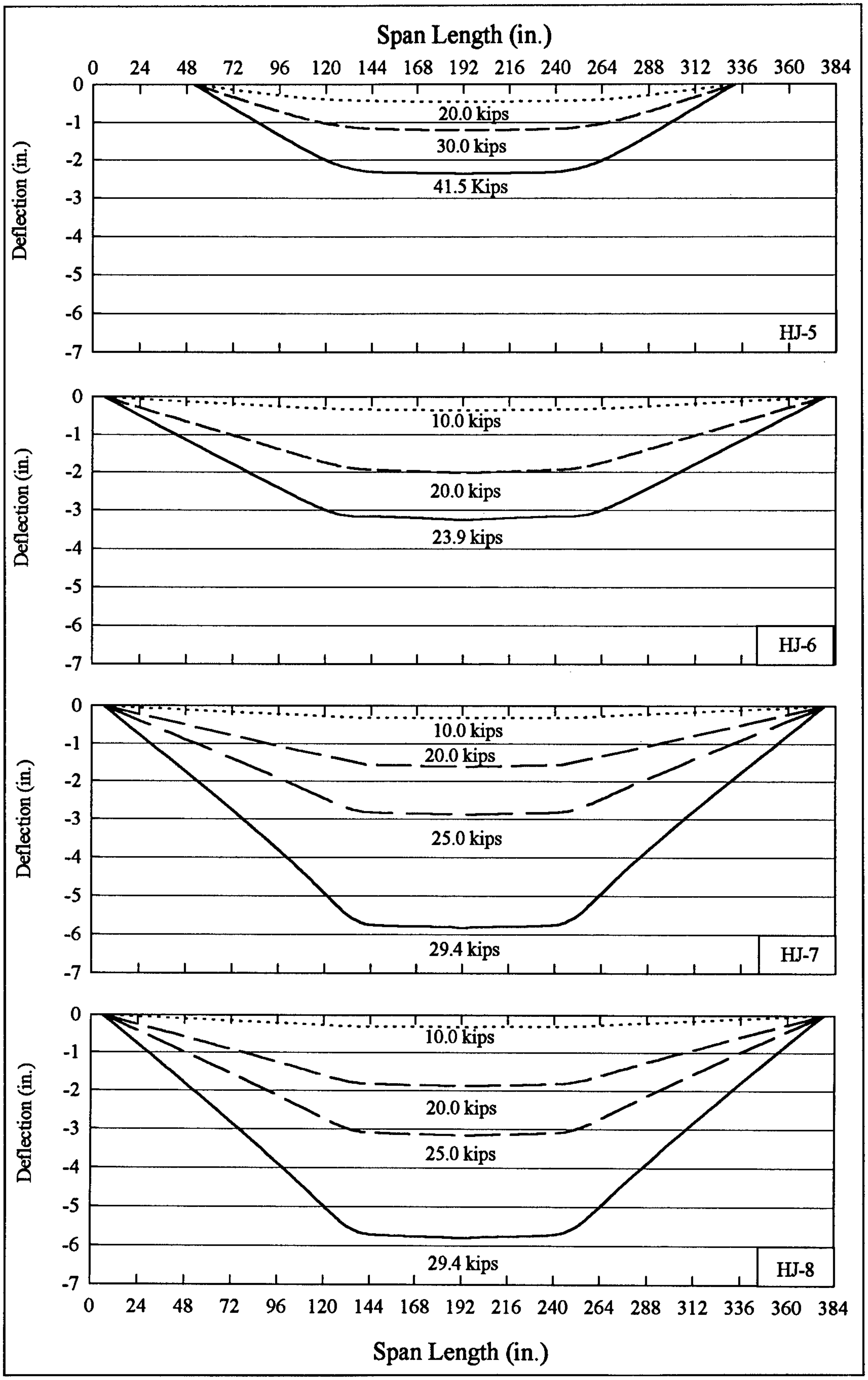

Figure 6.5. Deflected shapes for HJ-5 – HJ-8.

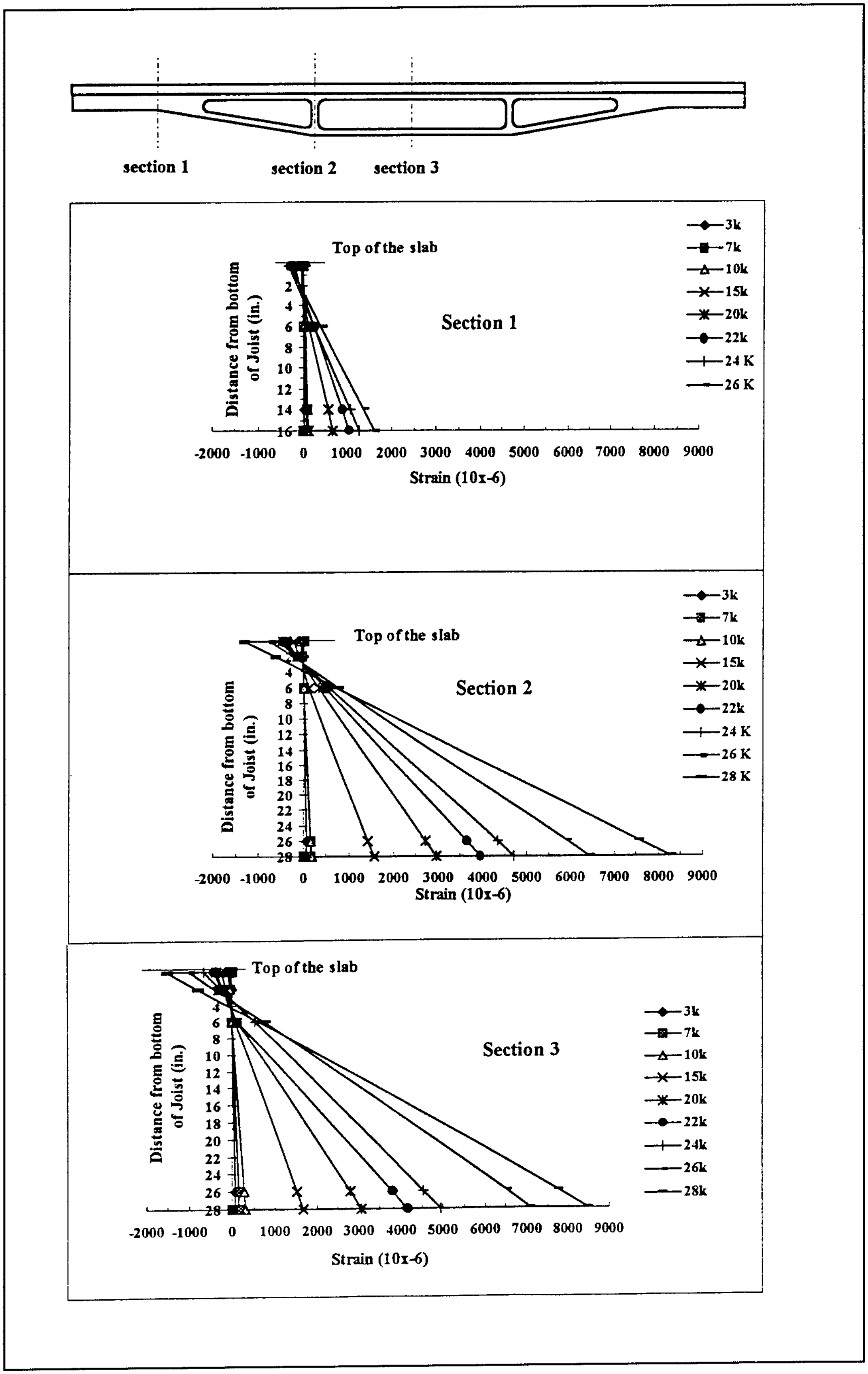

Figure 6.6. Strain distribution for HJ-1.

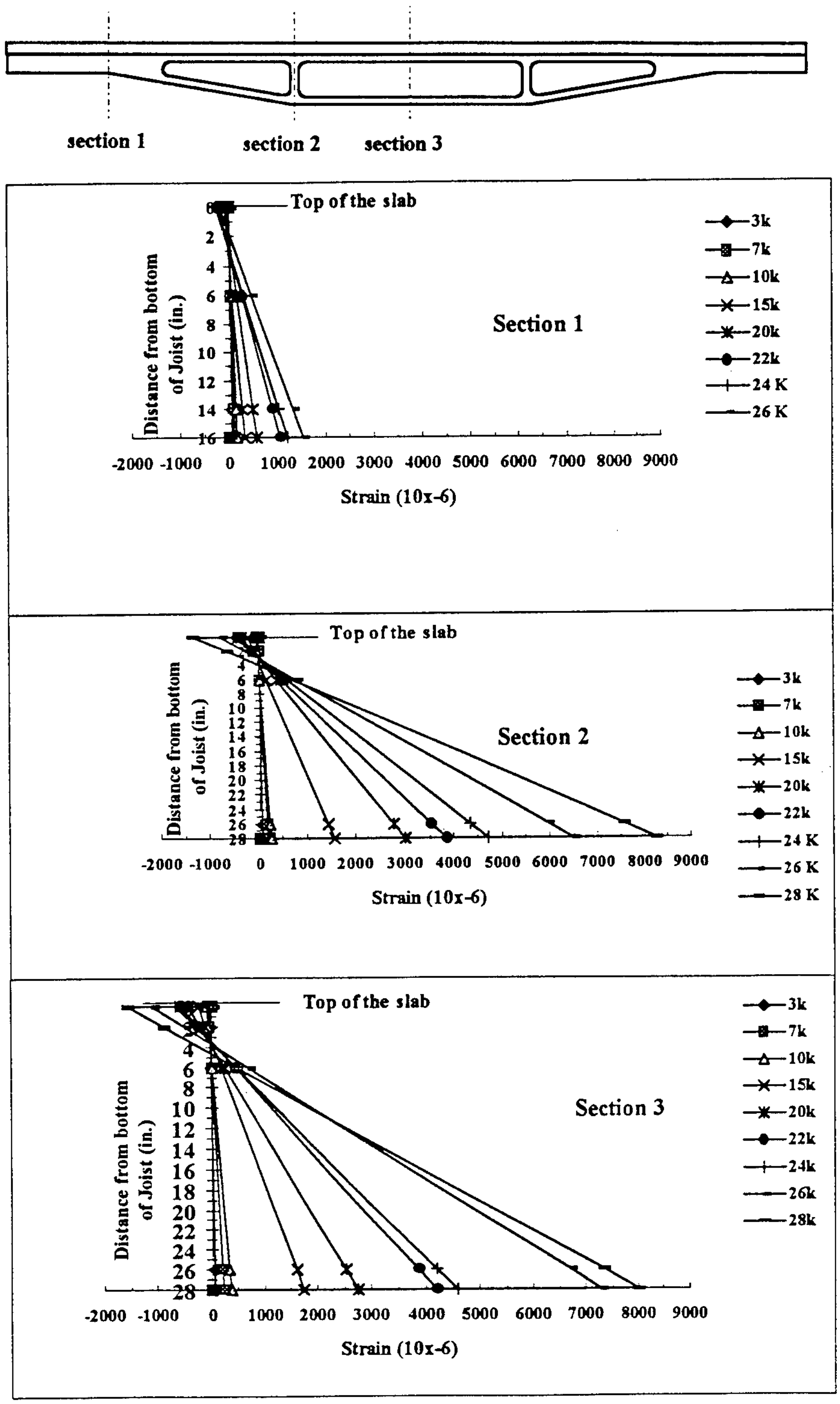

Figure 6.7. Strain distribution for HJ-2.

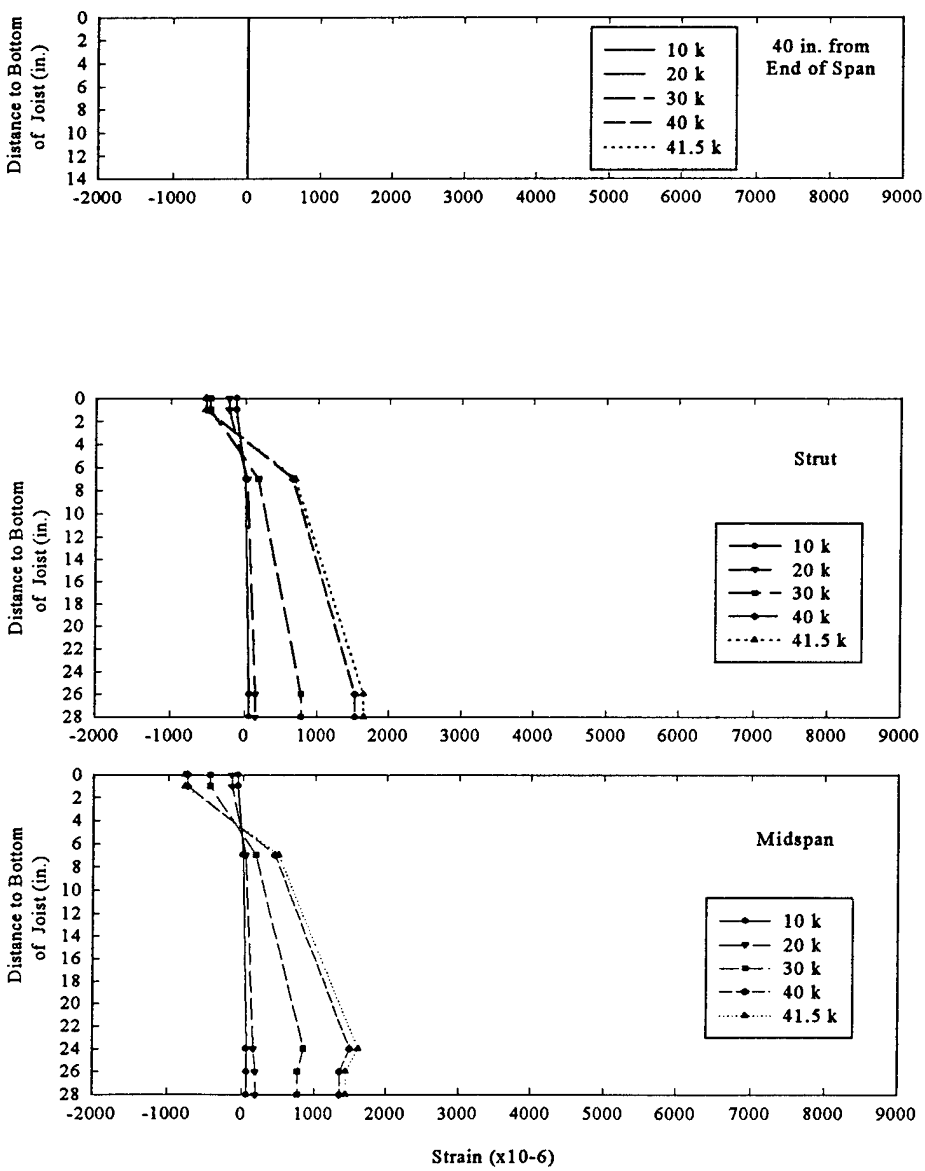

Figure 6.8. Strain distribution for HJ-5.

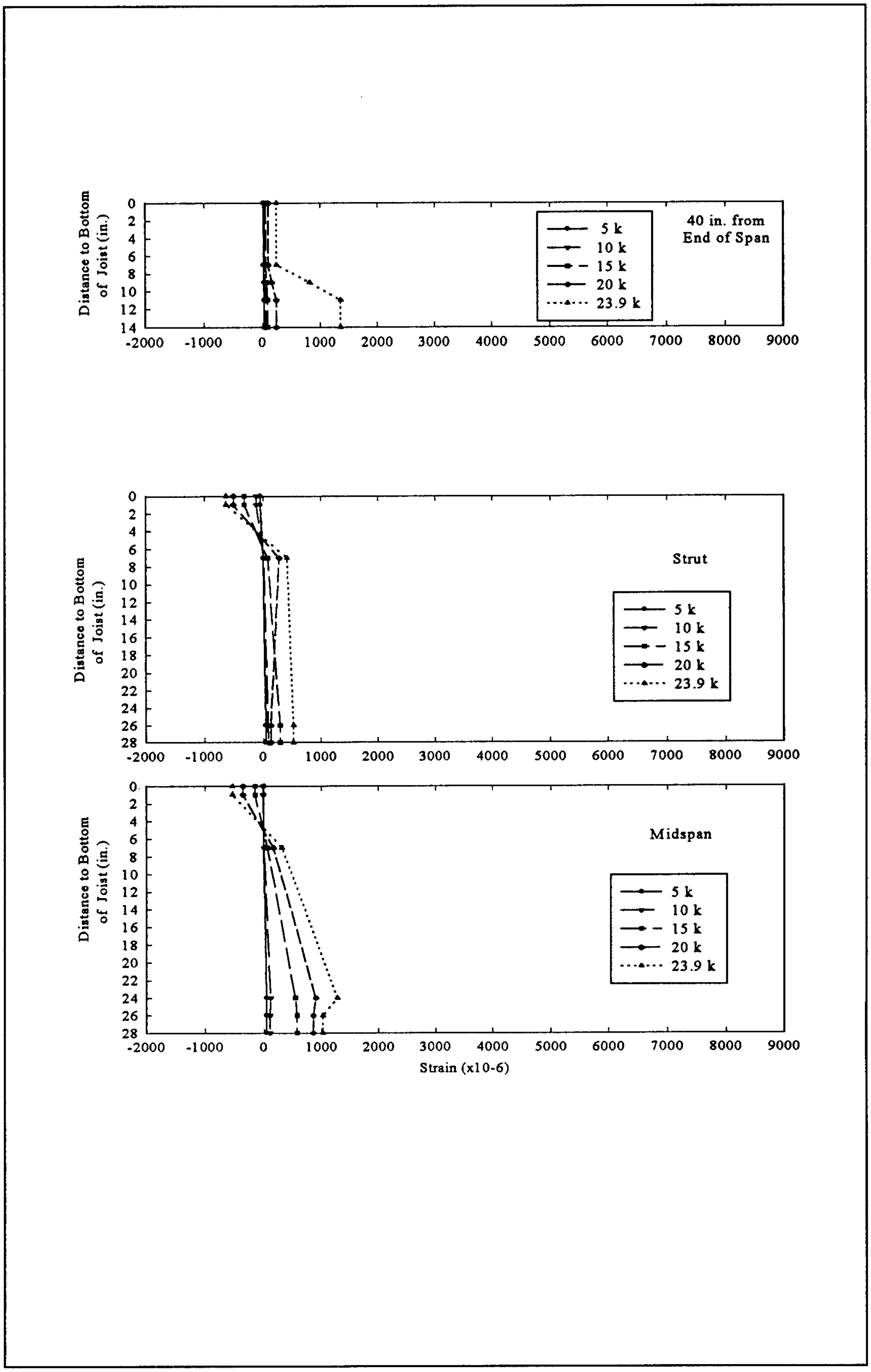

Figure 6.9. Strain distribution for HJ-6.

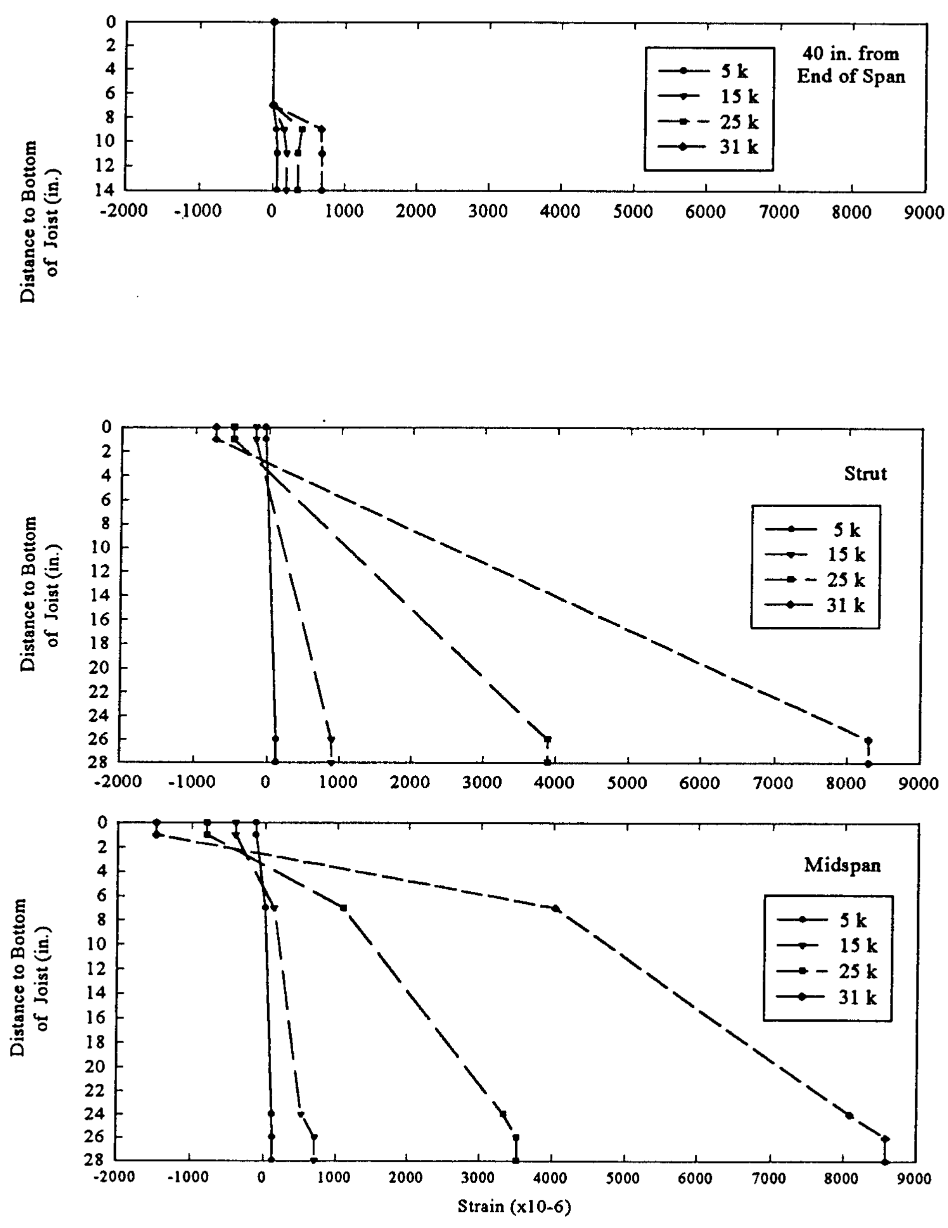

Figure 6.10. Strain distribution for HJ-7.

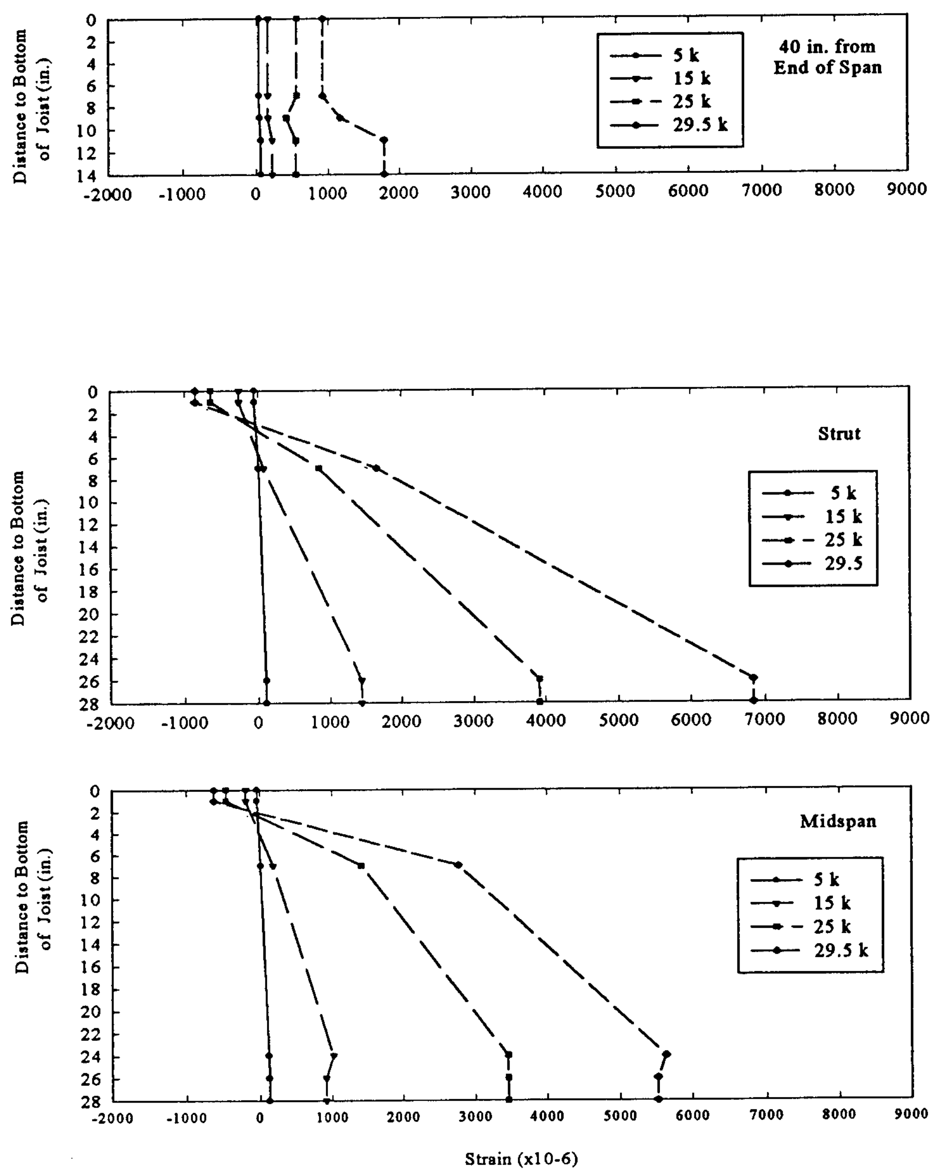

Figure 6.11. Strain distribution for HJ-8.

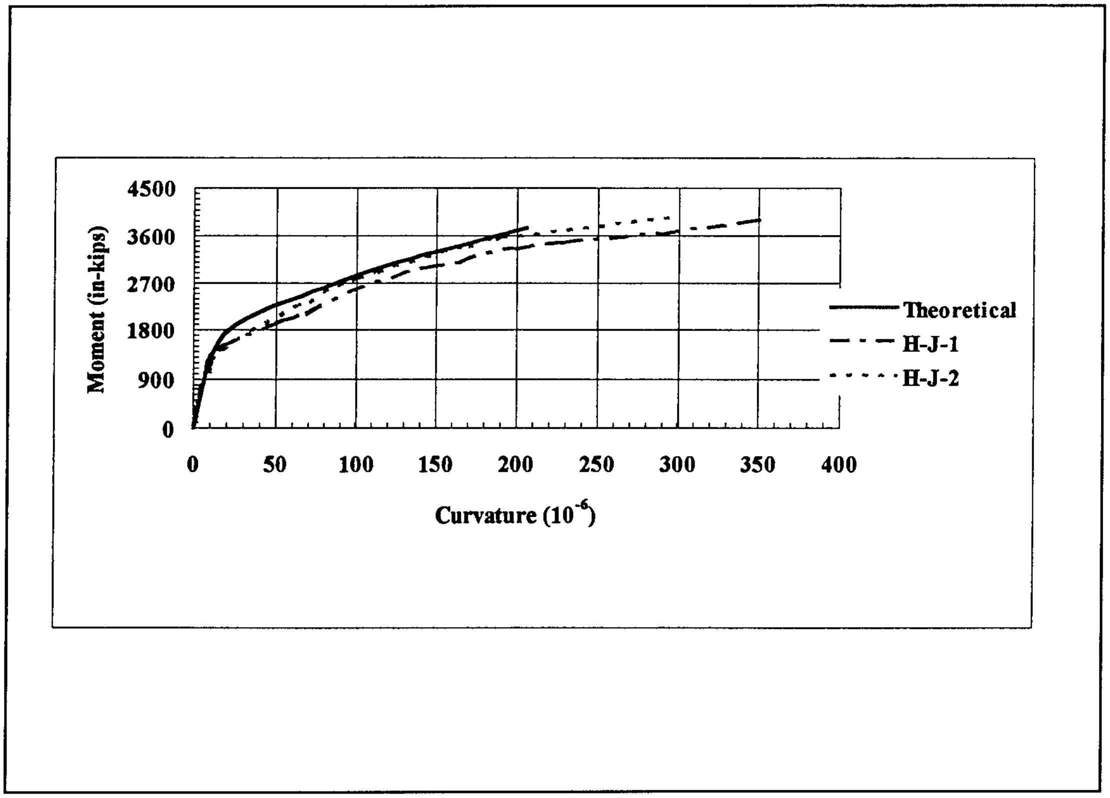

Figure 6.12. Moment vs curvature for HJ-1 and HJ-2.

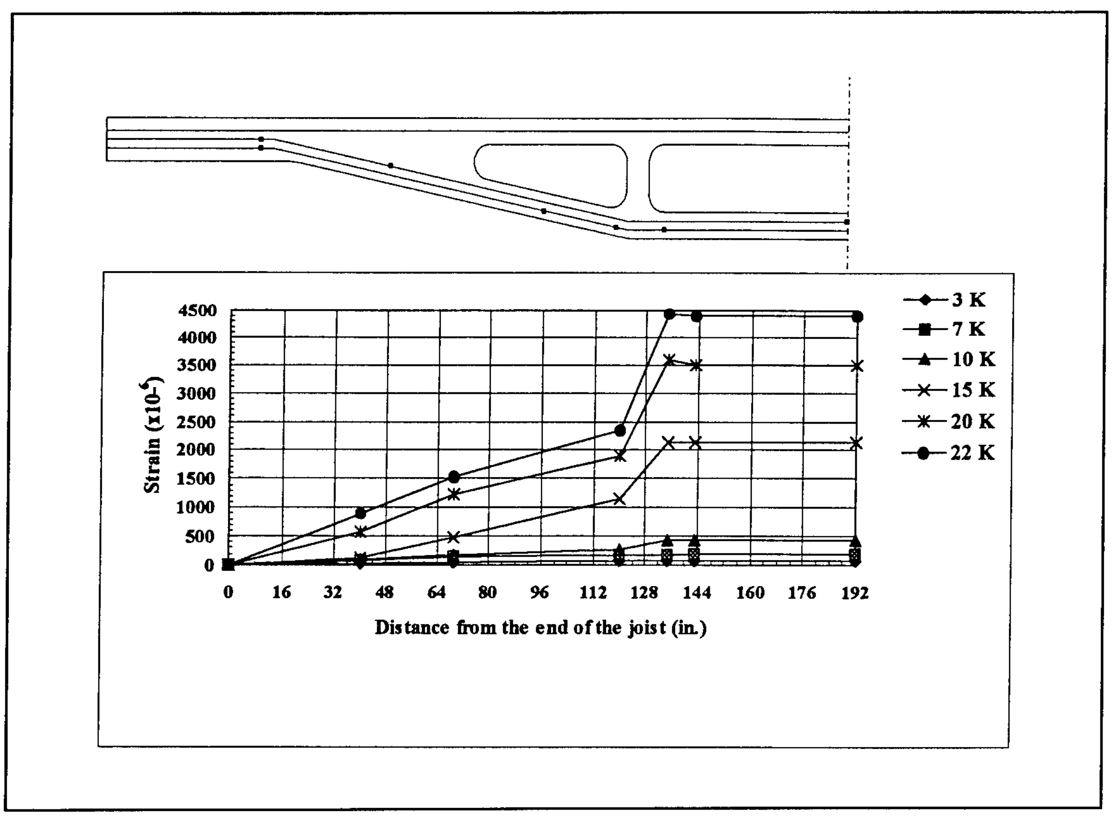

Figure 6.13. Strain distribution along strand length of HJ-1.

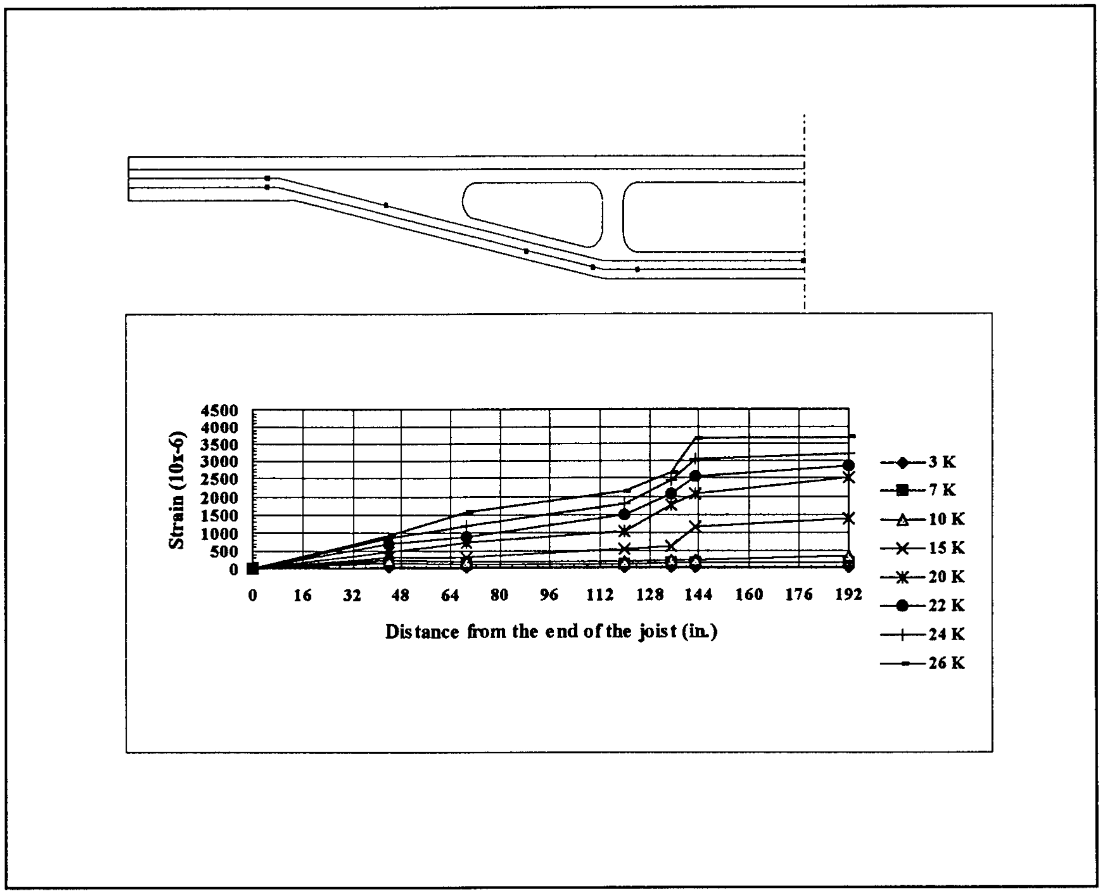

Figure 6.14. Strain distribution along strand length of HJ-2.

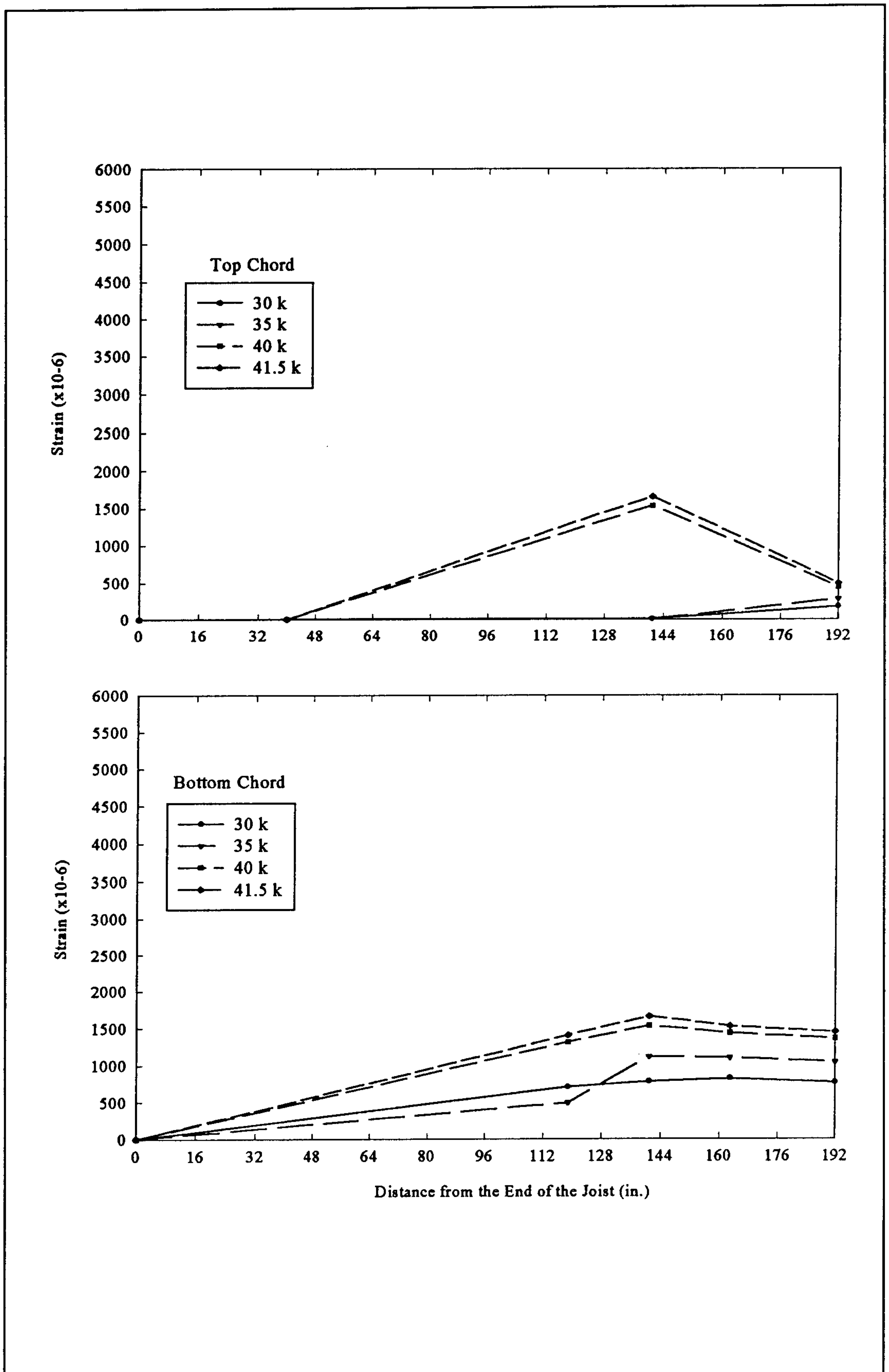

Figure 6.15. Strain distribution along strand length of HJ-5.

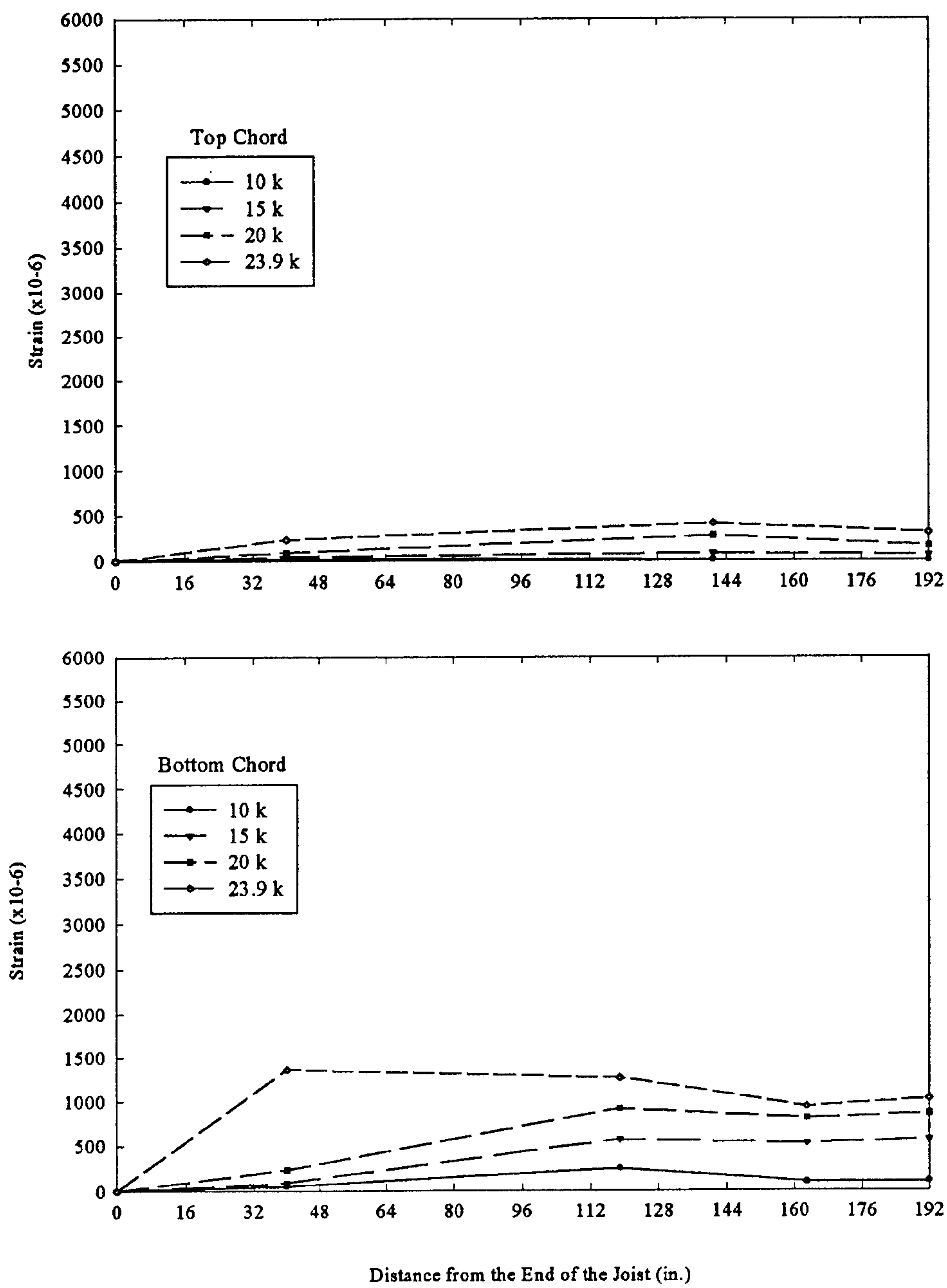

Figure 6.16. Strain distribution along strand length of HJ-6.

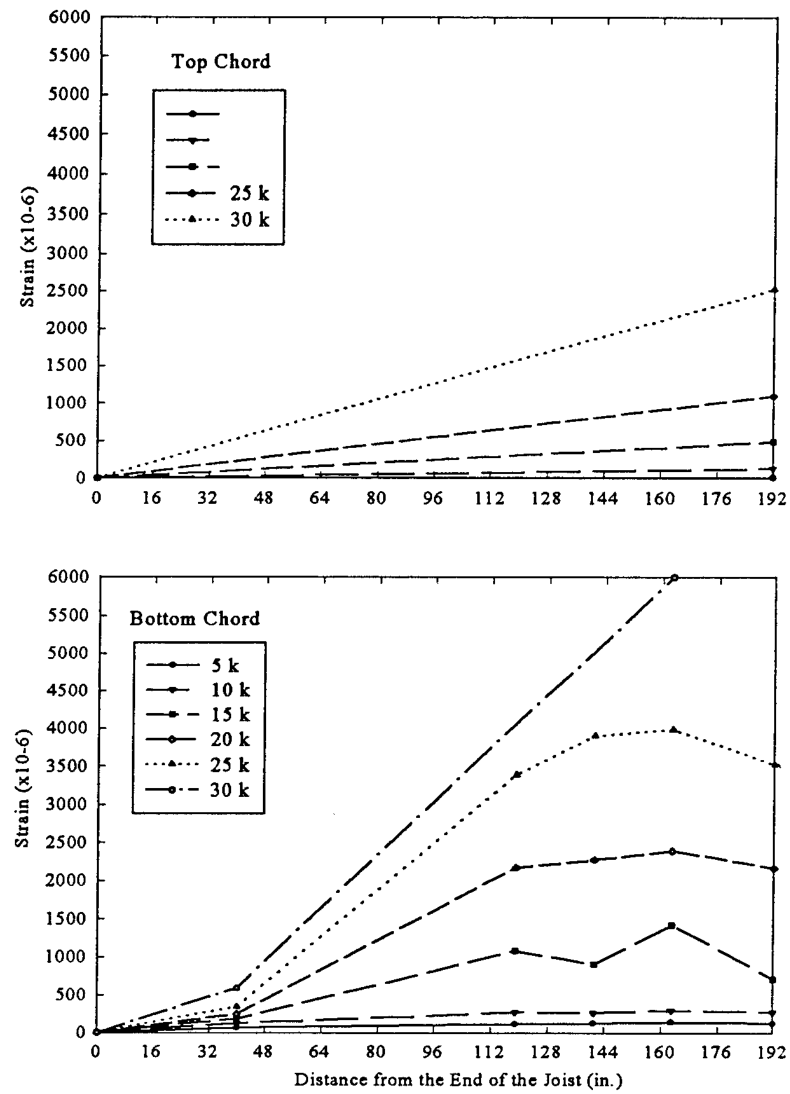

Figure 6.17. Strain distribution along strand length of HJ-7.

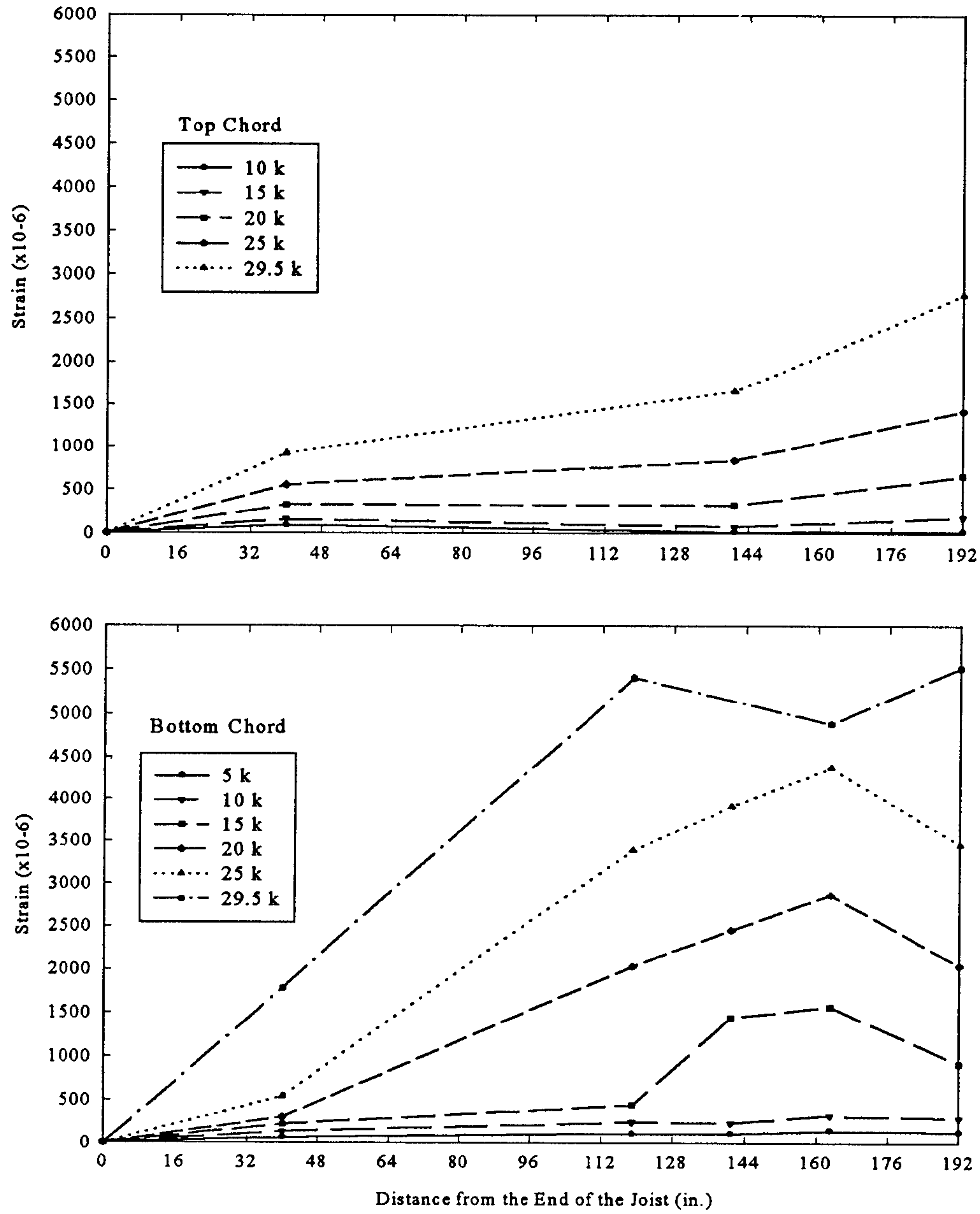

Figure 6.18. Strain distribution along strand length of HJ-8.

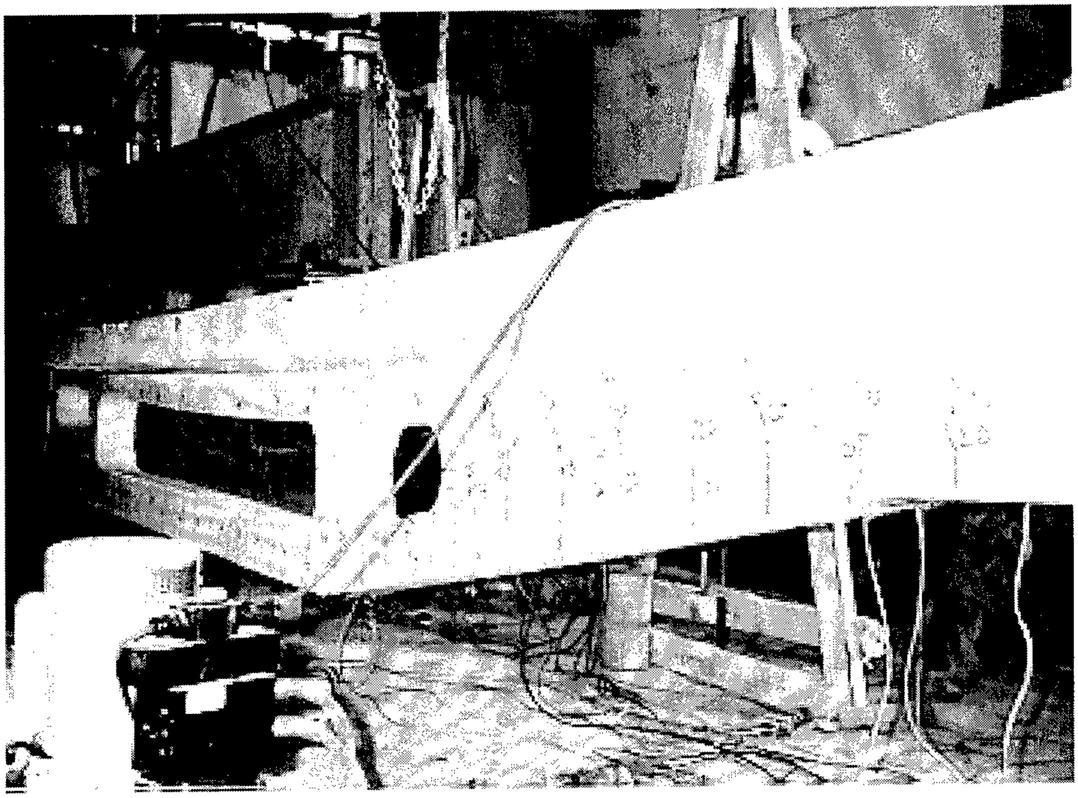

Figure 6.19. Cracking pattern for HJ-1.

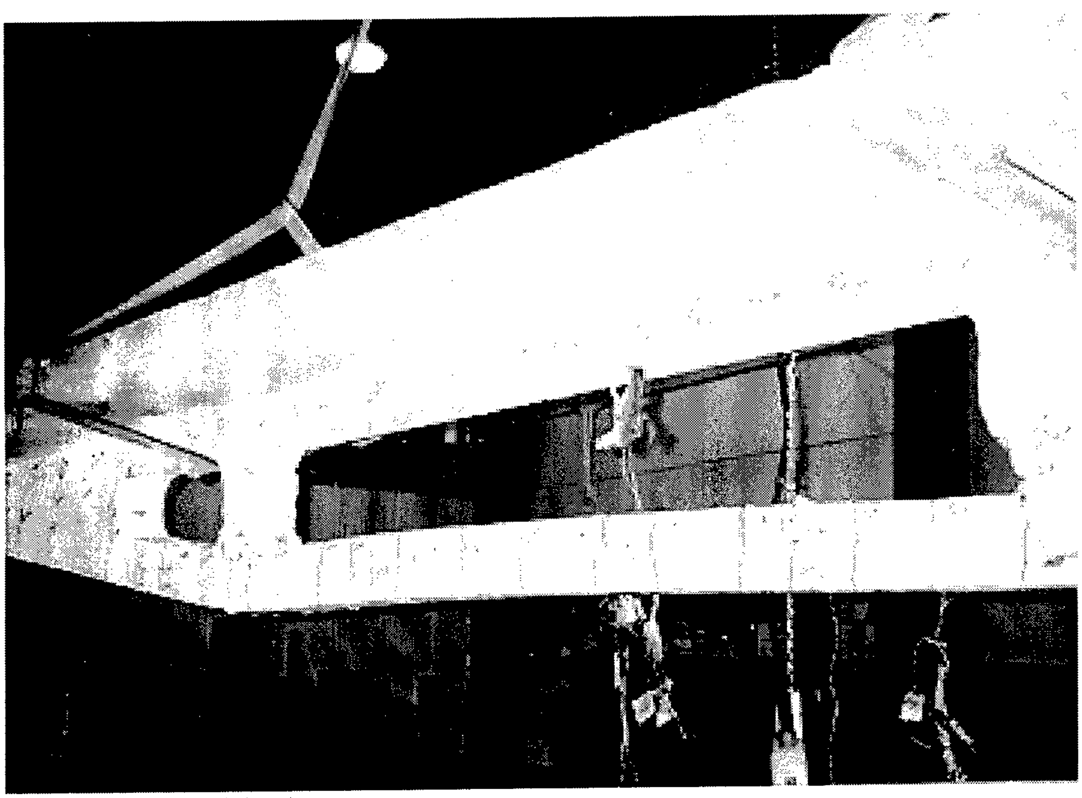

Figure 6.20. Cracking pattern for HJ-2.

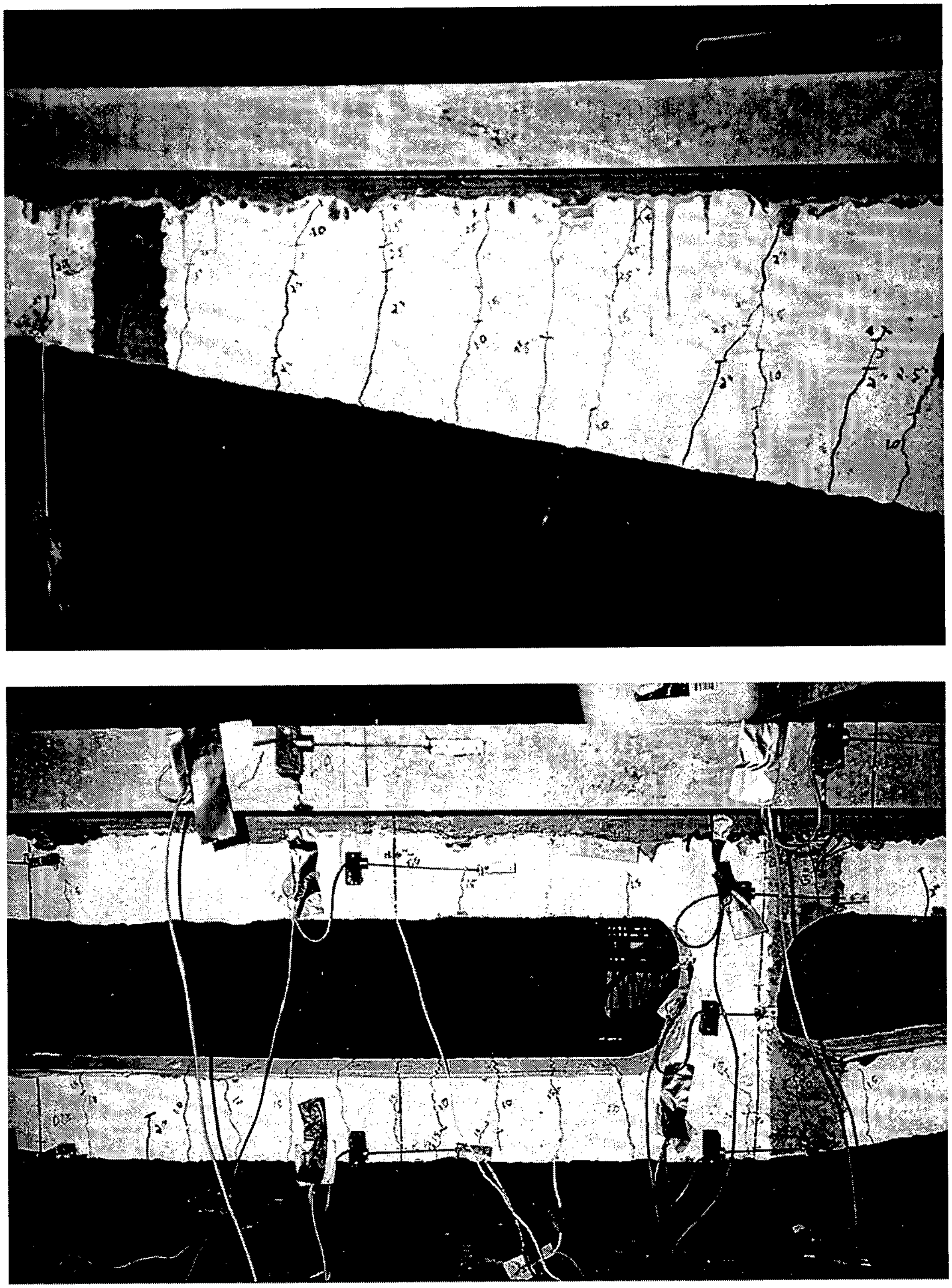

Figure 6.21. Crack patterns for HJ-7.

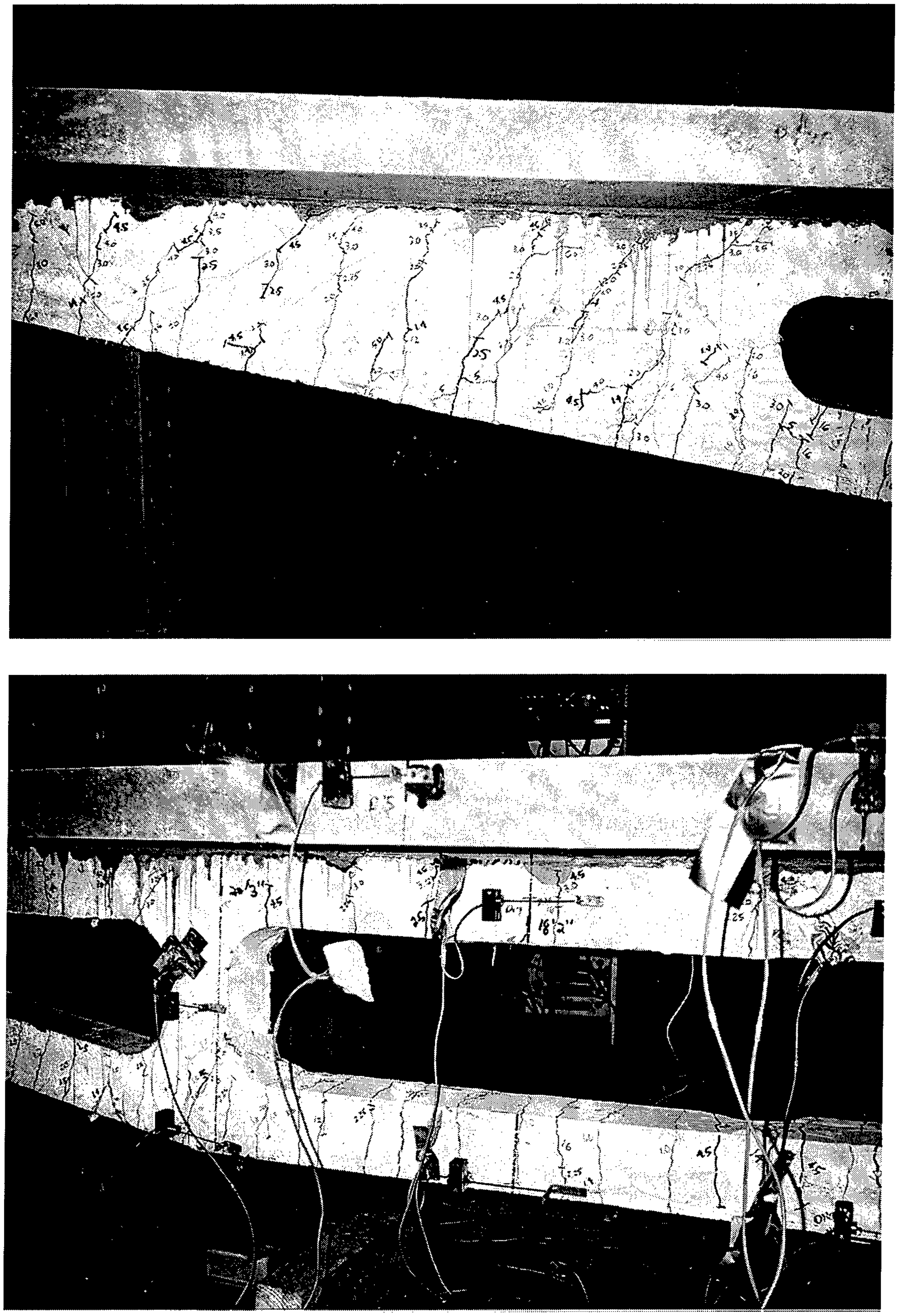

Figure 6.22. Crack patterns for HJ-8.

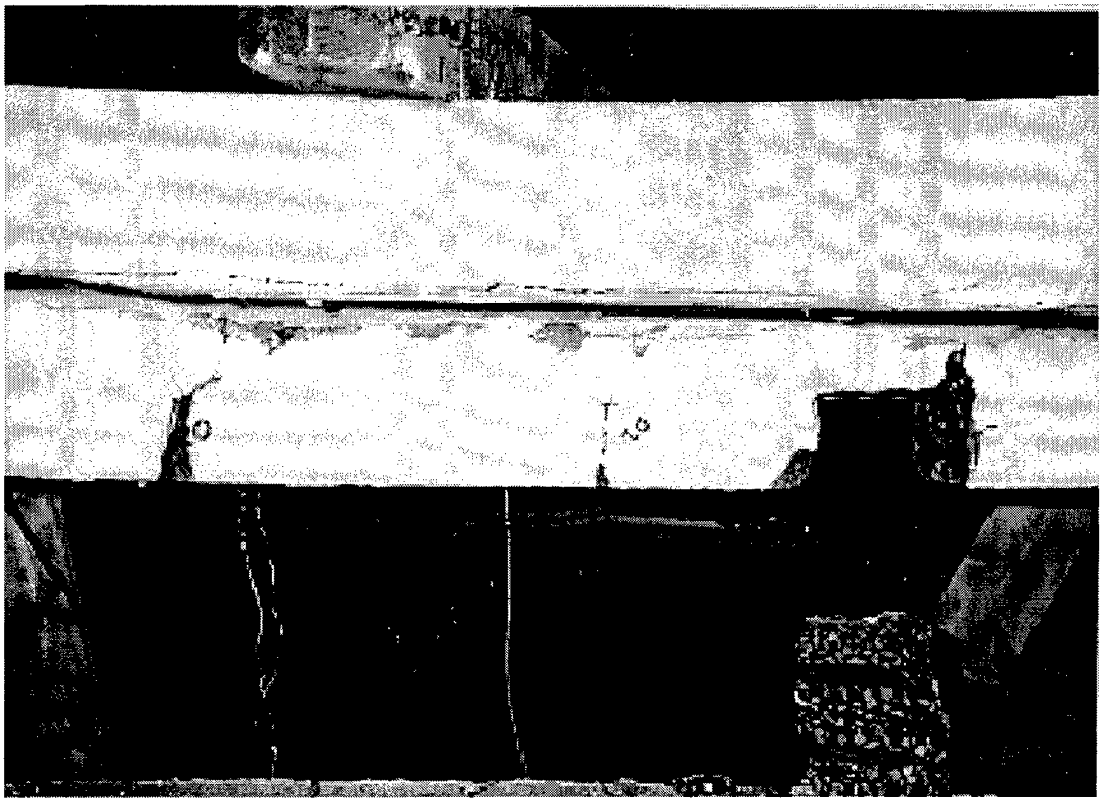

Figure 6.23. Failure of HJ-1.

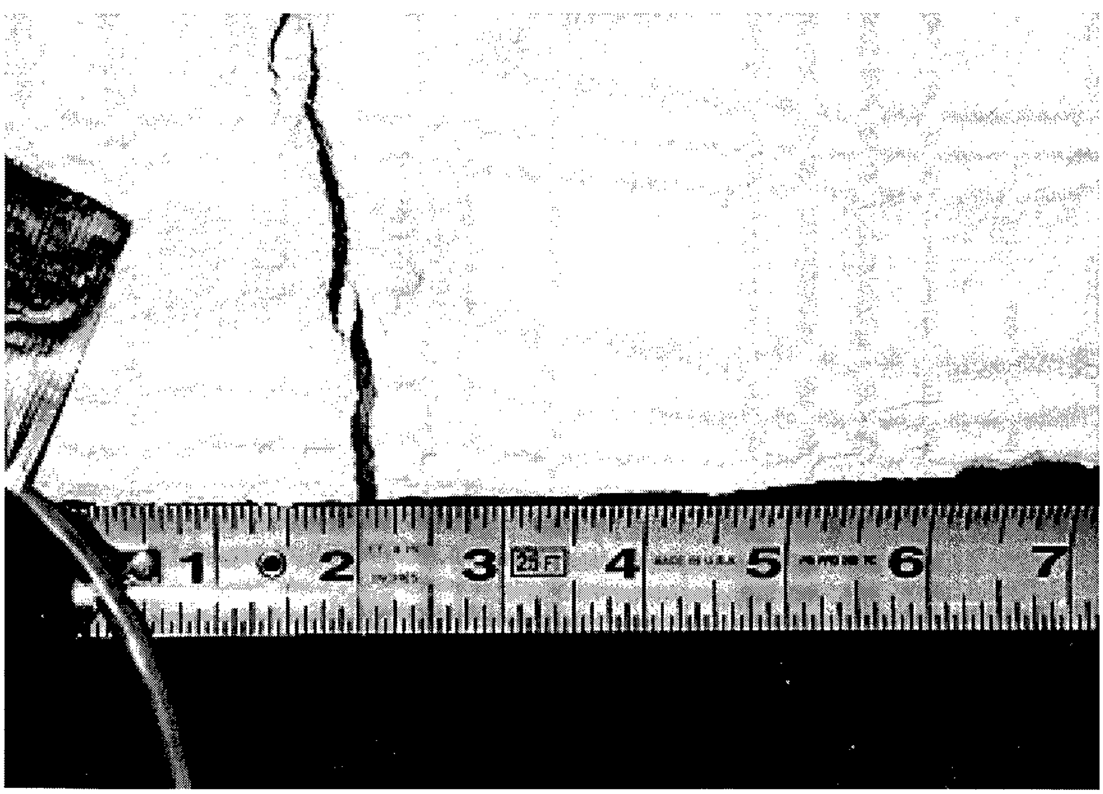

Figure 6.24. Crack in HJ-2 bottom chord.

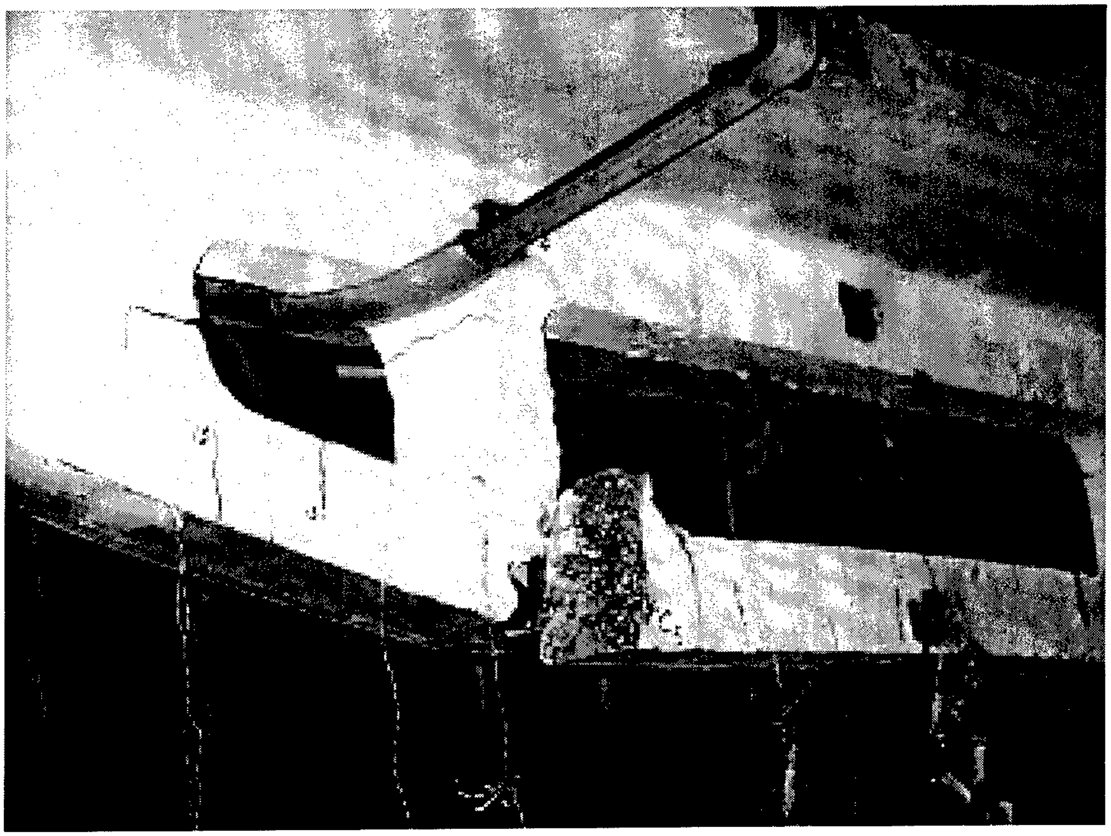

Figure 6.25. Failure of HJ-2.

Figure 6.26. Crack patterns for HJ-6.

Figure 6.27. Failure of HJ-6.

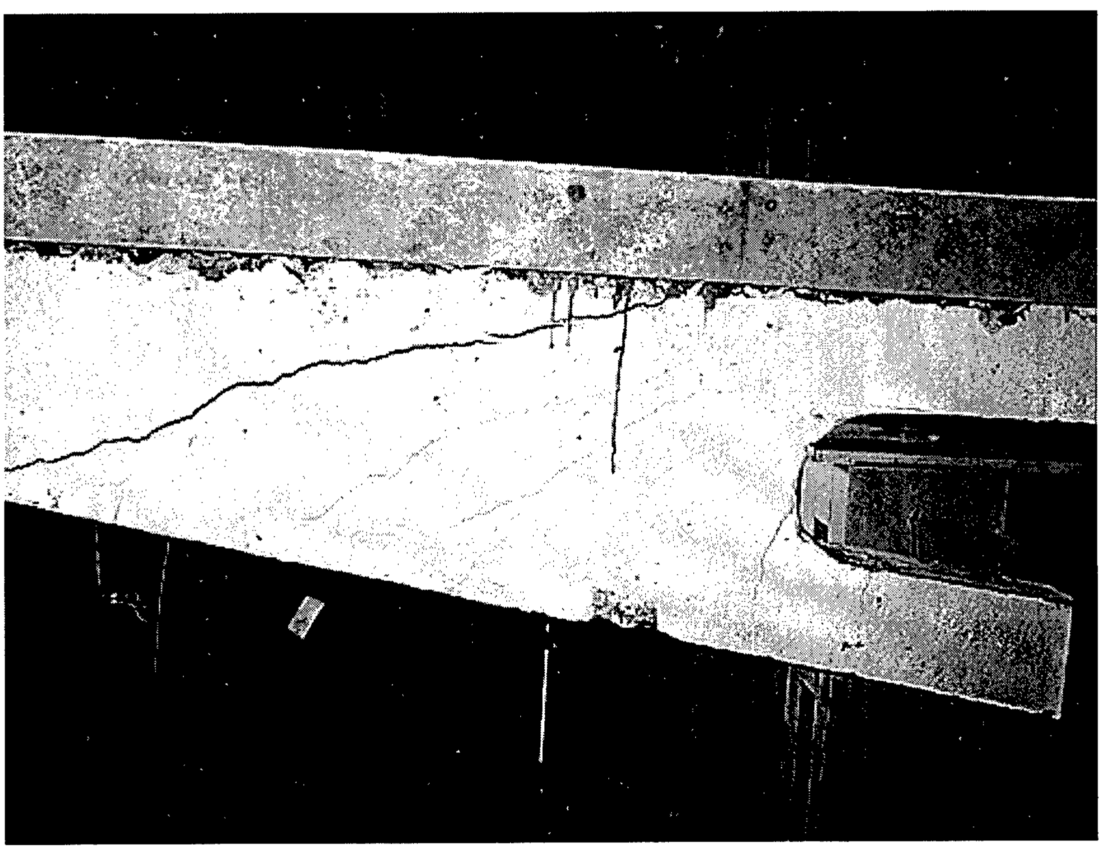

Figure 6.28. Crack patterns for HJ-5.

7 Design Procedure and Cost/Benefit Analysis

Introduction

Based on theoretical analyses and experimental tests a simple procedure was developed to design hybrid joists. This design procedure is a step by step process wherein load demands are assessed, a member cross-section is selected, prestressing and shear reinforcement are designed, and stresses and deflections are checked. Figure 7.1 shows the flowchart for the joist design procedure. A design aid and design example are presented in Appendix A to facilitate understanding of the design procedure and the use of hybrid joists.

Design Criteria and Assumptions

Design criteria are based on *Building Code Requirements for Reinforced Concrete*, ACI 318-95 (1995). Load and strength reduction factors as specified by the code are used. Flexural strength is calculated using strain compatibility. The flange flexural and shear strengths are not considered as limiting criteria.

The joist is designed as a floor member with a tributary width of 6 ft. It is designed as a partially prestressed concrete member; flexural tensile cracking is assumed to occur under service loads. The joist web is assumed to support a 4 in. thick cast-in-place slab. The following construction sequence is assumed:

1. The joists are cast horizontally.
2. The prestressing strands are released.
3. The joists are erected in place and lightweight forms are supported from the joists for casting the slab.
4. The slab is cast and the forms are removed.

The joist is assumed to be uniformly loaded at all stages with a simple span and roller supports. *Caution*: the results of the current study do not support the use

of hybrid joists under concentrated loads. Follow-on research will be needed to determine whether this type of hybrid joist can be configured and optimized to handle concentrated loads.

Design Procedure

Select Configuration

The suggested configuration of the joist is shown in Figure 7.2. The length L_2 depends on the depth of the joist only, and is fixed for all spans with the same depth. The strand profile is assumed to be the same as that shown in Figure 7.3. Choose a section using the preliminary load tables provided in Tables A.1 through A.3.

Define Loading

As stated above, uniform loading of the beam is assumed. Service loading is defined as the unfactored load. This will generally be a combination of the beam self-weight, superimposed dead load, and live load. Ultimate load is typically defined as:

$$\text{Ultimate Load} = 1.4 * DL + 1.7 * LL \qquad \textbf{[Eq 7.1]}$$

where DL is the sum of the self-weight and superimposed dead load

LL is the live load

Calculate the service load for each loading stage. Calculate the ultimate loads acting on the joist. Again, it must be noted that the CPAR test results do not support the use of this type of hybrid joist where concentrated loads will be applied.

Check Stresses

Flexural, shear, and axial stresses should be checked for all loading stages. A suggested analytical model for computing internal member stresses is shown in Figure 7.4.

Check stresses due to the release of prestress. For this condition the analytical model should include the joist web only. Critical sections for this loading

condition are at the joist ends and the top chord at midspan, sections 1 and 3 in Figure 7.5. End stresses are calculated at 50 strand diameters from the section end, the theoretical point of full transfer.

Check stresses due to the construction loads. The joist web alone is the appropriate model for this condition.

Check stresses due to service loads. All sections of the joist — sections 1 through 4 of Figure 7.5 — should be evaluated at this loading condition.

Check stresses at ultimate loading using ACI 318-95 approximate equations or the strain compatibility method. The critical section at ultimate load is at the joist midspan; in particular, the local behavior of the top chord should be checked. If the tension stresses in the top or bottom chord exceed $6\sqrt{f_c'}$, the stresses should be checked against the crack width limitation of ACI code. Using the ACI 318-95 provision (Section 10.6.4), the maximum crack width should be determined using the following equation:

$$\omega = 0.076 \qquad \beta_n f_s \; \sqrt[3]{dcA} \qquad \textbf{[Eq 7.2]}$$

where ω = crack width at tension face of the beam, in.

β_n = the ratio of the distance to the working stress neutral axis from the extreme tension fiber and from the centroid of the main tension reinforcement. To simplify practical design, an approximate value of 1.2 is used.

f_s = service load stress in the steel (ksi)

d_c = thickness of concrete cover measured from the extreme tension fiber to center of the bar located closest thereto (in.)

$A = \frac{Ae}{m}$, effective tension area of concrete surrounding the main tension reinforcing bars and having the same centroid as the reinforcement divided by the numbers of bars (sq in). Permissible stresses in concrete are in

accordance with the requirements of ACI 318-95, Section 18.4, and Savage et al. (1996)[15]. These are summarized below.

Stresses in concrete immediately after prestress transfer:

extreme fiber stress in compression	$0.80\, f'_{ci}$
extreme fiber stress in tension	$6\sqrt{f'_{ci}}$
extreme fiber stress in tension at the ends	$3\sqrt{f'_{ci}}$

where f'_{ci} = compressive strength of concrete at time of initial prestress

Stresses in concrete at service loads:

extreme fiber stress in compression due to prestress force plus sustained loads or total loads $0.60\, f'_c$

extreme fiber stress in tension due $6\sqrt{f'_c}$

ACI 318-95 limits crack width to 0.016 in. for interior exposure and 0.013 in. for exterior exposure.

Design Shear Reinforcement

Design the shear reinforcement as if the joist had no openings. The critical joist section is at a distance h/2 from the face of support where h is the total depth of the section in this location. The recommended shear reinforcement is as shown in Figure 7.6.

Check Deflections

Deflections should be checked using structural analysis methods. Estimated cambers should be based on elastic members. The estimated long-term deflec-

---

[15] The compression stresses at release are restricted in ACI 318-95 to 0.6 f'_{ci}. In a study to assess the effect of a higher compression stress level on the concrete at prestress release, Tadros et al. indicated that this limit is low. An 18 in. x 18 in. prestressed member was evaluated to determine how different levels of prestressing forces affect concrete strain, prestress losses, and concrete stress at time of release. This study included linear elastic and nonlinear analyses. The study showed that the stress in the concrete at release can be increased to 0.86 f'_{ci} and still have a safety factor of 1.5 for ultimate crushing of concrete.

tion should account for superimposed dead load but does not include live load. The governing section is at the top chord midspan. For calculating the deflection limitation, the length of the opening should be considered as L3 = 1 ft.

Cost /Benefit Analysis

The following cost analysis (Table 7.1) was made to compare the materials-only cost of hybrid joists with (a) conventional double-tee joists without web openings and (b) double-tee joists with web openings. The assumptions used in the cost analysis of all systems are listed below.

Assumptions for cost analysis

Span .... 50 ft
Live load .... 50 psf
Partitions, floor covering & miscellaneous dead load .... 15 psf
Double tee top flange .... 4 in.
Cast-in-place slab for the hybrid joist .... 4 in.
Double tee web spacing .... 4 ft
Hybrid joist spacing .... 6 ft
Double tee depth .... 24 in.
Hybrid joist depth .... 24 or 36 in.
28-day concrete strength .... 7000 psi for double-tee joists
.... 10,000 psi for hybrid joists
Strands .... 1/2 inch diameter 270 ksi low relaxation

Table 7.1. Materials cost analysis.

		Unit	Material quantity / unit floor area							
Item		*Cost ($)*	*Solid double tee*		*Double tee with web openings*		*Hybrid joist, 24 in. depth*		*Hybrid joist, 36 in. depth*	
			Quantity	Cost	Quantity	Cost	Quantity	Cost	Quantity	Cost
Strands, ft/ft^2		0.50/ft	2.00	1.00	2.25	1.13	2.03	1.02	3.01	1.51
Reinforcing bars, lb/ft^2		0.35/lb	---	---	0.50	0.18	0.21	0.07	0.29	0.10
Welded wire fabric, lb/ft^2		0.50/lb	1.22	0.61	1.41	0.55	0.43	0.22	0.43	0.22
Hold-down devices		18.00/piece	0.01	0.18	0.01	0.18	0.01	0.18	0.01	0.18
Concrete	Precast, ft^3/ft^2	120/yd^3	0.51	2.27	0.47	2.09	0.11	0.49	0.17	0.76
	CIP, ft^3/ft^2	60/yd^3	---		---	---	0.17	0.38	0.17	0.38
Total/ ft^2				4.06		4.13		2.36		3.15

This analysis shows that the materials required for producing hybrid joists—both those with a 24 in. and 36 in. web depth—would cost less than the materials used in conventional solid double-tee joists. Initially the cost of producing hybrid joists may be slightly higher than that for solid double-tee joists due to the requirement for new forms and modification of the standard manufacturing process. However, as the modified process became routine, the manufacturing cost of hybrid joists could reasonably be expected to decrease. The use of hybrid joists in construction would provide additional cost savings over conventional double-tee construction because the building's environmental systems could be passed through the webs of the joists. This design advantage would require less overall building height, saving in wall material costs and reducing the overall cost of the building by reducing its weight.

Other benefits are associated with the use of hybrid joists over conventional joist systems. An analysis was conducted to evaluate the stiffness of the hybrid joists to floor vibration. A detailed discussion of this analysis is contained in Saleh (1996). After a careful review of the state-of-the-art procedures for evaluating floor vibration perceptibility, a method by Allen (1990) was used to predict floor system response and acceptability. The hybrid joist was evaluated against three other joist types:

1. System 1, an open-web steel joist with 4 in. cast-in-place slab
2. System 2, prestressed precast concrete double tees with solid webs with 2 in. cast-in-place topping
3. System 3, prestressed double tees with web openings with 2 in. cast-in-place topping.

Table 7.2 shows the first four frequencies for all systems. The important frequency is the lowest frequency, which is associated with the first mode of vibration. This table shows that the System 1 has the lowest natural frequency, and therefore the greatest flexibility. System 2 has the highest natural frequency, and therefore is the stiffest. The two new systems (System 3 and System 4) have natural frequency values that lay in between the previous values. The natural frequencies for all four systems are comparable. All system frequencies fall within acceptable limits per Allen (1990). The openings in the double tees have little effect on the dynamic characteristics of the system. The stiffness of the hybrid joist was increased by using a higher concrete strength, which refines its dynamic characteristics.

Table 7.2. Natural frequencies of systems evaluated.

Frequency no.	System 1	System 2	System 3	System 4
1	2.053	3.535	3.363	3.393
2	2.074	3.566	3.404	3.666
3	2.157	3.849	3.676	3.906
4	2.344	4.446	4.287	4.510

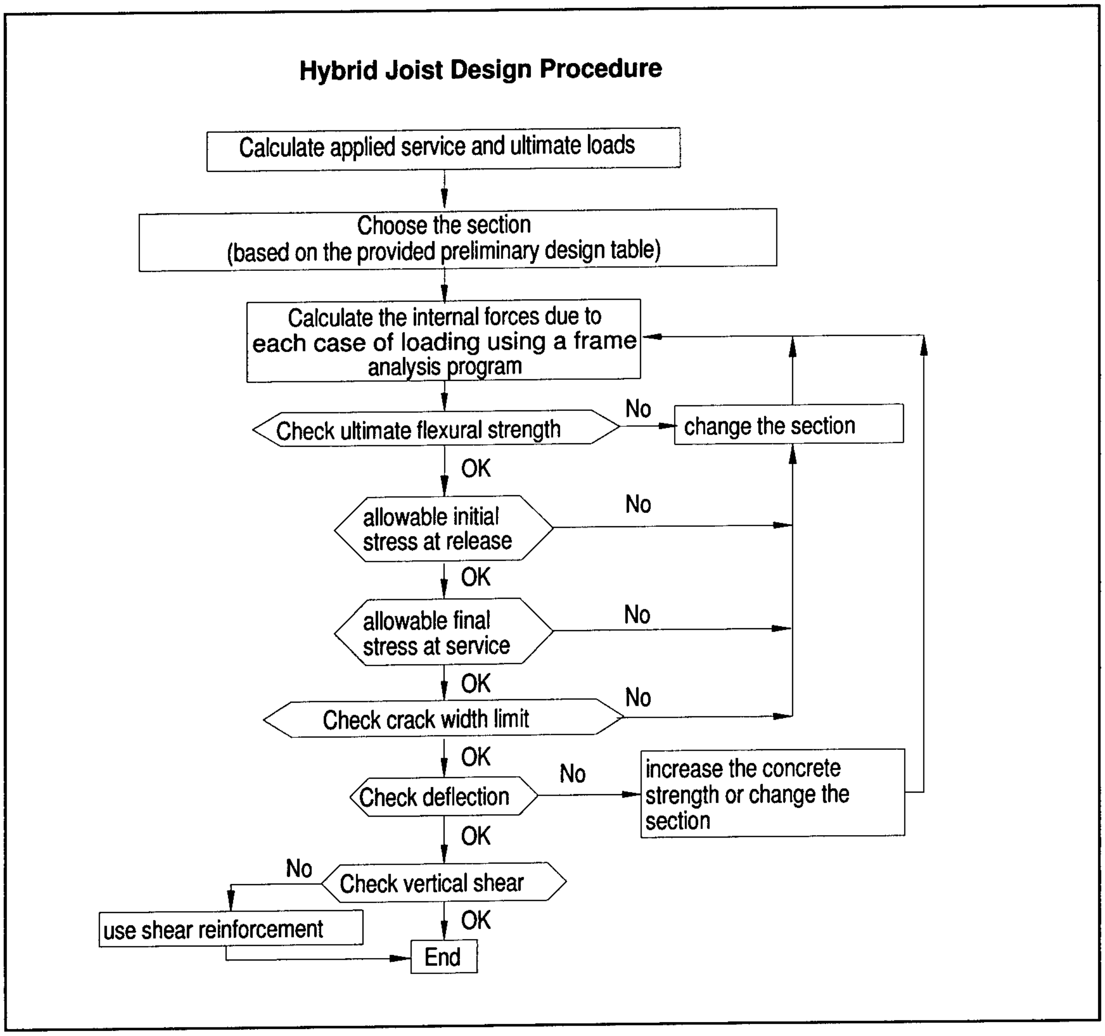

Figure 7.1. Flowchart of hybrid joist design procedure.

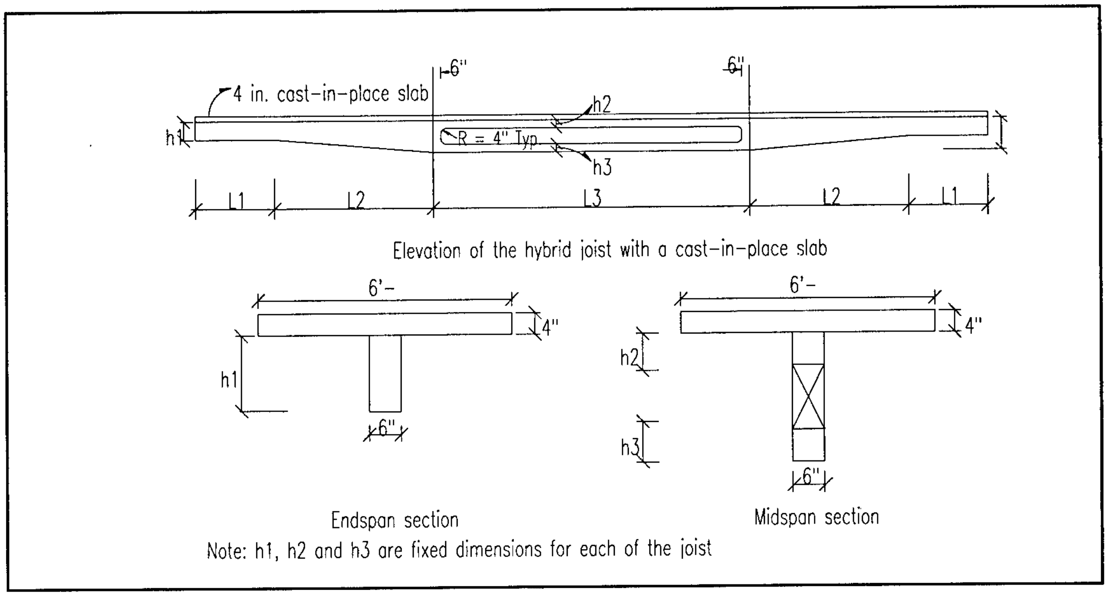

Figure 7.2. Recommended joist configuration.

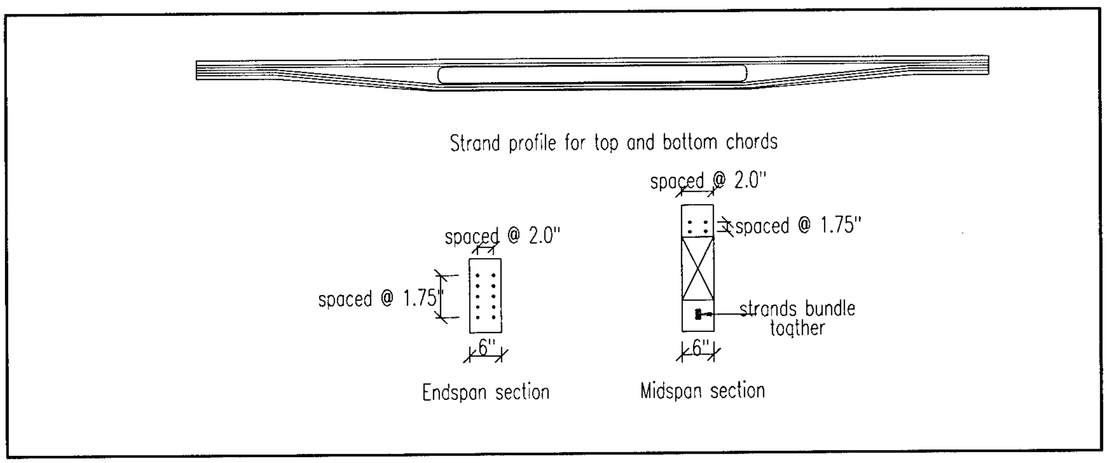

Figure 7.3. Recommended strand profile.

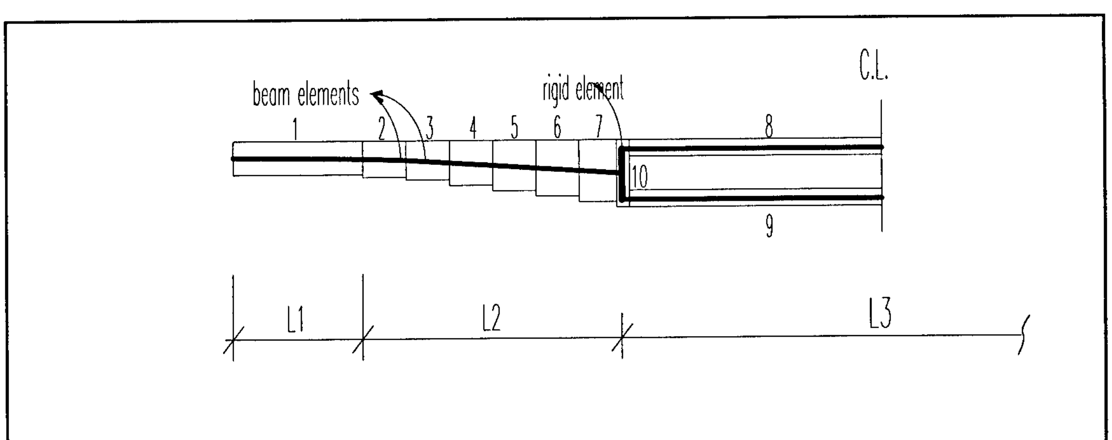

Figure 7.4. Beam element model for the hybrid joist.

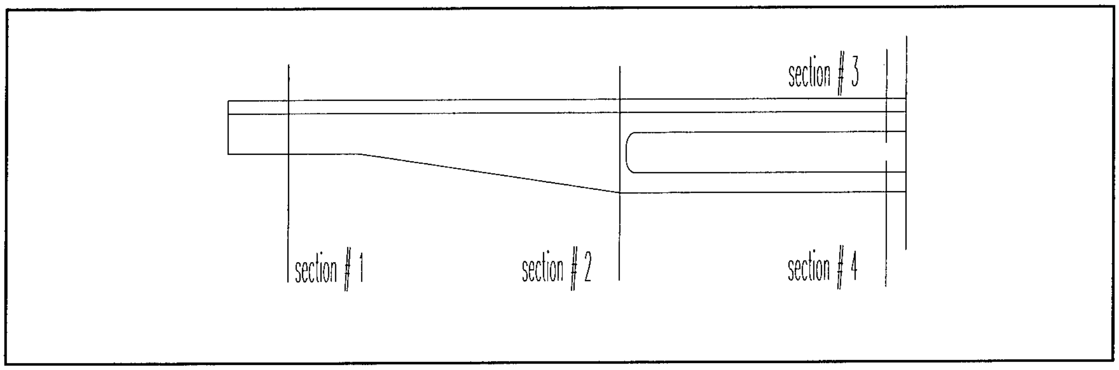

Figure 7.5. The critical sections for the hybrid joist.

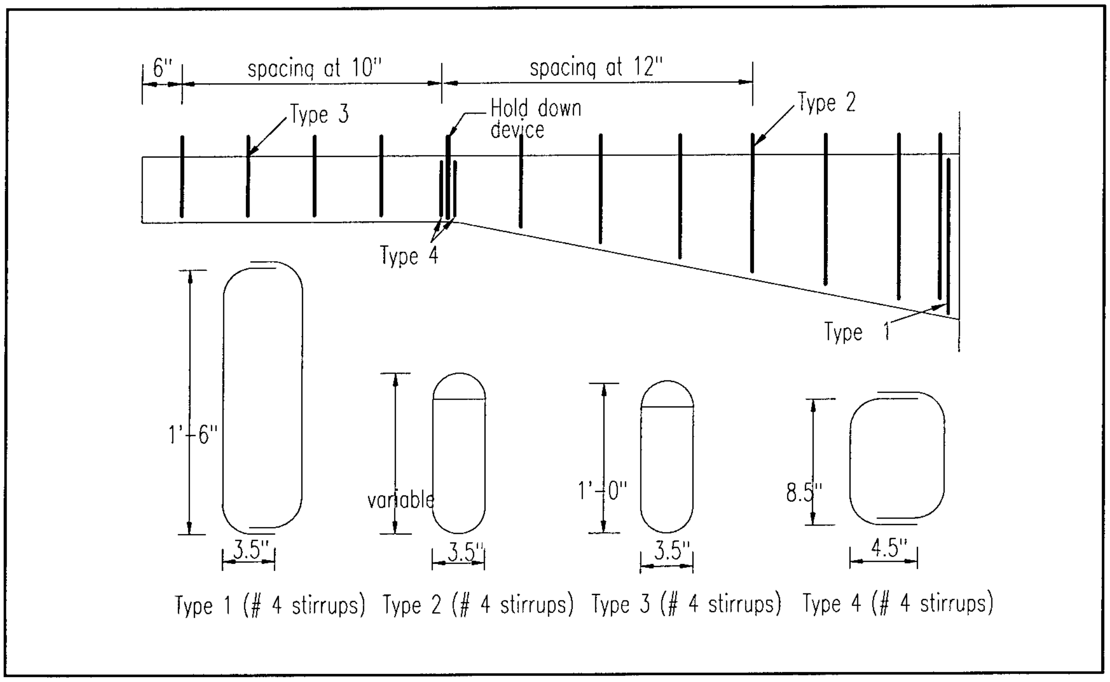

Figure 7.6. Recommended shear reinforcement.

8 Conclusions, Recommendations, and Commercialization

Conclusions

The new hybrid joist has remarkable performance and the capability to behave like a conventional double-tee beam. The behavior of the new hybrid joist meets the requirements of ACI 318-95. Experimental failure loads were very high compared with design service and ultimate loads.

Both the analytical and experimental results indicate that the proposed hybrid joist has a predictable ductile response. The experimental results verify that the analytical model provides a reliable and simple method for determining the load-deflection response of the hybrid joist. Vibration analysis also showed that the hybrid joist has acceptable response to established criteria and compares well with the response of both concrete and steel bar joists.

Based on the tests and analyses, a design procedure was developed to help the user select the proper hybrid joist size for different applications. The proposed design procedure contains design steps for assessing load demands, selecting a member cross-section, designing prestressing and shear reinforcement, and checking stresses and deflections. The design procedure is explicitly limited to applications where the joist will be uniformly loaded, such as the floors and roofs of typical office buildings. The results of this study do not support the use of this type of hybrid joist where concentrated loads are to be applied; follow-on research would have to be conducted to determine whether this type of hybrid joist could be configured and optimized to handle concentrated loads.

Recommendations

The final hybrid joist designs evaluated in this experimental and analytical research program are recommended for use by the Corps of Engineers and the construction industry to replace standard double-tee beams in prestressed

precast reinforced concrete floor and roof construction where only uniform loading will occur. The hybrid joists are not recommended for conditions where concentrated loads may be present.

Joist shear reinforcement, as shown in Figure 4.3 (Chapter 4) is recommended. Positive anchorage of shear reinforcement into the cast-in-place slab is essential. The top surface of the web should also be roughened to ensure good composite action between the web and the cast-in-place slab.

Further analysis and testing of hybrid joist designs is recommended to evaluate their behavior under special loading conditions including concentrated loads, fatigue loading, and vibrations. Additionally, the effects of long-term loading (e.g., creep) should be assessed. For greater optimization of the joist design, other issues to investigate would be the effects of varying degrees of partial prestress force and increased spacing between the webs (i.e., a wider flange width). Simplification of the shear reinforcement details in the hybrid joist system to reduce the cost of labor and forms would also be of value.

Technology Transfer and Commercialization Plan

The Prestressed Concrete Institute (PCI) is the primary organization in the United States dedicated to the advancement of the design, manufacture, and use of prestressed and precast concrete. PCI disseminates information on the latest concepts, techniques, and design data to the architecture and engineering professions through regional and national programs and technical publications. This organization will be employed as the essential vehicle for the publication and marketing of the hybrid joist design to the engineering profession and precast concrete industry.

The design procedure for hybrid joists has been submitted to PCI for review and inclusion in its design handbooks. PCI handbooks provide guidance to engineers in designing and specifying precast concrete products in accordance with commonly accepted industry practice and codes. PCI's review process is expected to take 6 months.

As design professionals, engineers, and architects increasingly specify hybrid joists for their construction projects, it can be assumed that the precast concrete industry will respond to the commercial demand. The PCI could facilitate this process by promoting commercialization of the hybrid joist as a standard product of the precast concrete industry nationally. As an industry participant in the

research that produced the hybrid joist designs, the Precast Concrete Association (PCA) of Nebraska supports the commercialization of this product.

As the primary design and construction agent of the U.S. military services, the U.S. Army Corps of Engineers should actively disseminate design information and potential applications for hybrid joists. Information on the hybrid joist design was published in the newsletter *Structural Engineering For Military Programs* (HQUSACE, October 1996). An article describing hybrid joist benefits, a design procedure, and sample configurations is provided at Appendix B. A version of this information may be prepared for publication in a future issue of *Structural Engineering For Military Programs*.

Applicable Corps guide specifications, Civil Works Guide Specification (CWGS) 03425, *Precast-Prestressed Concrete,* and Corps of Engineers Guide Specification (CEGS) 03550, *Precast/Prestressed Concrete Floor and Roof Units,* currently specify that designs conform to ACI and PCI standards. Neither of these guide specifications prohibits the use of joists with openings. CWGS 03425 states that shop drawings are to show all openings greater than or equal to 12 in. wide cast into members. CEGS 03550 states that "Structural analysis shall include evaluation of the effects of... holes. Units shall be designed for... additional loads imposed by openings...". Inclusion of the design of hybrid joists in the PCI handbooks will further facilitate Corps application of these joists.

References

Allen, D. E., "Building Vibrations from Human Activities," *Concrete International*, Vol 12, No. 6, June 1990, pp 66-73.

American Concrete Institute [ACI] Committee 318, *Building Code Requirements for Structural Concrete and Commentary*, ACI 318-95 (ACI, 1995).

ACI Committee 544.3R-93, *Guide of Specifying, Proportioning, Mixing, Placing and Finishing Steel Fiber Reinforced Concrete* (ACI, 1 May 1993).

Barney, G.B., W.G. Corley, J.M. Hansan, and R.D. Parmelee, "Behavior and Design of Prestressed Concrete Beams," *PCI Journal*, November/December 1977, vol. 22, no. 6, pp. 32-61.

Carrasquillo, R.L., A.H. Nilson, and F.O. Slate, "Properties of High Strength Concrete Subject to Short-Term Loads," *ACI Structural Journal*, vol 78, no. 3 (May-June 1981).

Dinakaran, V., and M.K.L.N. Sastry, "Behavior of Post-Tensioned Prestressed Concrete I-Beams with Large Web Openings," *Indian Concrete Journal* (February 1984).

Kennedy, J.B., and H. Abdalla, "Static Response of Prestressed Girders with Openings," *ASCE Journal of Structural Engineering*, vol. 118, no. 2 (February 1992)

Kennedy, J.B., and A.M. El-Laithy, "Cracking at Openings in Prestressed Beams At Transfer," *ASCE Journal of the Structural Division*, vol. 108, pp. 1250-1265.

Ragan, H.S. and J. Warwaruk, "Tee Members with Large Web Openings," *PCI Journal*, vol. 12, no. 4 (August 1967), pp. 53-65.

Salam, S.A., and J. Harrop, "Prestressed Concrete Beams with Transverse Circular Holes," *Proceedings of the Structural Division*, vol. 105, no. ST3 (ASCE, March 1979).

Saleh, M.A., "Optimization of Prefabricated Joists," Doctoral Dissertation (University of Nebraska, December 1996).

Savage, J.M., *Optimized Prefabricated Concrete Joist Systems* (Master's Thesis, University of Nebraska, December 1993).

Savage, J.K., M.K. Tadros, P. Arumugasaamy, and L.G. Fischer, "Behavior and Design of Double Tee with Web Openings," *PCI Journal*, January/February 1996, vol. 41, no. 1, pp. 46-62.

Steel Joists and Joist Girders (Vulcraft, a division of NUCOR Corp., 1991 and 1995).

Appendix A: Design Aids and Example

Design Aid

This appendix presents design aids for three hybrid joist sections. The sections chosen represent hybrid joists with web depths of 24 in., 36 in., and 48 in. Information is provided for spans between 32 ft and 70 ft. The joist spans used in the tables are the effective span lengths between support center lines. The joist spacing was assumed as 6 ft.

Tables A.1, A.2, and A.3 provide section property details for the three joist sections used in the design aids. These joists are designated HJ-24, HJ-36 and HJ-48. Figures A.1, A.2, and A.3 show the joist configurations for representative spans.

Design Assumptions

Concrete material properties for the joist web are assumed to be ≥ 12,000 psi for compressive strength, f'c, at 28 days and 9000 psi at the time of prestressing release. This strength is required to avoid overstresses at release, control deflections, and provide adequate shear capacity. Joist flange concrete compressive strength is assumed to be f'c ≥ 5000 psi. The concrete weight is 150 pcf. All strands are ½ in. diameter with an ultimate strength of 270 ksi and have low relaxation properties. Epoxy coated strands are recommended for protection from corrosion and fire in this application based on the assumption that service loads will produce cracking in the member. The initial prestress value is assumed to be 0.65 of ultimate prestressing strength, or 0.65 f_{pu}. Stresses at transfer of prestress are assumed to be 90 percent of the initial stresses. Effective prestress is assumed 80 percent of initial.

Load Table Description

The load tables (Tables A.4, A.5, and A.6) show joist self-weight, allowable uniform superimposed service load, estimated camber at the time of erection,

estimated long-term deflection, live load deflection, and required vertical shear reinforcement for hybrid joists of 24 in., 36 in., and 48 in. depths.

The allowable uniform superimposed service load includes dead load of 15 psf typical for floor members. A construction load of 10 psf was assumed to account for forming the cast-in-place slab.

The values for safe superimposed uniform service load are based on the capacity of the section as governed by ultimate flexural strength, service load flexural stresses, crack width, deflection, or shear strength. The dead load portion of the safe load is specifically identified for the purpose of applying load factors and determining cambers and deflections.

The criteria used to determine the allowable superimposed load are based on Building Code Requirements for Reinforced Concrete ACI 318-95/318R-95. The Code provisions used in the development of these load tables are as follows:

The joists are designed for use as floor members.

Capacity governed by design flexural strength:

Load factors: 1.4 D.L. + 1.7 L.L.

Strength reduction factor, F = 0.90

Calculation of design moments assumes simple spans with roller supports. The joist is modeled with beam elements. Flexural strength is calculated using strain compatibility.

Capacity governed by deflection:

for floor members, the live load deflection should not be more than $\frac{L}{360}$

for roof member the live load deflection should not be more than $\frac{L}{240}$

Capacity governed by crack width:

Using the ACI Code provision (section 10.6.4), the maximum crack width should be determined from the following equation:

$$\omega = 0.076\, \beta_n\, f_s \sqrt[3]{d_c\, A}$$

where ω = crack width at tension face of the beam, in.

β_n = the ratio of the distance to the working stress neutral axis from the extreme tension fiber and from the centroid of the main tension reinforcement. To simplify practical design, an approximate value of 1.2 is used.

f_s = service load stress in the steel (ksi)

d_c = thickness of concrete cover measured from the extreme tension fiber to center of the bar located closest thereto, in.

A = $\frac{A_e}{m}$, effective tension area of concrete surrounding the main tension reinforcing bars and having the same centroid as the reinforcement divided by the numbers of bars, in^2.(Figure A.4).

The ACI Code limits crack width to 0.016 in. for interior exposure and 0.013 in. for exterior exposure.

Capacity governed by shear strength:

Load factors: 1.4 D.L. + 1.7 L.L.

Strength reduction factor, F = 0.85

End stresses are calculated 50 strand diameters from the end of the section, the theoretical point of full transfer.

The flange flexural and shear strengths are not considered as limiting criteria.

The estimated cambers and deflections shown are calculated using the multipliers given in the PCI Handbook.

Estimated cambers are based on the elastic member properties. The estimated long-term deflection includes superimposed dead load, but does not include live load. The estimated long-term deflection was calculated using PCI Handbook multipliers before the application of superimposed live loads. Live load deflection is calculated using a frame analysis program. The governing section is

the midspan section of the top chord. For calculating the limitation of the deflection, the length of the opening should be considered as (L3 - 1 ft).

Design Example

Design Conditions and Joist Configuration

Design a hybrid joist floor member for 50 ft span length. Joist web depth is 24 in. and web width is 6 in. The joists are spaced at 6 ft on center and have a 4 in. thick cast-in-place (CIP) slab. Figure A.4 shows the typical dimensions of the hybrid joist section. Design the joist to carry 15 psf superimposed dead load (SIDL) and 50 psf live load (LL) in addition to its self weight.

Material properties are as defined below:

HJ 24 web concrete strength at release $f'_{ci} = 9000$ psi

concrete strength at 28-days $f'_c = 12000$ psi

modulus of elasticity[16]

at release E= 4795 psi

at 28-days E= 5382 ksi

CIP slab concrete strength at 28-days $f'_c = 5000$ psi

modulus of elasticity

at 28-days $E = (w_c)^{1.5}\,(33)\,\sqrt{f'_{ci}} = 4287$ ksi

Prestressing strand: 1/2" diameter, low relaxation.

ultimate strength $f'_s = 270$ ksi

yield strength $f^*_y = 0.9\ f'_s = 243$ ksi

[16] Carrasquillo et al. showed that the ACI equation for computing modulus of elasticity overestimates the stiffness of concrete with strengths greater than 6000 psi. The authors recommend the stiffness of normal-weight concrete be calculated as $E_c = 40000\ \sqrt{f'_c}\ + 1000000$

initial prestressing f_{si} $= 0.75\ f_s' = 202.5$ ksi

modulus of elasticity E_s $= 28000$ ksi

Reinforcing bars:

yield strength f_{sy} $= 60000$ psi

The beam element model described in Chapter 7 is used to determine the internal forces of the elements. Figure A.5 shows this model. Figure A.6 shows the critical joist sections. Table A.7 shows the section properties for non-composite and composite sections.

Figure. A.7 shows the strand profile and the cross section at the end and mid-span. The end element has 12 strands distributed at a spacing of 1.75 in.; the center of gravity (c.g.) of the strands is 5.38 in. from the bottom of the element. The top chord has 4 strands distributed at 1.75 in. and the c.g. of the strands is 2.50 in. from the bottom of the top chord. The bottom chord has 8 strands bundled together and the c.g. of the strands is 2.75 in. from the bottom of the bottom chord.

Define Loading and Internal Forces

Loads

self weight = calculate weight of the joist and then distribute over the span

=

$$\left[\frac{12}{12}x15+\frac{1}{2}x\frac{12}{12}x10+\frac{20}{2}x2-\left(\frac{20}{2}-\frac{1}{2}\right)x\frac{12}{12}\right]x2x\frac{6}{12}x150x\frac{1}{50}$$

= = 92 plf

CIP slab $= \frac{4}{12}$ x 6 x 150 = 300 plf

construction load = 10 psf x 6 = 60 plf

superimposed dead load = 15 psf x 6 = 90 plf

live load = 50 psf x 6 = 300 plf

ultimate loads = (92 + 300 + 90) * 1.4 + 300 * 1.7 = 1184 plf

Internal forces

The joist is cast horizontally (that is on its side). The construction stages are as follows:

1. release of prestressing force acting on non-composite sections.
2. self weight + CIP slab + construction loads acting on non-composite section.
3. SIDL + LL acting on composite section.

Using a the beam element model with a standard structural analysis program, the internal forces at the critical sections can be determined. Table A.8 shows the internal forces for each loading case.

Check Stresses

The flexural capacity of the joist should be evaluated for two critical sections. These sections are: (1) the midspan section composed of the CIP slab, and top and bottom web chords, and (2) the midspan section composed of the web top chord and CIP slab only.

The top strands can be ignored when calculating the capacity of the overall joist section. The number of strands in the bottom chord is 8 strands with a strand c.g. of 2.75 in. from the joist bottom.. The ultimate moment is calculated assuming the joist acts as simple beam.

$$M_u = \frac{w\ L^2}{8} = \frac{1.184 \times (50)^2}{8} = 370 \text{ ft-kips}$$

h = 28.00 in.

d_{ps} = 28 - 2.75 = 25.25 in.

b = 72.00 in.

A_{ps} = 8 x 0.153 = 1.224 in^2

for f'_c = 5000 psi, β_1 = 0.80

γ_p = 0.28 for low relaxation strand

$$\rho_p = \frac{1.224}{72.00 \text{ x } 25.25} = 0.00067$$

$$f_{ps} = 270\left[1 - \frac{0.28}{0.80} \text{x} \, 0.00067 \, \text{x} \frac{270}{5}\right] = 267 \text{ ksi}$$

$$a = \frac{1.224 \, \text{x} \, 267}{0.85 \, \text{x} \, 5 \, \text{x} \, 72} = 1.07 \text{ in.} < \text{thickness of the slab} = 4 \text{ in.}$$

$$\phi M_n = 0.90 \text{ x } 1.224 \text{ x } 267 \left(25.25 - \frac{1.07}{2}\right)\frac{1}{12}$$

$$= 606 \text{ ft-k} > M_u = 370 \text{ ft-k}$$

There are four strands in the top chord, with a strand c.g. of 2.50 in. from the bottom of the top chord. The ultimate moment in this case is calculated using the beam element model.

M_u = 39.92 ft-kips

h = 10.00 in.

d_{ps} = 10 - 2.50 = 7.50 in.

b = 72.00 in.

A_{ps} = 4 x 0.153 = 0.612 in^2

for $f_c' = 5000$ psi, $\beta_1 = 0.80$

γ_p = 0.28 for low relaxation strand

$$\rho_p = \frac{0.612}{72.00 \text{ x } 7.50} = 0.001133$$

$$f_{ps} = 270\left[1 - \frac{0.28}{0.80} \text{x} \, 0.001133 \, \text{x} \frac{270}{5}\right] = 264 \text{ ksi}$$

$$a = \frac{0.612 \, \text{x} \, 264}{0.85 \, \text{x} \, 5 \, \text{x} \, 72} = 0.53 \text{ in.} < \text{thickness of the slab} = 4 \text{ in.}$$

$$\phi M_n = 0.90 \times 0.612 \times 264 \left(7.50 - \frac{0.53}{2}\right)\frac{1}{12}$$

$$= 88 \text{ ft-k} > M_u = 39.92 \text{ ft-k (at mid span)}$$

Allowable working stresses are:

1. Stresses in concrete immediately after prestress transfer:

extreme fiber stress in compression $0.8\ f'_{ci} = 7200$ psi

extreme fiber stress in tension $6\sqrt{f'_{ci}} = 569$ psi

extreme fiber stress in tension at the ends $3\sqrt{f'_{ci}} = 285$ psi

Assume losses are 10% $f_{si} = 0.75 \times 270 \times 0.90 = 182$ ksi

2. Stresses in concrete due to services load:

extreme fiber stress in compression due to prestress force plus sustained loads or prestress force plus total loads

$0.60\ f'_c = 7200$ psi

extreme fiber stress in tension $6\sqrt{f'_c} = 657$ psi

Assume losses are 20% $f_{se} = 0.75 \times 270 \times 0.80 = 162$ ksi

Check working stresses. At release the only force acting on the joist is the prestressing force.

At the transfer section, Section 1 (see Figure A.4), force in the strands immediately after release:

$P_i = 0.153 \times 12 \times 182 = 334$ kips

$y_b = 6.00$ in.

The c.g. of the strands to the bottom of the joist = 5.38 in.

eccentricity = 6.00 - 5.38 = 0.62 in.

$$f_b = -\frac{334}{72} - \frac{334 \text{ x } 0.62}{144} = -4.639 - 1.450 = -6.089 \text{ ksi} \quad \text{O.K.}$$

$$f_t = -\frac{334}{72} + \frac{334 \text{ x } 0.62}{144} = -4.639 + 1.450 = -3.189 \text{ ksi} \quad \text{O.K.}$$

At the midspan section, the top chord section (Section 3; see Figure A.4), force in the strands immediately after release:

P_i = 0.153 x 4 x 182 = 111 kips

y_b = 3.00 in.

The c.g. of the strands to the bottom of the joist = 2.50 in.

eccentricity = 3.00 - 2.50 = 0.50 in.

$$f_b = -\frac{111}{36} - \frac{111 \text{ x } 0.50}{36} = -3.083 - 1.542 = -4.625 \text{ ksi} \quad \text{O.K.}$$

$$f_t = -\frac{111}{36} + \frac{111 \text{ x } 0.50}{36} = -3.083 + 1.542 = -1.541 \text{ ksi} \quad \text{O.K.}$$

At midspan section, bottom chord section (section # 4), force in the strands immediately after release:

P_i = 0.153 x 8 x 182 = 223 kips

y_b = 3.00 in.

The c.g. of the strands to the bottom of the joist = 2.75 in.

eccentricity = 3.00 - 2.75 = 0.25 in.

$$f_b = -\frac{223}{36} - \frac{223 \text{ x } 0.25}{36} = -6.194 - 1.549 = -7.743 \text{ ksi}$$

$$f_t = -\frac{223}{36} + \frac{223 \text{ x } 0.25}{36} = -6.194 + 1.549 = -4.645 \text{ ksi} \quad \text{O.K.}$$

Though the compression stress at the bottom fiber of the bottom chord is slightly higher than the allowable stress there will be a CIP slab on the top of the joist, these stresses will therefore be redistributed between the joist and the slab. The stress is acceptable.

Check final stresses. The applied loads are prestressing force, self weight, CIP slab, construction load, superimposed dead load (SIDL) and live load (LL). These loads will be checked in two stages. First, the sum of the prestressing force, self weight, CIP slab and construction loads act on the non-composite section. Second, the sum of the prestressing force, self weight and CIP slab act on the non-composite section and the sum of the SIDL and LL acting on the composite section.

The c.g. of the strands measured for the bottom of each element for each critical section are as follows:

Section 1	**5.38 in.**
Section 2	**8.46 in.**
Section 3	**2.50 in.**
Section 4	**2.75 in.**

The following general equations are used to compute flexural stresses:

$$f_b = -\frac{P_e}{A} - \frac{P_e\, e}{S_b} + \frac{M}{S_b}$$

$$f_t = -\frac{P_e}{A} + \frac{P_e\, e}{S_t} - \frac{M}{S_t}$$

Table A.9 shows the stresses at the bottom and top fibers of the sections under consideration. All stresses shown in Table A.9 are less than the allowable stresses. Stresses in the bottom fibers of all sections did not exceed the allowable tension stresses ($6\sqrt{f_c'}$), therefore crack width limitation need not be checked.

Design Shear Reinforcement

Design the shear reinforcement as if the joist has no openings. The ultimate uniform load is 1.18 plf. Effective section depth, (h), is 16 in.. Distance from the c.g. of the strand to the top of the section, (d), is 16 - 5.38 = 10.62 in.

At the critical section (h/2):

Ultimate shear, V_u= 28.51 kips

Using ACI Code equation (11-9)

$$V_c = \left[0.60\sqrt{f'_c} + 700\,\frac{V_u\,d}{M_u}\right] b_w\, d$$

where ultimate moment, M_u, occurs simultaneously with V_u = 17.56 ft-kips

b_w = section width = 6.00 in.

$\frac{V_u\,d}{M_u} = \frac{28.51 \text{ x } 10.62}{17.56 \text{ x } 12}$ = 1.44 > 1.00, Then, this value should be taken as 1.00

$$V_c = \left[0.60 \text{ x } \sqrt{12000} + 700 \text{ x } 1.00\right] \text{x } \frac{6.00 \text{ x } 10.62}{1000} = 48.82 \text{ kips}$$

$$\text{minimum } V_c = 2\sqrt{f'_c}\, b_w\, d = 2 \text{ x } \sqrt{12000}\,\frac{6.00 \text{ x } 10.62}{1000} = 13.97 \text{ kips}$$

$$\text{maximum } V_c = 5\sqrt{f'_c}\, b_w\, d = 5 \text{ x } \sqrt{12000}\,\frac{6.00 \text{ x } 10.62}{1000} = 34.92 \text{ kips}$$

So, V_c = 34.92 kips

$V_u < V_c$ but $> V_c/2$

So, minimum shear reinforcement should be used.

Assume spacing of the ties, S= 12 in.

$$A_{v\text{-min}} = \frac{50\ b_w\ S}{f_y} = \frac{50 \times 6.00 \times 12}{60000} = 0.06\ \text{in}^2/\text{ft}$$

Use $A_v = 0.06\ \text{in}^2/\text{ft}$

The reinforcement required for the critical section should be used as closed stirrups extending into the CIP slab. This reinforcement should cover the distance from the end of the joist to the edge of the openings. Two closed stirrups should be placed at the edge of the openings to control the cracking. Figure A.5 shows the details of the shear reinforcement.

Check Deflections

The deflection for force at the critical section (section # 3) is as follows:

Initial prestress force, Δ_{pi} = 1.07 in. (camber)

Final prestress force, Δ_{pe} = 0.84 in. (camber)

Joist self weight, Δ_{sw} = 0.45 in. (deflection)

CIP slab, Δ_{CIP} = 1.48 in. (deflection)

Superimposed dead load, Δ_{SIDL} = 0.14 in. (deflection)

Live load, Δ_{LL} = 0.46 in. (deflection)

Initial camber, Δ = 1.07 in. (camber)

Table A.10 shows the long term deflection using PCI multipliers.

Compute the allowable deflection due to live load. The live load deflection should be considered only for the length of the top chord (L3 = 20 ft).

$$\Delta = \frac{L}{360} = \frac{20 \times 12}{360} = 0.66\ \text{in.}$$

Live load deflection:

$\Delta_{LL} = 0.46$ in. < 0.66in. OK

Allowable total deflection due to sustained loads and LL

$$\Delta = \frac{L}{240} = \frac{20*12}{240} = 1.00\,\text{in.}$$

Total final deflection:

$$\Delta = 0.42 + 0.46 = 0.88\,\text{in.} < 1.00\text{in. OK}$$

Table A.1. Section properties for HJ-24.

	Section 1		Section 2		Section 3		Section 4	
	non-comp.	*composite*	*non-comp.*	*composite*	*composite*	*non-comp.*	*composite*	*non-comp.*
A, in²	72	302	144	374	36	266	36	36
y_b*, in.*	6.00	12.10	12.00	20.62	3.00	7.32	3.00	3.00
y_t*, in.*	6.00	3.90	12.00	7.38	3.00	2.68	3.00	3.00
I, in⁴	864	4682	6912	24588	108	1194	108	108
S_b*, in³*	144	387	576	1193	36	163	36	36
S_t*, in³*	144	1199	576	3330	36	446	36	36

Dimension details for HJ-24					
End element		***Top chord***		***Bottom chord***	
depth, in.	*# of strands*	*depth, in.*	*# of strands*	*depth, in.*	*# of strands*
12	12	6	4	6	8

Table A.2. Section properties for HJ-36.

	Section 1		Section 2		Section 3		Section 4	
	non-comp.	*composite*	*non-comp.*	*composite*	*composite*	*non-comp.*	*composite*	*non-comp.*
A, in²	108	338	216	446	48	278	60	60
y_b*, in.*	9.00	16.49	18.00	28.32	4.00	8.97	5.00	5.00
y_t*, in.*	9.00	5.51	18.00	11.68	4.00	3.03	5.00	5.00
I, in⁴	2916	12121	23328	68229	256	1993	500	500
S_b*, in³*	324	735	1296	2409	64	222	100	100
S_t*, in³*	324	2199	1296	5843	64	657	100	100

Dimension details for HJ-36					
End element		***Top chord***		***Bottom chord***	
depth, in.	*# of strands*	*depth, in.*	*# of strands*	*depth, in.*	*# of strands*
18	18	8	6	10	12

Table A.3. Section properties for HJ-48.

	Section 1		Section 2		Section 3		Section 4	
	non-comp.	*composite*	*non-comp.*	*composite*	*composite*	*non-comp.*	*composite*	*non-comp.*
A, in²	144	374	288	518	60	290	84	84
y_b in.	12.00	20.62	24.00	35.56	5.00	1055	7.00	7.00
y_t in.	12.00	7.38	24.00	16.44	5.00	3.45	7.00	7.00
I, in⁴	6912	24588	55296	142131	500	3140	1372	1372
S_b in³	576	1193	2304	3997	100	298	196	196
S_t in³	576	3330	2304	8643	100	911	196	196

Dimension details for HJ-48					
End element		***Top chord***		***Bottom chord***	
depth, in.	*# of strands*	*depth, in.*	*# of strands*	*depth, in.*	*# of strands*
24	22	10	8	14	14

Table A.4. HJ-24 loads and deflections.

HJ-24 with 12 strands	Span (ft)									
	32	***34***	***36***	***38***	***40***	***42***	***44***	***46***	***48***	***50***
Self weight, plf	100.78	99	98	97	96	95	94	93	92	92
Allowable SIDL, psf	410	360	315	275	240	215	165	135	115	85
Camber at release, in.	0.36	0.42	0.48	0.54	0.62	0.73	0.89	0.89	0.97	1.07
LL deflection, in.*	-0.55	-0.63	-0.71	-0.79	-0.87	-0.91	-0.78	-0.78	-0.78	0.65
Shear reinforce., in.2/ft	1.11	1.02	0.92	0.82	0.73	0.67	0.46	0.34	0.26	0.11
Distance L1, ft	1	2	3	4	5	1	2	3	4	5
Distance L3, ft	10	10	10	10	10	20	20	20	20	20

(For the top chord only)
L2=10 ft

Table A.5. HJ-36 loads and deflections.

HJ-36 with 18 strands	Span (ft)									
	42	***44***	***46***	***48***	***50***	***52***	***54***	***56***	***58***	***60***
Self weight, plf	155	153	152	150	149	147	146	145	144	143
Allowable SIDL, psf	505	455	410	375	340	310	285	260	235	220
Camber at release, in.	0.14	0.17	0.20	0.24	0.30	0.11	0.14	0.17	0.21	0.26
LL deflection, in.*	-0.69	-0.76	-0.85	-0.94	-1.04	-1.00	-1.07	-1.13	-1.18	-1.29
Shear reinforcement, in.2/ft	1.51	1.41	1.32	1.25	1.16	1.09	1.03	0.97	0.89	0.86
Distance L1	1	2	3	4	5	1	2	3	4	5
Distance L3	10	10	10	10	10	20	20	20	20	20

L2 = 15 ft

Table A.6. HJ-48 loads and deflections.

HJ-48 with 22 strands	Span (ft)									
	52	*54*	*56*	*58*	*60*	*62*	*64*	*66*	*68*	*70*
Self weight, plf	211	208	206	204	203	201	199	198	196	195
Allowable SIDL, psf	495	455	420	385	355	330	305	285	265	245
Camber at release, in.	0.05	0.06	0.07	0.08	0.10	0.03	0.04	0.05	0.06	0.08
LL deflection, in.*	-0.75	-0.82	-0.90	-0.97	-1.05	-0.97	-1.02	-1.09	-1.16	-1.18
Shear reinforcement, in.2/ft	1.61	1.53	1.46	1.38	1.30	1.25	1.18	1.14	1.08	1.02
Distance L1, ft	1	2	3	4	5	1	2	3	4	5
Distance L3, ft	10	10	10	10	10	20	20	20	20	20

L2 = 20 ft

Table A.7. HJ-24 section properties.

	Section 1		Section 2		Section 3		Section 4
	non-comp.	*composite*	*non-comp.*	*composite*	*non-comp.*	*composite*	
h, in.	12	16	24	28	6	10	6
A, in^2	72	302	144	374	36	266	36
y_b *in.*	6.00	12.10	12.00	20.62	3.00	7.32	3.00
y_t *in.*	6.00	3.90	12.00	7.38	3.00	2.68	3.00
I, in^4	864	4682	6912	24588	108	1194	108
S_b *in*^{3}	144	387	576	1193	36	163	36
S_t *in*^{3}	144	1199	576	3330	36	446	36

Table A.8. Internal forces due to each loading case (kips, ft-kips).

Section #	Self weight		CIP slab		Construction load	
	Axial	Moment	Axial	Moment	Axial	Moment
1	0.00	10.23	0.00	33.37	0.00	6.67
2	0.00	23.80	0.00	77.62	0.00	15.52
3	-13.20	2.64	-43.03	8.61	-8.61	1.72
4	+13.20	0.27	+43.03	0.90	+8.61	0.18

Table A.8 (cont'd.)

Section #	SIDL		LL		Ultimate load
	Axial	Moment	Axial	Moment	Moment
1	0.00	10.01	0.00	33.38	131.70
2	0.00	23.29	0.00	77.63	306.40
3	-12.30	3.03	-41.01	10.11	39.92
4	+12.30	0.15	+41.01	0.48	1.91

Table A.9. Stresses in top and bottom fibers (psi), Stage I.

Section #	Prestressing force		Self weight		CIP slab		Construction load		Total	
	f_b	f_t	f_b	f_t	f_b	f_t	f_b	f_t	f_b	f_t
1	-5.422	-2.840	+0.853	-0.853	+2.781	-2.781	+0.556	-0.556	-1.232	-7.030
2	-3.893	-0.238	+0.496	-0.496	+1.617	-1.617	+0.323	-0.323	-1.457	-2.674
3	-4.130	-1.377	+0.513	-1.247	+1.675	-4.065	+0.334	-0.812	-1.608	-7.501
4	-6.885	-4.131	+0.457	+0.277	+1.496	+0.896	+0.299	+0.179	-4.633	-2.779

Table A.9. Stresses in top and bottom fibers (psi), Stage II (cont'd.)

Sec. #	Prestress. force		Self weight		CIP Slab		SIDL		LL		Total	
	f_b	f_t	f_b	f_t	f_b	f_t	f_b	f_t	f_b	f_t	f_b	f_t
1	-5.422	-2.840	+0.853	-0.853	+2.781	-2.781	+0.310	+0.002	+1.035	-0.008	-0.443	-6.480
2	-3.893	-0.238	+0.496	-0.496	+1.617	-1.617	+0.234	+0.038	+0.781	+0.128	-0.765	-2.185
3	-4.130	-1.377	+0.513	-1.247	+1.675	-4.065	+0.177	-0.087	+0.590	-0.289	-1.175	-7.065
4	-6.885	-4.131	+0.457	+0.277	+1.496	+0.896	+0.392	+0.292	+1.299	+0.979	-3.241	-1.687

Table A.10. Long-term deflection (in.).

Load case	At release	Multiplier	Erection	Multiplier	Final
prestressing	+ 1.07	1.80	+ 1.93	2.45	+ 2.62
self weight			- 0.45	2.70	- 1.22
CIP slab			1.48	2.70	- 4.00
SIDL			- 0.14	3.00	- 0.42
LL					- 0.46

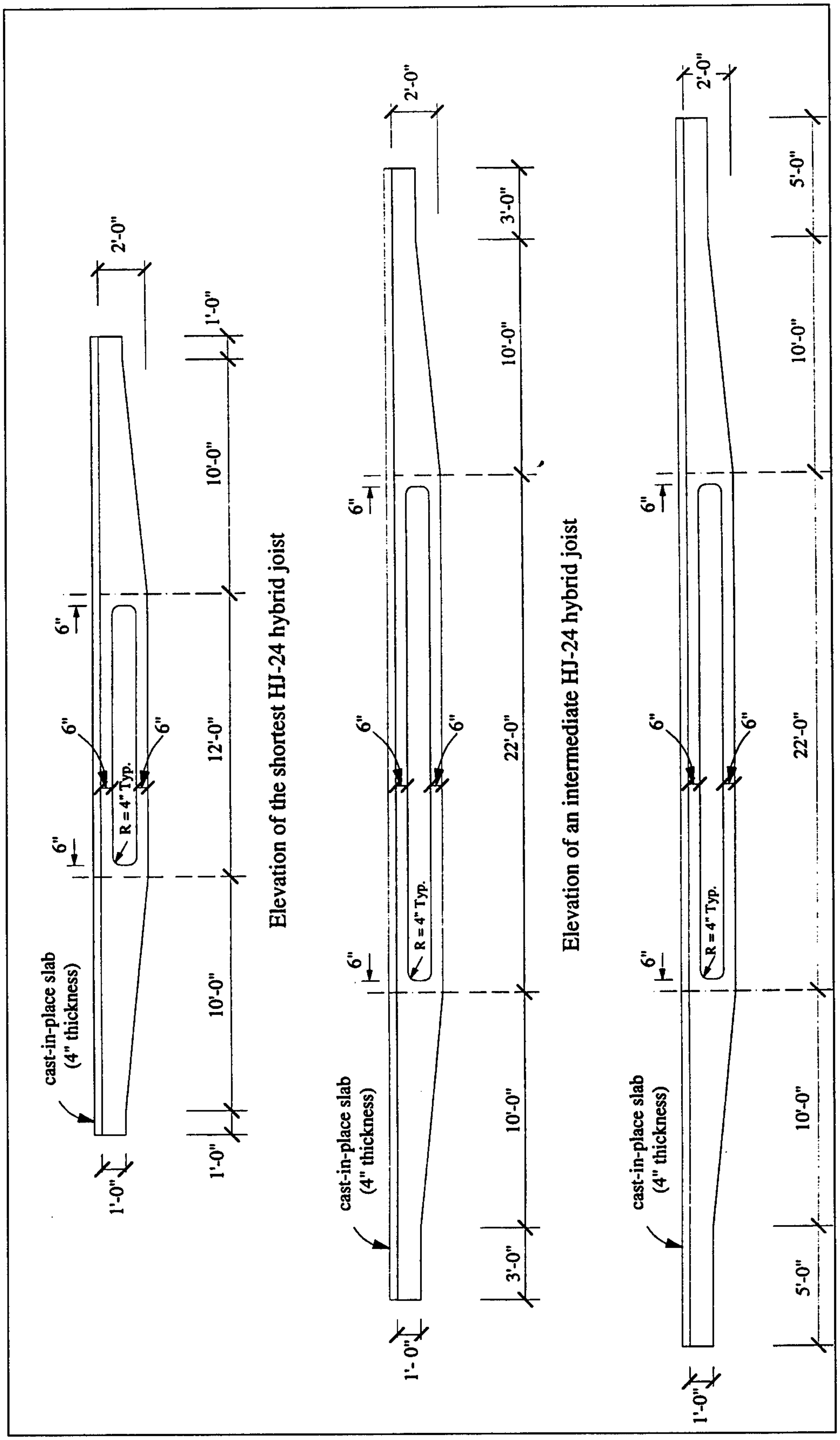

Figure A.1. Typical dimensions of HJ-24.

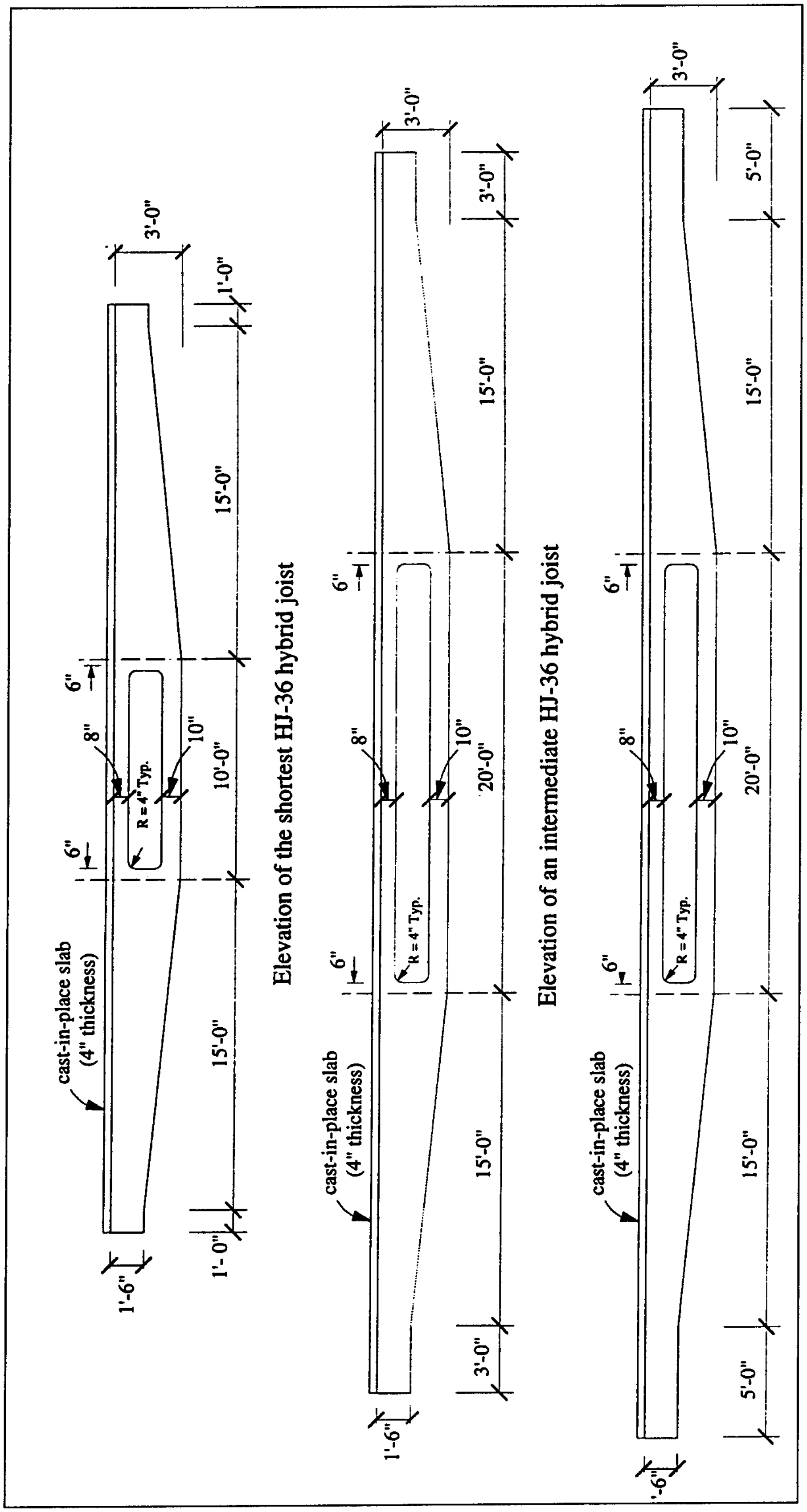

Figure A.2. Typical dimensions of HJ-36.

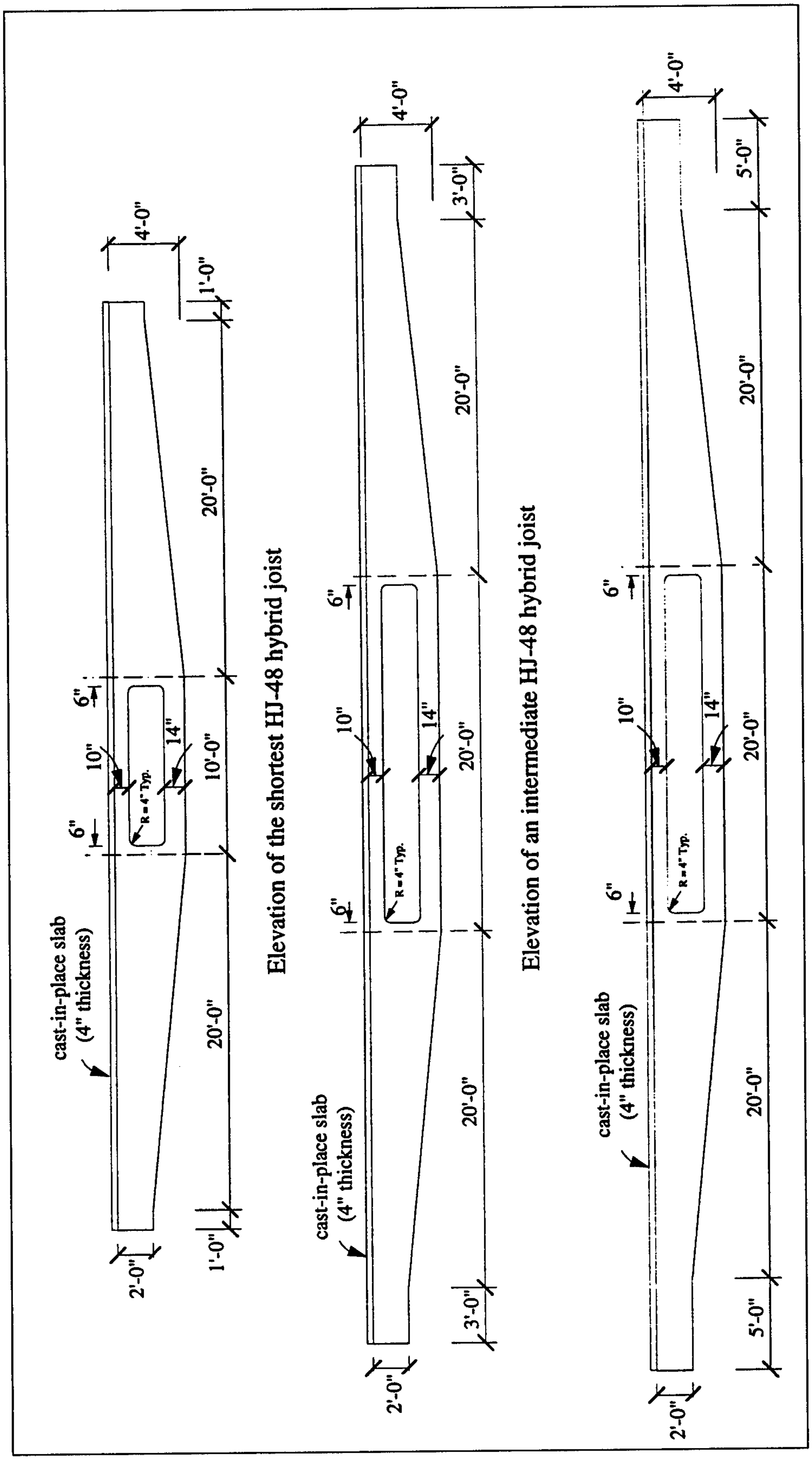

Figure A.3. Typical dimensions of HJ-48.

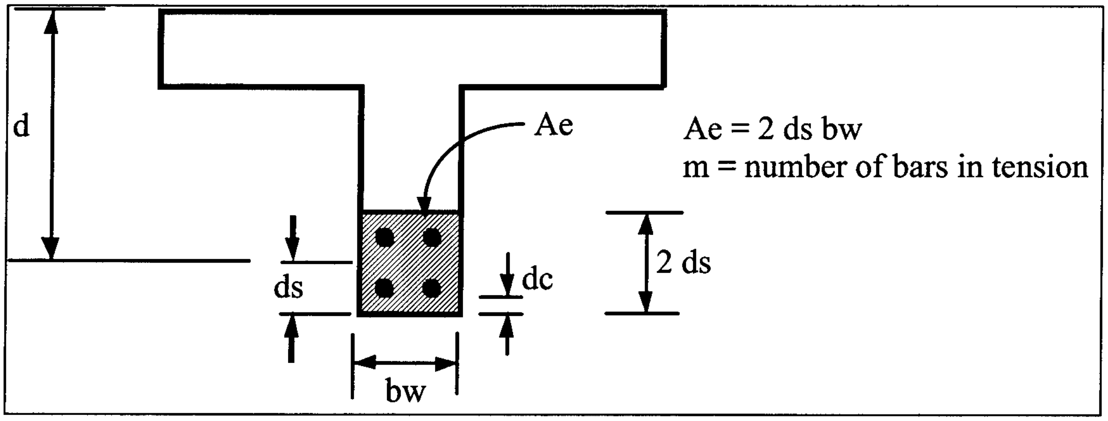

Figure A.4. Section properties for crack width computation.

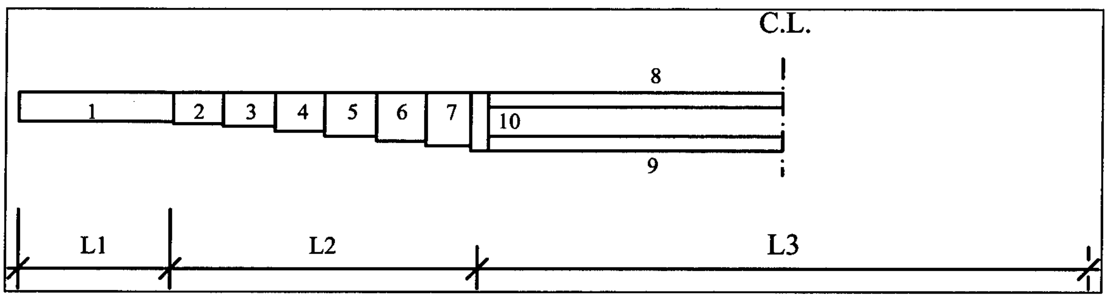

Figure A.5. The beam element model.

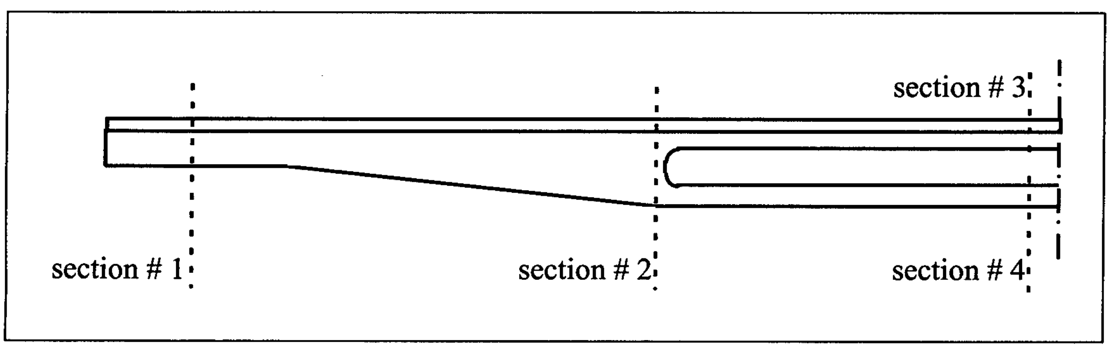

Figure A.6 Critical joist sections.

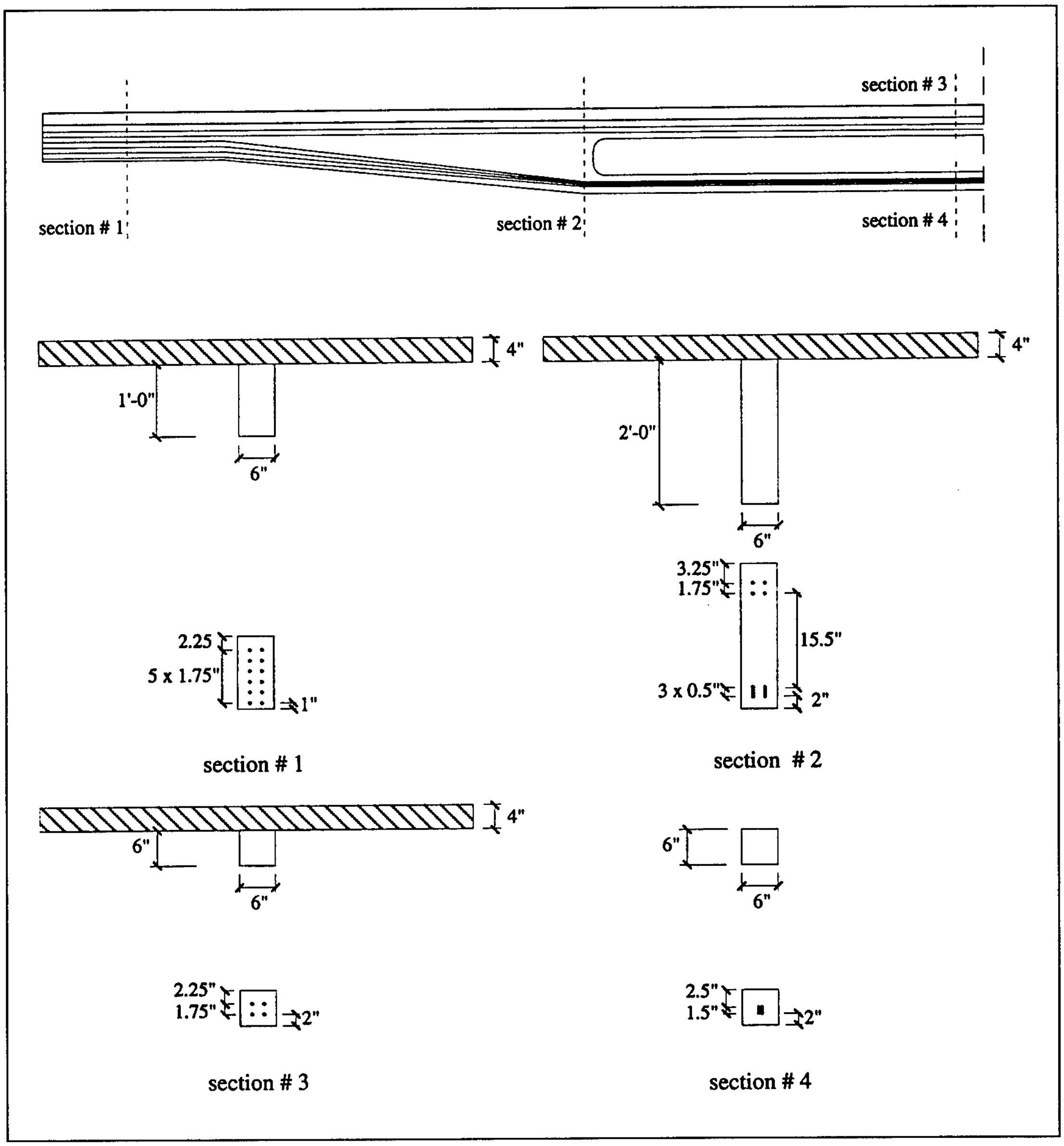

Figure A.7. Section details and strand profile.

USACERL DISTRIBUTION

Chief of Engineers
ATTN: CEHEC-IM-LH (2)
ATTN: CEHEC-IM-LP (2)
ATTN: CEMP-CE (2)
ATTN: CEMP-ET (2)
ATTN: CERD-C (2)
ATTN: CERD-L
ATTN: CERD-M

US Army Engineer District
ATTN: Library (40)

US Army Engineer Divisions
ATTN: Library (11)

Defense Tech Info Center 22304
ATTN: DTIC-O (2)

65
03/97